# MODELLING INVESTIGATION OF INTERACTION BETWEEN ARCTIC SEA ICE AND STORMS: INSIGHTS FROM CASE STUDIES AND CLIMATOLOGICAL HINDCAST SIMULATIONS

By

Alexander Semenov, B.S.

A Dissertation Submitted in Partial Fulfillment of the Requirements

for the Degree of Doctor of Philosophy

in

Atmospheric Sciences

University of Alaska Fairbanks

May 2019

APPROVED:

Dr. Xiangdong Zhang, Committee Chair
Dr. Uma Bhatt, Committee Member
Dr. Jennifer Hutchings, Committee Member
Dr. Nicole Mölders, Committee Member
Dr. Javier Fochesatto, Chair
*Department of Atmospheric Sciences*
Dr. Leah Berman, Dean
*College of Natural Sciences and Mathematics*
Dr. Michael Castellini, *Dean of the Graduate School*

## Abstract

The goal of this study is to improve understanding of atmosphere, sea ice, and ocean interactions in the context of Arctic storm activities. The reduction of Arctic sea ice extent, increase in ocean water temperatures, and changes of atmospheric circulation have been manifested in the Arctic Ocean along with the large surface air temperature increase during recent decades. All of these changes may change the way in which atmosphere, sea ice, and ocean interact, which may in turn feedback to Arctic surface air warming.

To achieve the goal, we employed an integrative approach including analysis of modeling simulation results and conducting specifically designed model sensitivity experiments. The novelty of this study is linking synoptic scale storms to large-scale changes in sea ice and atmospheric circulation. The models were used in this study range from the regional fully coupled Arctic climate model HIRHAM-NAOSIM to the ocean-sea ice component model of the Community Earth System Model CESM and the Weather Research and Forecasting (WRF) model.

Analysis of HIRHAM-NAOSIM simulation outputs shows regionally dependent variability of storm count with a higher number of storms over the Atlantic side than over the Pacific side. High-resolution simulations also reproduce higher number of storms than lower resolution reanalysis dataset. This is because the high-resolution model may capture more shallow and small size storms. As an integrated consequence, the composite analysis shows that more numerous intense storms produce low-pressure systems centered over the Barents-Kara-Laptev seas and the Chukchi-East Siberian seas, leading to anomalous cyclonic circulation over the Atlantic Arctic Ocean and Pacific Arctic Ocean. Correspondingly, anomalous sea ice transport occurs, enhancing sea ice outflow out of the Barents-Kara-Laptev sea ice and weakening sea ice inflow into the Chukchi-Beaufort seas from the thick ice area north of the Canadian Archipelago. This change in sea ice transport causes a decrease in sea ice concentration and thickness in these two areas. However, energy budget analysis exhibits a decrease in downward net sea ice heat fluxes, reducing sea ice melt, when more numerous intense storms occur. This decrease could be attributed to increased cloudiness and destabilized atmospheric boundary layer associated with intense storms, which can result in a decrease in downward shortwave radiation and an increase in upward turbulent heat fluxes.

The sea ice-ocean component CICE-POP of Community Earth System Model (CESM) was used to conduct sensitivity experiment to examine impacts of two selected storms on sea ice. CICE-POP is generally able to simulate the observed spatial distribution of the Arctic sea-ice concentration, thickness, and motion, and interannual variability of the Arctic sea ice area for the period 1979 to 2011. However, some biases still exit, including overestimated sea-ice drift speeds, particularly in the Transpolar Drift Stream, and

overestimated sea-ice concentration in the Atlantic Arctic but slightly underestimated sea ice concentration in the Pacific Arctic. Analysis of CICE-POP sensitivity experiments suggests that dynamic forcing associated with the storms plays more important driving role in causing sea ice changes than thermodynamics does in the case of storm in March 2011, while both thermodynamic and dynamic forcings have comparable impacts on sea ice decrease in the case of the August 2012. In case of March 2011 storm, increased surface winds caused the reduction of sea ice area in the Barents and Kara Seas by forcing sea ice to move eastward. Sea ice reduction was primarily driven by mechanical processes rather than ice melting. On the contrary, the case study of August 2012 storm, that occurred during the Arctic summer, exemplified the case of equal contribution of mechanical sea ice redistribution of sea ice in the Chukchi – East Siberian – Beaufort seas and melt in sea ice reduction.

To understand the impacts of the changed Arctic environment on storm dynamics, we carried out WRF model simulations for a selected Arctic storm that occurred in March 2011. Model output highlight the importance of both increased surface turbulent heat fluxes due to sea ice retreat and self-enhanced warm and moist air advection from the North Atlantic into the Arctic. These external forcing factor and internal dynamic process sustain and even strengthen atmospheric baroclinicity, supporting the storm to develop and intensify. Additional sensitivity experiments further suggest that latent heat release resulting from condensation/precipitation within the storm enhances baroclinicity aloft and, in turn, causes a re-intensification of the storm from its decaying phase.

**Acknowledgements**

Firstly, I would like to thank my advisor Prof. Xiangdong Zhang for advising and supporting my Ph.D study and related research. Besides, I would like to express my sincere gratitude to the rest of my thesis committee: Prof. Uma Bhatt, Prof. Nicole Mölders, and Prof. Jennifer Hutchings, for their encouragement and useful comments, and incitement to widen my research from various perspectives. I would like to thank the M.S. student Paula Doubrawa and the visiting scientist Junming Chen at Xiangdong Zhang's group for their helps with the WRF model and POP-CICE model setups, configurations, and experiments, respectively.

Second, I would also like to acknowledge Dr. Annette Rinke and her group at Alfred Wegener Research Institute, Helmholtz Center for Polar and Marine Research, Germany, for providing the data outputs of the hindcast simulations with the model with the model HIRHAM-NAOSIM, which laid the basis for the research presented in Chapter 2, I am gratefully indebted to Dr. Annette Rinke, Wolfgang Dorn, and Klaus Dethloff for their valuable contributions to this collaborative research.

This study was supported by the NSF Grant #1023592 and ONR-Glable Grant #N62909-13-1-V219, which were awarded to Prof. Xiangdong Zhang. The collaboration on HIRHAM-NAOSIM modeling study between the UAF and AWI groups was initiated by ONR-Global Grant #N62909-13-1-V219. The HIRHAM-NAOSIM modeling experiments were supported by German DFG Grant #SFB/TR17. Computational resources were provided by the Arctic Region Supercomputing Center (ARSC)/now Research Computing System at University of Alaska Fairbanks.

Finally, I want to express my very profound gratitude to my family and friends, in particular to Julie Lageson, Ian Zola Simons, Cece Borries, Soumik Basu, Oliver Dyre Dammann, and Gregory Deemer, for providing me with their support and continuous encouragement throughout my years of study and through the process of researching and writing this thesis. This accomplishment would not have been possible without them. Thank you.

## Table of Contents

Page

## List of Figures

Page

## List of Tables

Page

# Chapter 1 Introduction and Motivation

## 1.1 Arctic Climate System: Current State and Mechanisms of Ongoing Change

The Arctic climate system is a set of closely linked physical systems of land, ocean, cryosphere, and atmosphere. It plays a critical role in governing the global ocean and atmospheric circulation [*Serreze and Barry,* 2011].

The Arctic region is marked by the largest global climate warming evident in the instrumental record, paleoclimatic records, and in climate model projections through the 21st century [*Manabe and Wetherald,* 1975; *Johannessen et al.,* 2004]. Air temperature increase in the Arctic over the past few decades has been documented in many studies [*Serreze et al.,* 2000; *Alekseev et al.,* 2000; *Polyakov et al.*, 2003; *Bengtsson et al.,* 2004; IPCC 2007] and is believed to be driven by the Earth's response to increasing atmospheric greenhouse gas concentrations [e.g., *Manabe and Stouffer,* 1980; *Robock,* 1983; *Hansen et al.,* 1984; *Washington and Meehl,* 1996; *Holland and Bitz,* 2003; *Hall,* 2004]. Extensive sea ice loss has occurred within the Arctic Ocean [*Koyama et al.,* 2017].

Present Arctic warming is amplified due to shrinking and thinning sea ice extent, alterations of ocean currents, and hemispheric-scale changes in atmospheric variability [*Curry and Mauritzen,* 2005; *Francis et al.,* 2005; *Meehl et al.,* 2005; *Stroeve et al.,* 2005; *Schiermeier,* 2006, *Barber et al.,* 2008].

## 1.2 Arctic Climate System Feedbacks

Individual components of the Arctic Climate System can change concurrently and that interaction may amplify Arctic warming through feedback mechanisms [*Manabe and Wetherald,* 1975] and [*Serreze and Barry,* 2011; *Pithan and Mauritsen,* 2014]. Arctic climate feedbacks that modify the state of the Arctic Climate System and accelerate the warming include (i) ice albedo feedback; (ii) cloud and water vapor feedback; (iii) air temperature feedback; (iv) methane release due to thawing permafrost; and (v) Arctic greening [*McGuire et al.,* 2006; *Soden et al.,* 2008].

One of the primary contributors to Arctic polar amplification is the surface albedo feedback [*Crook et al.,* 2011; *Taylor et al.,* 2013]. Sea ice covered with snow reflects about 70% of sunlight whereas the ocean reflects less than 10% except in the sun glint [*Wiscombe and Warren*, 1980]. Therefore, the melting of sea ice, which reveals the ocean surface, causes an increase in the absorption of solar radiation further

adding an increased surface ocean temperature [*Perovich et al.,* 2007]. In this warmer climate, the summer sea ice melt season lengthens and causes a larger exposure of open water areas that readily absorb solar radiation. This effect fosters further melt of the high albedo ice and solar radiation and increases the sensible heat content of the oceanic mixed layer [*Perovich et al.,* 2007].

Cloud feedback was discovered to be the second largest contributor to the Arctic amplification [*Winton,* 2006; *Taylor et al.,* 2013]. Cloud cover and water vapor feedback refers to the mechanism that causes the presence of clouds to augment the downward longwave radiation flux to the surface [*Winton et al.,* 2006; *Pithan and Mauritsen,* 2014]. In contrast to the effect of cloud coverage in the low- and mid-latitudes, the net effect of Arctic clouds, exemplified mainly by low stratiform clouds, was found to warm the surface [*Intrieri et al.,* 2002; *Kay and L'Ecuyer,* 2013]. Recent scientific literature indicates that Arctic water vapor content has increased during recent decades due to increased transport of heat and moisture from mid latitudes [*Lucarini and Ragone,* 2011; *Zhang et al.,* 2012], and via enhanced local evaporation [*Bintanja and Selten,* 2014].

Another potentially large contributor to warming of the Arctic atmosphere is permafrost degradation. Thawing permafrost results in the release of methane, a greenhouse gas, which constitutes a positive feedback to the climate system [*Walter et al.,* 2006; *Jorgenson et al.,* 2006; *Anisimov* 2007].

In response to Arctic warming, high-latitude ecosystem changes include animal habitat migration [*Sturm et al*., 2001], a prolonged growing season [*Jeoung et al.,* 2011], and enhanced photosynthetic activity [*Xu et al.,* 2013]. These changes are generally referred to as Arctic "greening". Studies utilizing observations collected over the last several decades indicate an extension of shrub areas [*Tape et al.,* 2006; *Bunn and Goetz* 2006; *Potter et al.,* 2013] and northward migration of the Arctic tree line [*Pearson et al.,* 2013]. Increasing air temperatures will likely cause Arctic vegetation zones to shift, resulting in wide-ranging impacts. Rising temperatures are expected to favor a northward expansion of boreal forest into the tundra, and of tundra into the polar desert increasing the radiation absorption properties of the Arctic coasts [*Bhatt et al.,* 2010]. Sea ice decline along the coast results in warming and enhanced tundra productivity [*Bhatt et al.,* 2010]. Greening in the Arctic can amplify Arctic warming two to seven times due to decreased surface albedo [*Levis et al.,* 2000; *Chapin et al.,* 2005; *Bonan,* 2008].

The depletion of the ice pack leads to a rise in subsurface heat content as more of the ocean surface becomes exposed to the solar radiation [*Johannessen et al.,* 2004]. The additional heat absorbed by an increasingly ice-free Arctic Ocean in summer is already accelerating local and regional warming and preventing sea ice from recovering in winter. The incoming solar energy becomes trapped below the ocean surface layer and can reduce the growth of sea ice in winter, ultimately leading to earlier melting/retreat in

spring. Such a positive feedback may act in addition to ice-albedo feedback and further contribute to Arctic amplification. *Holland et al.*, [2006] argues that abrupt sea ice transitions are thermodynamically driven by enhanced open water production and increased solar radiation absorption.

### 1.3 Motivations

Extratropical cyclones are key atmospheric elements and represent major sources of energy, mass, and momentum transfer from the low and mid latitudes into the Arctic [*Barry and Carleton,* 2001; *Sorteberg and Walsh,* 2008a]. This motivates the investigation of another feedback mechanism that involves Arctic cyclones and sea ice and study how this feedback may also contribute to Arctic warming. Arctic cyclones play a critical role in the climate system by impacting precipitation, the radiation budget, cloudiness, and poleward heat and moisture transport [*Bengtsson et al.,* 2006; *Sorteberg and Walsh,* 2008a]. The transport of heat into the Arctic by both the ocean [e.g., *Polyakov et al.*, 2010] and atmosphere [e.g. *Serreze et al.*, 2009] has been shown to accelerate Arctic warming.

Sea level pressure exhibits a decreasing trend over the Arctic Ocean [*Serreze et al.*, 2000; *Polyakov et al.,* 2003]. The long-term decline in atmospheric pressure over most of the Arctic is consistent with the response typically simulated by climate models to greenhouse warming [*Vavrus et al.,* 2013] Analyses of the sea level pressure fields indicate that Arctic warming is linked to changes in atmospheric circulation due to increased energy influx into the Arctic [e.g. *Simmonds et al.,* 2008]. Atmospheric circulation may cause approximately 50% of the winter warming in the central Arctic region [*Serreze et al.,* 2000].

Whilst interaction between sea ice and storms affect Arctic temperatures in ways that may contribute to yet more climate change, the impact of increasing incidence and severity of Arctic cyclones is as yet not fully understood within the broad picture of global climate change. So far it has been discovered that decreasing sea level pressure trend in the Arctic is consistent with forcing mechanisms such as a poleward shift of storm tracks [*Bengtsson et al.,* 2006], boundary layer heating [*Deser et al.,* 2010], northward shifts in baroclinicity in the marginal ice zone *[Inoue and Hori*, 2011], and enhanced upward surface energy fluxes with greater open water coverage [*Simmonds and Keay,* 2009]. An increase in penetration of cyclones into the central Arctic has been observed during years of low ice content [*Inoue et al.,* 2012].

More studies recently have been dedicated to investigating the linkage between Arctic storm incidence and concurrent sea ice deterioration [e.g., *Asplin et al.,* 2012; *Zhang et al.,* 2013; *Boisvert et al.,*

2016]. In 2012, the historic minimum recorded sea ice extent was partially attributed to the occurrence of an Arctic cyclone in August that caused a sharp sea ice decline during its development [*Parkinson and Comiso,* 2013; *Zhang et al.,* 2013].

The hypothesis of sea ice reduction as a response of cyclones is not new in spite of recent increase in media and scientific community attention drawn to investigating the relationship between sea ice decline and cyclone activity. The existence of an amplified pace of Arctic air-sea interaction under cyclonic conditions was first introduced in the 1980's. Studies demonstrated that there is a linkage between summer cyclone regime and sea ice decline [e.g., *Barry and Maslanik,* 1989; *Serreze et al.,* 1989]. Since then, many studies documented that Arctic large-scale circulation, and cyclones in particular, can accelerate sea ice deterioration [*Deser and Teng,* 2008; *Ogi et al.,* 2010; *Ogi and Wallace,* 2012; *Asplin et al.,* 2012, *Overland et al.,* 2012, *Zhang et al.,* 2012].

Despite showing the frequency, duration, and intensity of cyclones that enter the Arctic region from the mid-latitudes increased significantly over the period 1948 - 2002 [*Serreze et al.,* 1997, 2000; *Orlanski* 1998; *McCabe et al*., 2001; *Zhang et al.,* 2004; *Wang et al.,* 2006], there is no conclusive finding to clearly assert if the increase in cyclone frequency or intensity is associated with sea ice loss [*Vavrus et al.,* 2016]. Changes in cyclonic activity in the Arctic leads to changes in temperature gradients between mid-latitudes and the poles, and changes in specific humidity as the atmosphere warms [*Vavrus et al.,* 2016]. Partly due to that, studies have reached different conclusions, with some studies suggesting a reduction in mid-latitude cyclone frequency and intensity during winter [e.g., *Gitelman et al.,* 1997; *Geng and Sugi,* 2003, *Vavrus et al.,* 2016], while others, suggesting an increase in frequency and strength of winter cyclones [*Bengtsson et al.,* 2006; *Simmonds et al.,* 2008; *Sorteberg and Walsh,* 2008b; *Simmonds and Keay,* 2009; *Stroeve et al.,* 2011].

While aforementioned Arctic studies alluded that cyclone and sea ice can contribute to Arctic climate warming, there is no general consensus on the mechanisms and this phenomenon is not well understood; therefore, the response of sea ice – storm interaction needs to be investigated as a fully coupled feedback mechanism by analyzing the impact of sea ice on Arctic cyclones in a thorough research framework. Whether the Arctic cyclones and sea ice as a feedback mechanism can accelerate Arctic warming remains unclear, but it motivates to study the response of sea ice on Arctic storms and vice versa as well as to assess of cyclones and sea ice interaction in the context of polar amplification.

Previous studies investigated the cyclonic impact on sea ice, and vice versa, on several time and spatial scales, utilizing different research approaches [e.g *Zhang et al.,* 2004; *Asplin et al.,* 2012; *Zhang et al.,* 2013; *Boisvert et al.,* 2016]. However, these studies lacked clarity on the broader context of cyclone –

sea ice interaction and its footprint on the Arctic warming. In this study, the objective is to conduct a comprehensive study of sea ice – cyclone interaction, encompassing different time and spatial scales and research methods, to identify the mechanisms that might be involved in a cyclone – sea ice feedback process.

Thus, in order to bridge the gap of previous research findings, we carried out an in-depth analysis of sea ice – cyclone response by deploying a series of coupled and stand-alone climate models to isolate and study in detail the following two processes:

(i) physical mechanisms influencing sea ice dynamics and thermodynamics under cyclonic conditions;

(ii) impact of sea ice recession observed in the last decades on Arctic cyclogenesis.

This study is aimed at providing a comprehensive understanding of the cyclone – sea ice interaction in an effort to aid the research community in improving the reliability of the climate model, to reduce the uncertainty of Arctic climate change projections, and to improve the accuracy of operational models.

### 1.4 Implications of Arctic Climate Change to Socio-economic Activity

Growing awareness of rapid changes in the Arctic climate, in conjunction with advances in technology, make the Arctic a new frontier for a variety of socio-economic activities including resource exploration, commercial shipping, tourism and societal activities [*Eicken et al.,* 2009]. Depending on the interest of a stakeholder, Arctic sea ice can be categorized as: (i) climate regulator, marine hazard, and coastal buffer; (ii) transportation and use as a platform; (iii) cultural services obtained from the "icescape"; and (iv) support of food webs and biological diversity [*Eicken et al.*, 2009]. Aforementioned categories may be at risk depending on weather conditions or ice regimes.

Sea ice retreat in the Arctic has significant implications for marine access and shipping that will impact natural resource development and regional trade [*Arctic Council*, 2009]. Shrinking sea ice coverage allows longer navigation seasons and new access to previously difficult-to-reach coastal regions [*Arctic Council*, 2009]. However, while year-round operations may become possible for the maritime industry, the longer season of navigation will cause greater risks of encountering adverse weather conditions as compared to times with larger sea ice extent.

Many Arctic-based operations are sea ice- and weather-dependent. To increase the feasibility of Arctic projects and timeliness of decision making, these operations demand quality data and an

understanding of the timing, intensity, and duration of ice incursions or cyclones so that decision makers may properly mitigate risks and hazards.

The Arctic is a challenging environment where risks of operating are increasingly high. Proximity to the sea ice edges and migration of low pressure systems pose additional environmental risks in the Arctic. Arctic low pressure systems are detrimental to Arctic offshore and onshore activities due to freezing spray (Fig. 1.1A), increasing wind speeds (Fig. 1.1C), greater wave height (Fig. 1.1D), increasing precipitation and the reduction of visibility (Fig. 1.1B), and, if sea ice is present, increased sea ice drift speed. High winds and sea state undermine the stability of offshore structures and vessels. Low visibility may limit navigational access for vessel-to-vessel work and helicopter flights. Icing during Arctic cyclones in transitional seasons is another hazard that Arctic stakeholders may have to contend with during storms. Ice accretion produces accumulation of ice on exposed structural components of ships and platforms above the water surface either on the coast or at sea (Fig. 1.1A).


Figure 1.1: Adverse weather conditions in the Arctic: ice build-up (Credit: http://www.ccg-gcc.gc.ca/) (A), poor visibility conditions (fog, mist) during Coast Guard search and rescue operations (Credit: http://alaska.coastguard.dodlive.mil/) (B), blizzard and strong winds conditions in Nunavut, Canada (Credit: http://www.cbc.ca/) (C), and destabilized beach barriers in Barrow on Aug. 27, 2015 (Credit: http://www.adn.com/) (D).

Arctic-based industries have incorporated meteorological, oceanographic and sea ice knowledge into their operational guidelines and implemented high cost plans to mitigate risks related to adverse weather conditions and ice encroachment. Ice management and ice defense plans detail potential impacts

of cyclones and sea ice on operations: e.g. causing downtime and damage to the equipment. Success of ice management, defense, and avoidance of operations depends upon the reliability of the atmosphere – ocean and sea ice models that, in turn, depends on sufficient physical knowledge of storm – sea ice interaction mechanisms.

Coastal erosion is another hazard that may accelerate following the reduction of sea ice under cyclonic conditions resulting in damages to coastal infrastructure [*Jorgenstern and Brown*, 2005; *Clow*, 2008; *Smith et al.,* 2010; *Holland-Bartels and Pierce*, 2011]. Sea ice acts as a buffer and protects coastal areas from erosion [*Eicken et al.*, 2009; *Wobus et al.*, 2011]. As the length of season with open water in the Arctic increases, coastal areas become more susceptible to erosion (Fig. 1.2). Stronger winds and higher waves that are often caused by cyclones tend to accelerate beach erosion by warming of permafrost [*Ogorodov et al.*, 2010]. Several Arctic communities along with industrial facilities have reported structural damages to the infrastructure as a result of erosion, and in future may face relocation [*Feifel and Gregg*, 2010]. Thawing ground can disrupt transportation, buildings, and other infrastructure, therefore posing significant engineering challenges for roads, buildings, pipelines, and industrial facilities.


Figure 1.2: Sandbags in Kivalina (Credit: Jan Van Der Woning/TCS/Zuma Press) (A), and Shishmaref (Credit: Shishmaref Alaska Erosion & Relocation Coalition) (B).

As a risk-mitigation tool in decision making, local communities, shipping, and resource development industries require accurate prediction of sea ice, ocean, and atmospheric conditions. Improved understanding of sea ice response to Arctic cyclones, and vice versa, may add value to developing better coupled algorithms for sea ice and weather/oceanographic forecast models. These models will become

essential aids for meeting the needs of Arctic shipping and resource development and forecasts that can be utilized by stakeholders.

In recent years, a number of intense storms in the Arctic Ocean have caused wide-spread environmental and socio-economic damage. A storm in August 2012 exemplified a low pressure system that caused notable environmental changes in the Central Arctic Ocean and a November 2011 cyclone resulted in both environmental and socio-economic damages to West Alaska coastal communities [*Zhang et al.,* 2012]. Sea ice extent in summer 2012 reached the lowest ever recorded since 1979 over the remote sensing period. As was later discovered, the abrupt sea ice reduction was occurring while a low pressure system was moving over the Arctic Ocean in early August of 2012 [*Zhang et al*., 2012]. Between August 7 and August 9, sea ice extent was reduced by nearly 200.000 square kilometers.

The November 2011 cyclone discussed in this thesis, is another example of a low pressure system that resulted in both adverse weather conditions and wide-spread coastal damage in the Arctic. The atmospheric low pressure system developed over the Bering Sea in November 2011 and moved northeast towards the western coast of Alaska bringing both near-gale and gale force winds and high sea state. Approximately 37 communities were affected by damages as a result of coastal erosion and flooding due to storm surge and large amount of precipitation [*Hopkins et al.,* 2011].

Improved knowledge of storm – sea ice interaction will aid maritime industry to enhance safety and ensure that proper risk mitigation practices are in place. To date, a number of oil and gas projects carried out in ice-infested waters incorporated extensive studies of Arctic and sub-Arctic sea ice and cyclone climatology.

### 1.5 Research Goal and Objectives

The purpose of this study is to investigate the interactive mechanisms between cyclones and sea ice in the context of Arctic climate change by following a two-step investigation scheme: (i) analyze coupling mechanisms in the context of a sea ice – cyclone feedback (e.g., cyclone impact on sea ice; sea ice response to cyclones); and (ii) assess the role of sea ice – cyclone feedback in the context of Arctic Climate System and Arctic amplification, and the robustness of this finding. The thesis objectives are two-fold: (i) to realistically represent Arctic sea ice, ocean and atmospheric conditions by applying coupled and stand-alone, global and regional climate models; and (ii) to investigate the multi-scale mechanisms of sea ice – storm interaction.

Within this framework, the following contributing factors will be discussed: investigation of long-term (climatology) and short-term (specific cases) cyclone – sea ice feedback mechanisms; investigation of the seasonality of cyclone – sea ice feedback by comparing cyclone activity in winter and summer; and investigation of geographical patterns of cyclone – sea ice feedback in two specific Arctic sectors: Atlantic and Pacific sides of the Arctic.

The project objectives are broad in scope and intended to advance knowledge, reduce uncertainty, and improve assessment of Arctic climate and predictions of Arctic weather, ocean and ice conditions.

### 1.6 Methods and Research Approach

We applied a multi-prong modeling approach to rigorously detail the results of both case studies and climatology analyses to bridge the gap of sparse findings of previously conducted studies on sea ice - storm physical interaction and to further investigate Arctic climate coupling mechanisms. In this study, we employed a scientific approach to analyze model data output produced by regional and global, stand-alone and coupled climate models. High-resolution models were applied to better understand the physical mechanisms driving the Arctic climate change and their interaction.

A hierarchy of climate models will provide greater insight into the interactive mechanisms of the climate system than using data from just one model. The employed models include the stand-alone regional atmospheric Weather Research and Forecasting model (WRF), coupled regional North Atlantic/Arctic Ocean climate atmosphere-ocean-sea ice (HIRHAM-NAOSIM), and coupled global ocean-sea ice Community Ice Code – Parallel Ocean Programming model (CICE-POP) (Table 1.2). WRF and CICE-POP were compiled and integrated as a part of the research project. Output of the HIRHAM-NAOSIM model was also used in this study. Models of various scales, (global and regional), allowed identification of feedback mechanisms, at both a medium and large geographic scale. Case studies and climatology analyses were utilized to differentiate long-term from short-term impacts of feedback mechanisms within the sea ice – cyclone coupled system.

CICE-POP and WRF models were used to carry out additional sensitivity analyses and investigating the role of independent sea ice – cyclone feedback mechanisms while only unperturbed simulations were used in HIRHAM-NAOSIM research study because the model data for that study was provided by Alfred Wegener Research Institute and not generated internally in the Arctic Research Supercomputing Center as was the case with CICE-POP and WRF models.

Table 1.1: Utilized weather and climate models

| | WRF Weather Research and Forecasting Model | HIRHAM-NAOSIM | CICE-POP Community Earth System Model |
|---|---|---|---|
| Model | National Center for Atmospheric Research (NCAR) | Alfred Wegener Institute for Polar and Marine Research (AWI) | National Center for Atmospheric Research (NCAR) |
| Scale | Regional | Regional | Global |
| Coupling | Stand-alone | Fully coupled | Two way coupled |
| Component | Atmosphere | Atmosphere – Ocean – Sea ice | Ocean – Sea ice |
| Resolution | 10 km | Spatially variable | Spatially variable |
| Time Frame | Case study | Climatology | Case studies |
| Objective | Investigate impacts of sea ice reduction on storm dynamics | Investigate impacts of Arctic cyclones on sea ice and ocean | Investigate impacts of Arctic cyclones on sea ice |

Impacts of sea ice and ocean on storms were investigated based on a case study of a cyclone event using the WRF model, while the impacts of storms on sea ice were studied using both coupled ice-ocean simulations of the case studies (CICE-POP simulations) and climatology (HIRHAM-NAOSIM simulations).

### 1.7 Thesis Structure

The structure of the thesis is as follows: Chapter 2 discusses the climatological impacts of Arctic storms on sea ice in summer, whereas chapter 3 describes the impacts of Arctic storms based on two case studies. Chapter 4 examines the impact of recent sea ice decline and ocean warming on Arctic storm dynamics. Research discussion and conclusions are given in chapter 5.

# Chapter 2 Climatology of Arctic Cyclones and Impacts on Sea Ice: Results from Regional Fully Coupled Model Hindcast Simulations

## 2.1 Introduction

Along with the amplified surface temperature increase over the Arctic, one prominent phenomenon in atmospheric circulation changes is a generally poleward shift of storm tracks and intensifying Arctic storm activities [*Zhang et al.,* 2004; *Sepp and Jaagus,* 2011]. Concurrently with observed atmospheric changes, sea ice cover and thickness has dramatically decreased in the last decades [*Kwok and Rothrock* 2009; *Stroeve et al.,* 2011]. The atmospheric impact upon underlying sea ice can become more severe as the reduction and thinning of Arctic sea ice continues to result in sea ice that is more susceptible to atmospheric and oceanographic changes. In particular, a number of studies reveal that the large-scale atmospheric circulation (e.g., associated with the North Atlantic Oscillation) has a strong impact on sea ice cover [e.g., *Liu and Curry,* 2004; *Ukita et al.,* 2007; *Strong and Magnusdottir,* 2011]. Analyzing the Arctic regional sea ice - ocean model output, *Zhang et al.* [2003] indicated that the large-scale atmospheric circulation is the driver of many of the changes manifested in the recent observations such as reductions of Arctic sea ice area and volume. Further, cyclones play an important role in the formation and destruction of sea ice. Thermodynamically, storms provide heat and moisture advection from lower latitudes to the Arctic and modify the surface radiation balance by changed cloud conditions. Dynamically, wind stress associated with storms can break open the ice cover such that cracks, leads and polynyas can form and open water affects the surface energy balance [*Wendler et al.,* 2013]. The influence of cyclones on sea ice has been discussed in studies based on both observations and models [e.g., *Zhang et al.,* 2010; *Mesquita et al.,* 2011; *Kriegsmann and Brümmer,* 2014]. The passage of storms over Arctic sea ice resulted in increased wind [*Zhang et al.,* 2013] and wave forcing on sea ice [*Asplin et al.,* 2012] as well as modification of freeze-melt cycles [*Bader et al.,* 2011].

Regional climate models are valuable tools to investigate such small scale coupled atmosphere-ice-ocean phenomena at high spatial and temporal resolutions. Additionally, the given 'ideal' lateral boundary forcing from reanalysis data provides the opportunity to study the effects of cyclones on sea ice in a 'controlled' environment. Previous investigations with the Arctic coupled atmosphere-sea ice – ocean model HIRHAM-NAOSIM showed that this model can reproduce the present-day Arctic atmospheric and sea ice conditions as compared to observations [*Dorn et al.,* 2009, 2012] and, it can be used to describe atmospheric feedbacks to sea ice anomalies associated with heat and moisture flux anomalies, modified baroclinicity and cyclone activity [*Rinke et al.,* 2013].

In this thesis, we evaluated the HIRHAM-NAOSIM simulated Arctic summer cyclone (i.e. storm) climatology and assess the average impact of intense storms on the underlying sea ice and ocean by analyzing the model output from 61-year-long (1948-2008) ensemble runs performed in Alfred Wegener Institute. [*Dorn et al.,* 2009] The analysis of sea ice-ocean-storm interaction was concentrated on sea ice melting season which was defined as July 1 – September 15 period. The focus on the summer months is two-fold: one of them is the seasonality of cyclone activity in the Arctic (summer is the most synoptically active period over the central Arctic Ocean [*Serreze and Barrett,* 2008]) and the other one, is the high susceptibility of sea ice to changes in atmospheric forcing. In particular, it was discussed if the model could reproduce the following known effects of intense storms on sea ice: reduction of sea ice concentration and thickness, modified surface energy fluxes, and changes in ice drift (i.e., increased divergence).

The structure of this chapter is as follows. Data and methods will be presented in Section 2.2, followed by documentation of the modeled storm climatology for various Arctic sectors (Section 2.3.1.) The influences of storms on sea ice and ocean conditions are discussed in Section 2.3.2. Section 2.3 presents the results and discussions.

## 2.2 Data and Methods

### 2.2.1 Model data

The employed data were from the regional coupled climate model HIRHAM-NAOSIM, which consists of the regional atmospheric model HIRHAM [*Dethloff et al.,* 1996] and the high-resolution version of the North Atlantic/Arctic Ocean sea ice model NAOSIM [*Karcher et al.,* 2003; *Kauker et al.,* 2003]. A detailed model description was given by *Dorn et al.* [2009].

The model generally well reproduces the observed summer sea ice variability over the last 6 decades, although with a less steep decline of sea ice extent over the last decade than observed, which is attributed to the summer atmospheric circulation and the sea ice volume at the beginning of the melting period in spring [*Dorn et al.,* 2012]. Atmosphere - sea ice interactions were realistically simulated, whereby strong regionally dependent feedback patterns can be imprinted [*Rinke et al.,* 2013].

The model was configured to cover the entire Arctic north of about 60°N at a horizontal grid increment of 0.5° (~ 50 km) for the atmosphere (HIRHAM) and of 0.25° (~25 km) for the ocean (NAOSIM).

A hindcast simulation over 1948-2008 with six ensemble members was carried out using the NCEP-NCAR reanalysis data as atmospheric lateral boundary conditions [*Kalnay et al.* 1996]. All ensemble members were started on 1 January 1948 and run through 31 December 2008 [*Dorn et al.* 2012]. The ensemble runs performed by *Dorn et al.* [2012] only differ in their initial ocean and sea ice fields, which were taken from different years of a preceding coupled spin-up run. The model ensemble simulations that was used in this study have been extensively described in *Dorn et al.* [2012].

### 2.2.2 Cyclone identification algorithm

To document the simulated climatology, variability, and changes of Arctic storm activities, a storm identification and tracking algorithm [*Zhang et al.,* 2004] was applied to daily sea level pressure (SLP) outputs. The principle of this algorithm is the identification of a low SLP center, which has a minimum SLP gradient of at least 0.15 hPa per 100 km with surrounding grid points and can survive for more than 12 hours. More details about this algorithm and its application with respect to Arctic storm track variability and changes can be found in *Zhang et al.* [2004].

As defined, the Arctic region was considered as poleward of 60°N. Considering the distinct geographical and climatological features as well as outstanding climatological storm activity near the ice-free Atlantic and Pacific Oceans, we divided the Arctic Ocean domain into eight subregions in this study: Barents-Norwegian Seas, Greenland Sea, Kara Sea, Laptev Sea, East-Siberian Sea, Chukchi Sea, Beaufort Sea, and Central Arctic (Fig. 2.1).

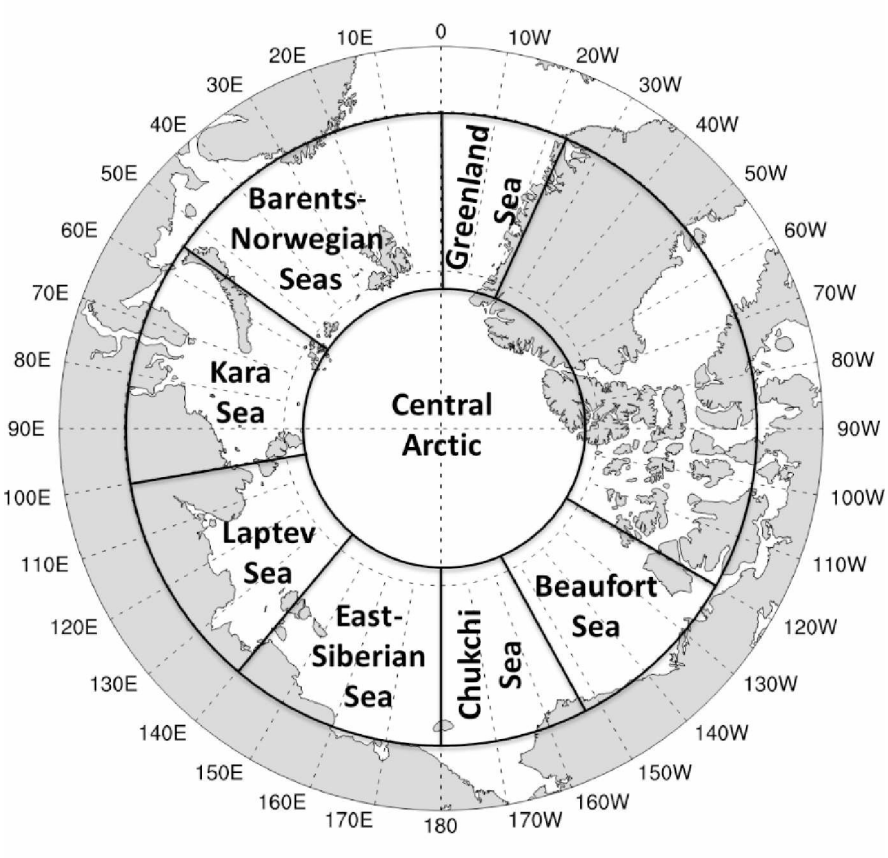


Figure 2.1: Defined regions of Arctic Ocean to discuss the storm activity: Barents/Norwegian Seas (BN), Greenland Sea (GS), Kara Sea (KS), Laptev Sea (LS), East-Siberian Sea (ESS), Chukchi Sea (CS), Beaufort Sea (BS), and Central Arctic (CA).

We analyzed two parameters to characterize the storm activity: storm count, and storm intensity. The sum of cyclone centers in each subregion in all time steps is denoted by a cyclone center count. The cyclone center count was found based on a composited map into 3.0 by 3.0 degree grid cells and represents a depiction of the Arctic cyclone activity. We analyzed overall storm count accounting for all storms in the domains and intense storm count comprised of only intense storms with central SLP less than 990 hPa. The other measure of storm activity that we investigated in the present study is the storm intensity, which we calculated based on the method described in *Zhang et al.* [2004]. Storm intensity is defined by the difference between the central SLP of the storm and the average monthly mean SLP at corresponding grid points. Therefore, positive values of storm intensity denote a positive departure of the central SLP of a storm from the climatological mean SLP at this grid point.

Considering that the number of Arctic storms climatologically reaches its maximum during summer [*Zhang et al.*, 2004; *Serreze and Barrett,* 2008], and the largest variability and decrease, as well as minimum value, of sea ice extent occur in summer, our analysis focused on the period from 1 July - 15 September of each year during the model simulation 61-year time period 1948-2008. The cyclone identification algorithm was applied to the daily SLP data from all six individual HIRHAM-NAOSIM ensemble members and from NCEP-NCAR reanalysis for late summer/early fall (JAS) 1948-2008.

### 2.2.3 Composite Analysis

The purpose of the composite analysis was to test the hypothesis that deeper and more intense storms produce a robust response of sea ice and ocean conditions. For this, composites of sea ice and ocean variables for identified low and high intense storm count cases were calculated and composite differences for "high minus low intense storms" are discussed. More concretely, we conducted the composite analysis based on the count of intense storms (central SLP < 990 hPa) over each of the subregions. The criterion for the composite analysis was based on exceeding the 1.5 standard deviation ($\sigma$) of intense storm count. Low intense storm cases were selected when the intense storm count was less than $-1.5\sigma$ whereas events of high intense storms were obtained when the intense storm count exceeded $+1.5\sigma$. We used the ensemble mean to calculate the composites (4697 low and 61 high intense storm cases within the 61 years for the Atlantic side of the Arctic and 4665 low and 23 high intense storm cases within the 61 years for the Pacific side of the Arctic) because of the low across-ensemble differences (Fig. 2.2). A Student's t-test was applied to assess the significance of the composite differences at the 95% confidence level.

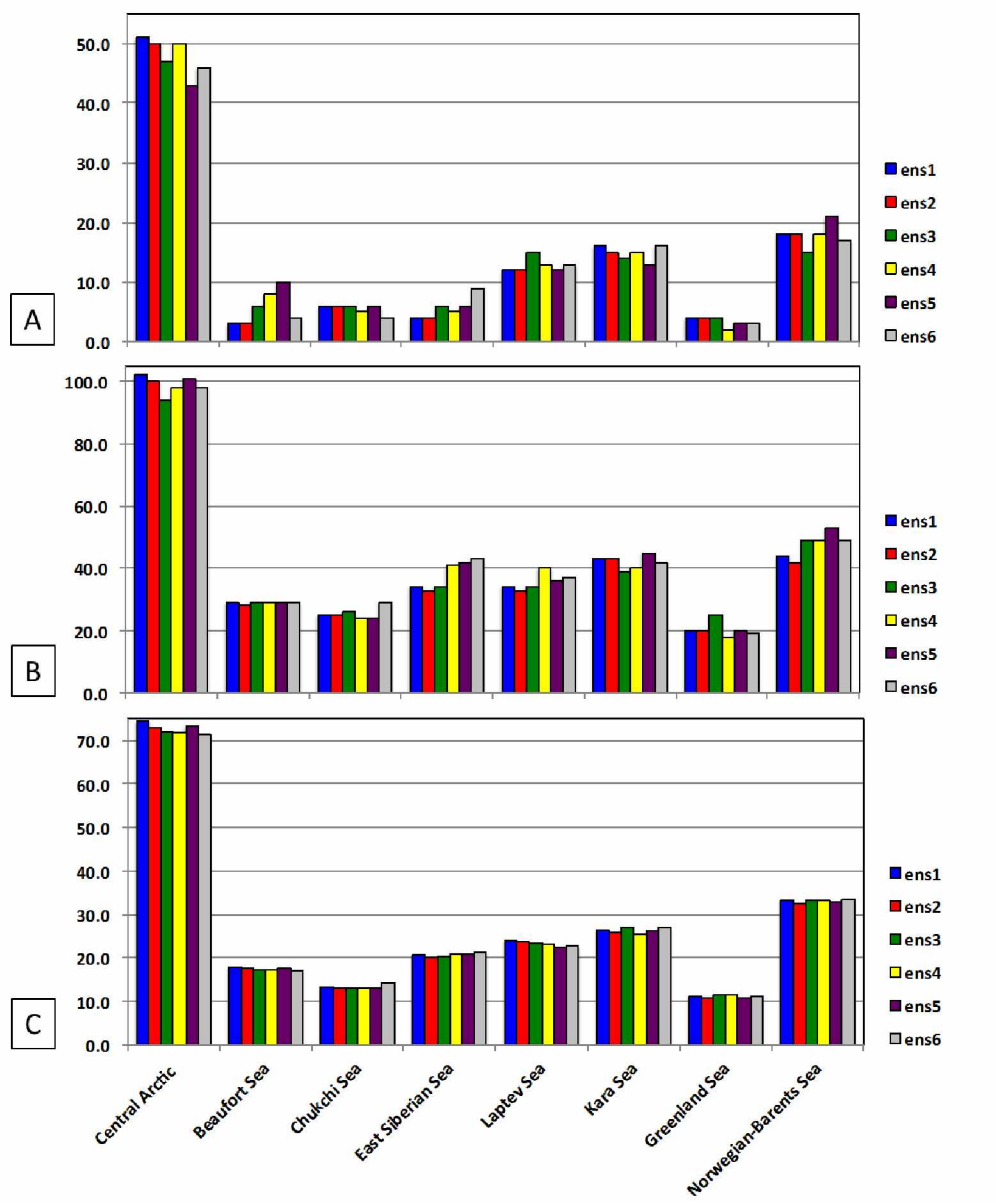


Figure 2.2: Summer storm count in HIRHAM various ensemble experiments (Unit: [storms per subregion]): maximum storm count in 61-year period of model integration (A), minimum storm count in 61-year period of model integration (B), average storm count in 61-year period of model integration (C).

For this composite analysis, we further partitioned the Arctic Ocean domain into two primary source regions: The Pacific side of the Arctic (storms originating over the Pacific Ocean) and the Atlantic side of Arctic Ocean (storms originating over the Atlantic Ocean). Both of these regions are characterized by frequent storm tracks associated with northeastward moving currents of warm ocean water – the Kuroshio Current and the Gulf Stream, respectively. The Pacific side of the Arctic covers the East Siberian,

Chukchi and Beaufort Seas while the Atlantic side of the Arctic Ocean encompasses the Greenland, Barents/Norwegian and Kara Seas. Both the Atlantic and the Pacific sides of the Arctic span the region from 60°N to 90°N and cover 60°W to 80°E and 140°E to 140°W, respectively.

## 2.3 Results and Discussion

### 2.3.1 Arctic Storm Analysis

#### 2.3.1.1 Regional and Temporal Variability of Storm Activity

Cyclone activity in the Arctic experiences substantial temporal and spatial variability. To evaluate the simulated cyclone activity climatology over different Arctic subregions, we analyzed the regional distribution and time series of storm count and intensity (Fig. 2.3-2.4).

The storm count is lower in NCEP than in HIRHAM-NAOSIM which is a result of lower resolution and inability to capture small scale low pressure systems that are resolved in HIRHAM-NAOSIM. The counts in NCEP and HIRHAM-NAOSIM are well-correlated. The intensity of storms in HIRHAM-NAOSIM is higher than in NCEP reanalysis data which is also a result of a higher model resolution in HIRHAM-NAOSIM.

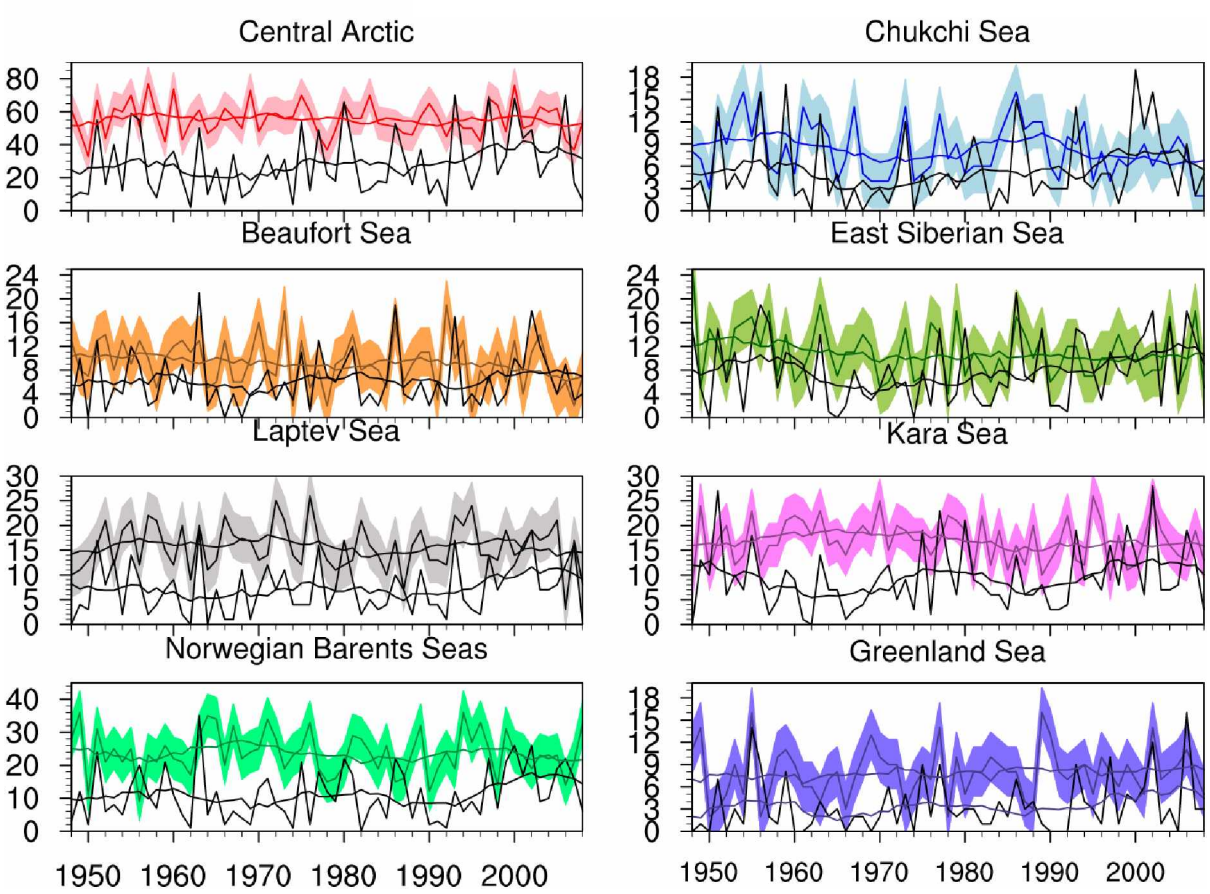


Figure 2.3: HIRHAM-simulated ensemble mean (colored lines) and NCEP-NCAR (black lines) storm counts in JAS for 1948-2008 (Unit: [storms per grid cell]). Smooth lines indicate 11-year running averages. The count is the accumulating number of storms occurring over each subregion based on the daily data. The across-ensemble standard deviation of the storm count is shown as shaded area.

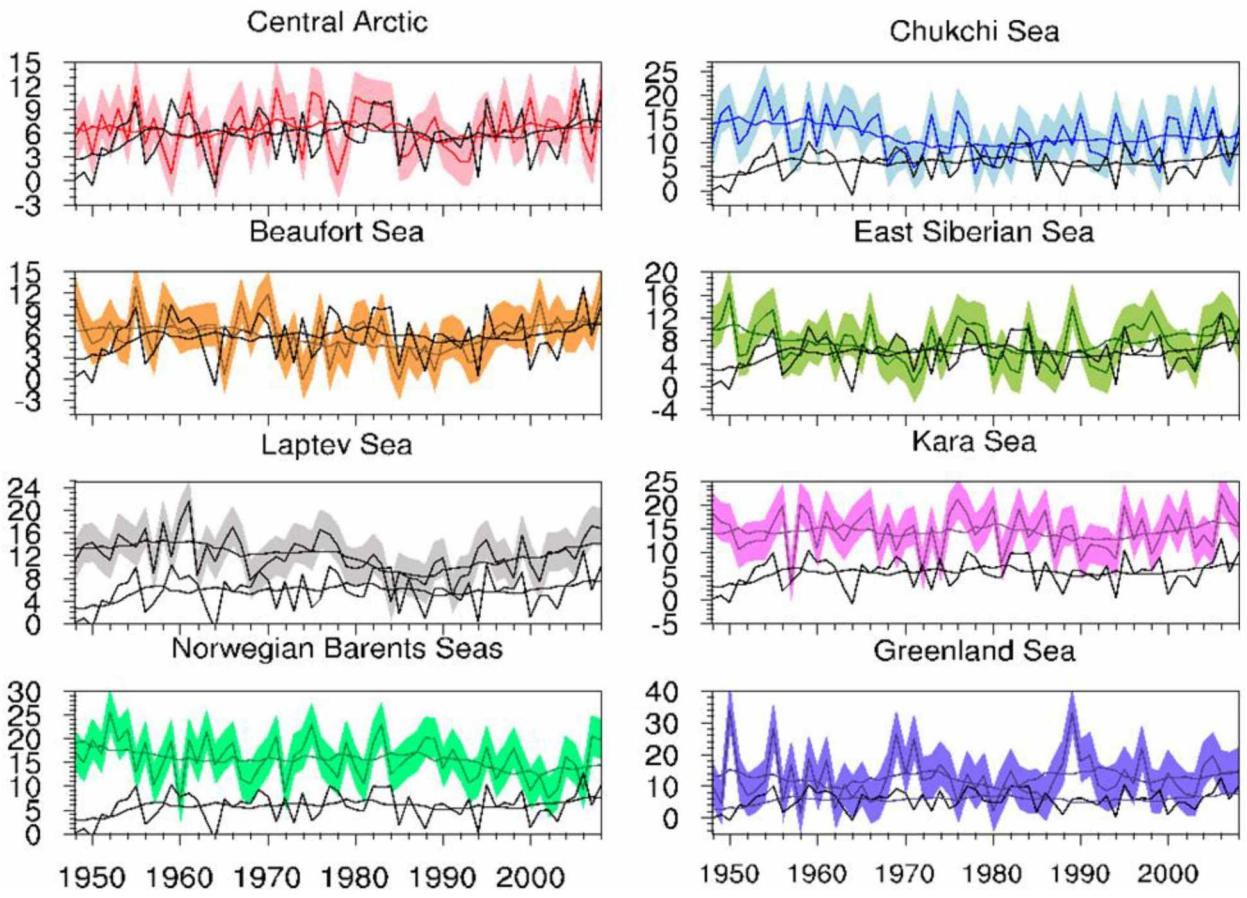


Figure 2.4: HIRHAM-simulated ensemble mean (colored lines) and NCEP-NCAR (black lines) storm intensity in JAS for 1948-2008 (Unit: [hPa]). Smooth lines indicate 11-year running averages. The count is the accumulating number of storms occurring over each subregion based on the daily data. The across-ensemble standard deviation of the storm count is shown as shaded area.

The ensemble mean storm count in the Arctic and pan-Arctic indicates the presence of several maxima of cyclone activity. The largest storm density in summer was observed around Iceland (over 300 storms) and southwestern Greenland (200-230 storms) attributed to a prominent North Atlantic storm track. On the Pacific side of the Arctic, the maxima of cyclone activity were observed around Alaska (230-260 storms), and Chukotka (250-300 storms) corresponding to the Pacific storm track (Fig. 2.5). Comparison with NCEP-NCAR data showed that the reanalysis had a lower number of storms than HIRHAM-NAOSIM, but the areas of maximum cyclone counts (around Greenland, Alaska, Far East of Russia) were co-located with those of HIRHAM-NAOSIM. Furthermore, the comparison demonstrated that the distribution and

magnitude of storm count was in an agreement with previous studies using the NCEP-NCAR reanalysis data [*Zhang et al.* 2004, *Serreze and Barrett,* 2008].

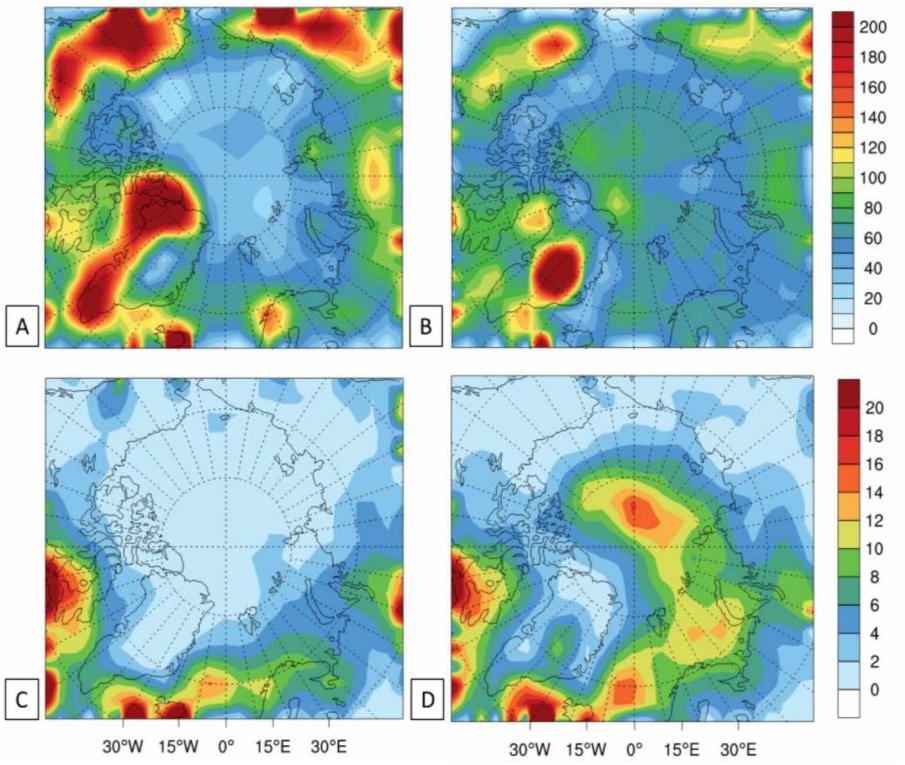


Figure 2.5: Ensemble mean storm counts (Unit: [number of storms per grid cell per 60 years (1948-2008)]). The count is the accumulated number of storms occurring over each region based on the daily data: all storms HIRHAM-NAOSIM (A), all storms NCEP-NCAR (B), deep storms (SLP < 990 hPa) HIRHAM-NAOSIM (C), deep storms (SLP <990 hPa) NCEP-NCAR (D).

There was a comparable spatial pattern of cyclone activity in the Arctic between the HIRHAM simulations and European Centre for Medium-Range Weather Forecasting reanalysis (ERA-40) with a maximum over the central Arctic Ocean [*Akperov et al.* 2014]. Specific values of Arctic storminess derived from NCEP-NCAR and HIRHAM-NAOSIM are given in Table 2.1. The average storm count in HIRHAM was approximately twice as high as in the NCEP-NCAR reanalysis for the Central Arctic (55 vs. 28 storms), Laptev Sea (16 vs. 7 storms), Kara Sea (17 vs. 9 storms), Greenland (8 vs. 3 storms) and Norwegian-Barents Sea sector (24 vs. 11 storms) (Table 2.1). The notable underestimation of storm counts over the Arctic in NCEP-NCAR reanalysis compared to HIRHAM-NAOSIM was likely to be caused by the higher spatial

model resolution allowing representation of small scale low pressure systems. This finding is in agreement with *Akperov et al.* [2014] who also found that the storm count in HIRHAM's is twice as large as in ERA-40 reanalysis data.

Table 2.1: Storm counts (accumulated number of storms over each region) for JAS 1948-2008. Max, Min indicate the maximum, minimum counts in the most extreme year.

| | | Central Arctic | Beaufort Sea | Chukchi Sea | East Siberian Sea | Laptev Sea | Kara Sea | Greenland Sea | Norwegian-Barents Sea | All Arctic |
|---|---|---|---|---|---|---|---|---|---|---|
| | | | | | | | | | | |
| HIRHAM | Max | 77 | 19 | 16 | 26 | 26 | 26 | 16 | 36 | 191 |
| | Min | 33 | 1 | 2 | 4 | 3 | 8 | 2 | 9 | 95 |
| | Ave | 55 | 9 | 8 | 11 | 16 | 17 | 8 | 24 | 148 |
| | | | | | | | | | | |
| NCEP-NCAR | Max | 70 | 21 | 19 | 21 | 19 | 28 | 16 | 35 | 186 |
| | Min | 2 | 0 | 0 | 0 | 0 | 0 | 0 | 0 | 10 |
| | Ave | 28 | 6 | 5 | 8 | 7 | 9 | 3 | 11 | 79 |

In various Arctic subregions, the cyclone activity experienced significant year-to-year fluctuations, both in terms of storm count and intensity shown in Fig. 2.3 and Fig. 2.4, respectively. The simulated storm count time series showed the maximum high storm count in summer over the Central Arctic (on average about 55 storms per summer, maximum of 77 storms in years of strong cyclone activity and about 33 storms in years of lowest cyclone activity; Fig.2.3). While the entire number of storms over the Central Arctic is high, their intensity is relatively low (Fig. 2.4). Storms normally move into the Central Arctic from the lower latitudes than 60°N. As the storms move in the Central Arctic area from the Atlantic, Pacific Ocean and Eurasia and due to the large distances traveled by them, their intensity is weak.

It should be noted that in the simulations, a large number of storms with high intensity was found in the Chukchi Sea with storm counts averaging about nine storms per summer with intensity up to 15 hPa. Other areas of high intensity storm count include the Norwegian, Barents and Kara Seas where frequent cyclone activity is associated with the North Atlantic storm track.

Similar to the storm count, the storm intensity experienced a large interannual variability of different magnitude for various Arctic subregions (Fig. 2.4). The comparison of HIRHAM-NAOSIM-simulated and NCEP-NCAR reanalysis derived cyclone intensity showed relatively similar temporal change. The smallest differences between the HIRHAM-NAOSIM and NCEP-NCAR cyclone intensities

were observed over the Central Arctic, Beaufort and East Siberian Seas. Storm intensity over the Chukchi, Laptev, Kara, Norwegian-Barents and Greenland Seas was greater in HIRHAM-NAOSIM than in the reanalysis, which was likely a result of higher resolution of the model.

The analysis of storm intensity over different Arctic regions demonstrated large interannual variability of cyclone intensity over seasonally ice-free areas of the Greenland Sea and the Barents-Norwegian Sea ranging from 0 hPa to 40 hPa, 5 hPa to 30 hPa in the Pacific side of the Arctic, respectively (Fig. 2.4). In contrast, the central Arctic that remained ice-covered in JAS, experienced lower storm intensity and less pronounced interannual temporal fluctuations of intensity than the aforementioned waters.

#### 2.3.1.2 Composites for High and Low Intense Storms

The major direct impact of intense storms events was displayed in associated SLP anomaly patterns. Composites of high intense storm cases over the Atlantic side of the Arctic showed a deep SLP center of about 997 hPa and occurred over the Kara Sea, extending to the Barents Sea, northern Greenland Sea and eastward to the Laptev Sea (Fig. 2.6A). The SLP difference between high and low intense storm cases was characterized by a statistically significant (95% confidence based on Student's t-test) negative anomaly of -13 hPa over the Kara Sea (Fig. 2.6C). Similarly, a deep SLP center of ca. 989 hPa was found over the central Chukchi Sea, covering western Beaufort Sea and eastern part of the East-Siberian Sea (Fig. 2.6D). The composite difference over the Pacific side of the Arctic showed a statistically significant at the 95% confidence level negative SLP anomaly of -16 hPa (Fig. 2.6D).

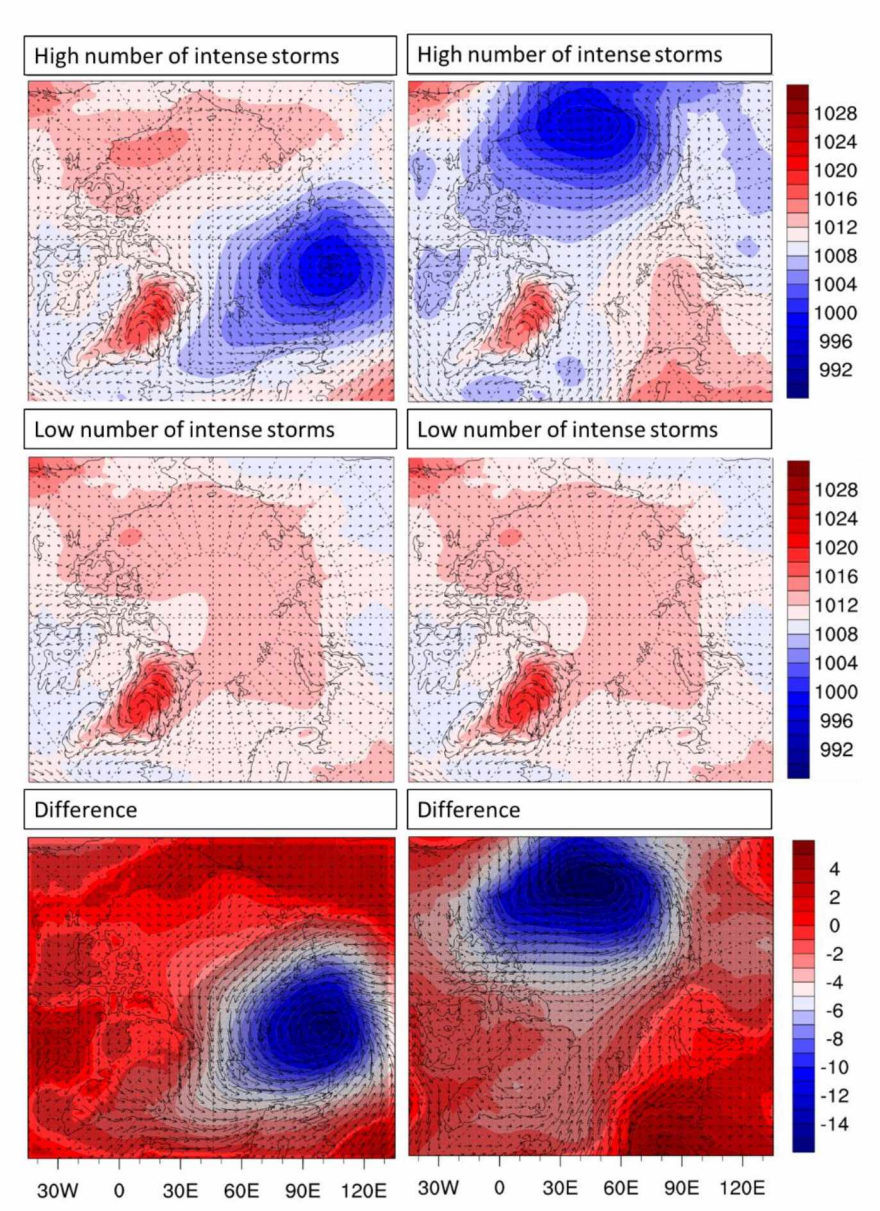


Figure 2.6: Composite differences of sea level pressure (Unit: [hPa]) over the Atlantic (left) and the Pacific (right) sides of the Arctic Ocean from a composite analysis of high and low intense storms during JAS 1948-2008. Differences between high and low intense storms with greater than 95% confidence are dotted.

### 2.3.2 Impact on Sea Ice and Ocean

We investigated the climatological response of sea ice concentration (SIC), thickness, and motion as well as ocean mixed-layer temperature (defined here as the uppermost ocean model layer of 0-20 m) to intense storms over the Atlantic and Pacific sides of the Arctic Ocean.

As illustrated by the composite differences of SIC in events of intense storms sea ice areal coverage was reduced. Persisting negative SIC anomalies in the NE part of the Barents and northern part of the Kara Seas indicate the areas predominantly affected by migration of Atlantic storms (Fig. 2.7A). Areas with negative SIC anomalies on the Atlantic side of the Arctic outlined marginal ice zones where ice is most frequently and strongly subject to changes in oceanic and atmospheric forcing. The most extensive negative SIC anomaly occurred in the SE Kara Sea, expanding from the eastern coast of Novaya Zemlya eastward to Yamal Peninsula. A coastal polynya to the east of Novaya Zemlya was a result of intense cyclone activity. Positive anomalies of SIC in the central Barents Sea were driven by cyclonic dynamic forcing where increased winds exerted on sea ice promoted NE drift in the area. The Svalbard Islands blocked sea ice movement to the NE with the drift that resulted in piling up of ice and consequently positive SIC anomalies. Another positive SIC anomaly found in the Pechora Sea was also the result of dynamic forcing exerted on sea ice due to strong winds.

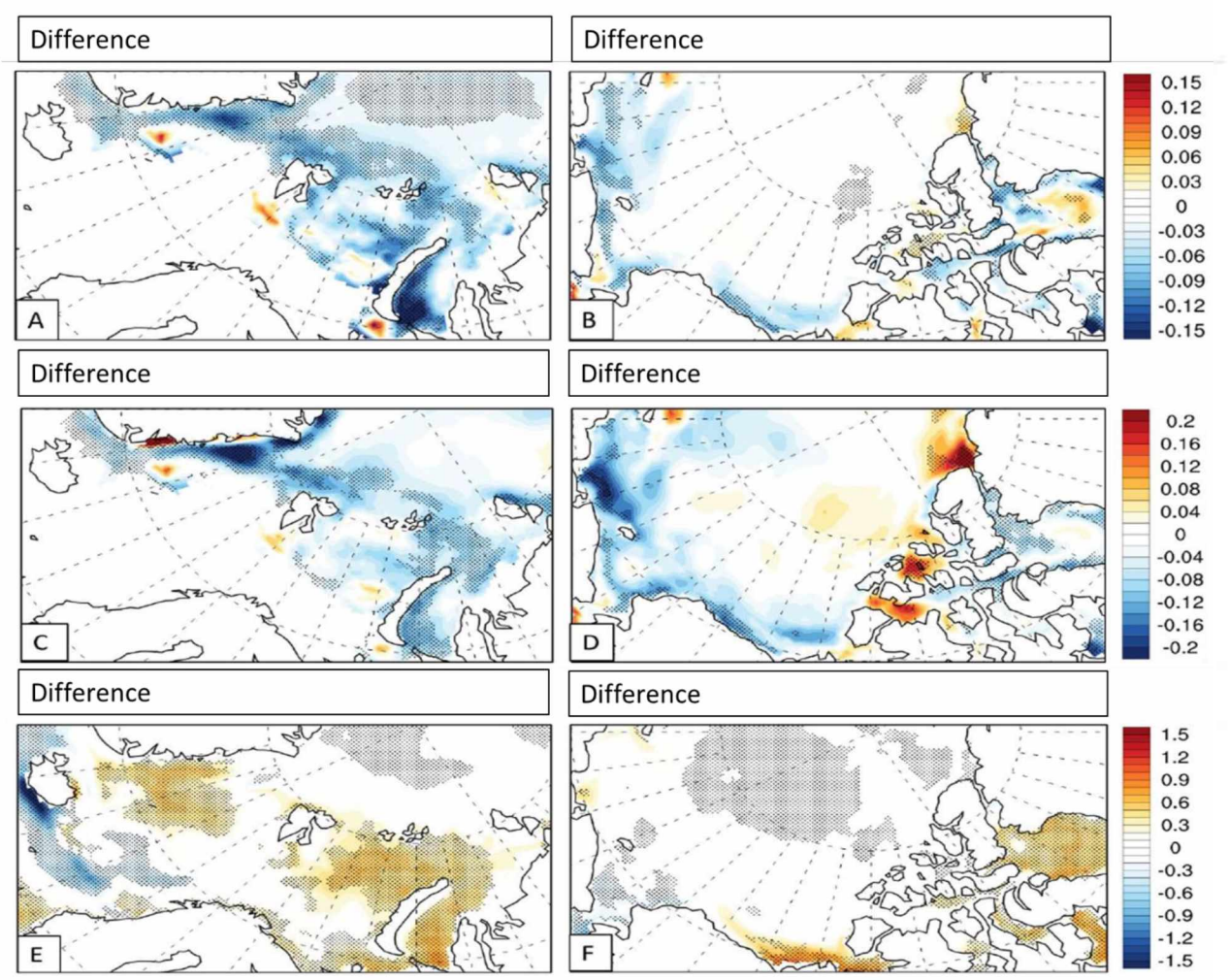


Figure 2.7: Composite differences between sea ice concentration (Unit: [fraction of 1]) for the Atlantic (A) and for the Pacific (B) side of the Arctic, sea ice thickness (Unit: [m]) for the Atlantic (C) and for the Pacific (D) side of the Arctic, surface sea temperature (Unit: [°C]) for the Atlantic (E) and for the Pacific (F) side of the Arctic of the composite analyses of high minus low intense storms during JAS 1948-2008. Differences between high and low intense storms with greater than 95% significance are dotted.

In events of intense storms on the Pacific side of the Arctic, negative anomalies of SIC occurred predominantly along the coasts where sea ice is most susceptible to cyclonic-driven forcing (Fig. 2.7B). As a result of cyclonic forcing, SIC in the Chukchi, Beaufort and East-Siberian Seas was reduced by approximately 9-12%. Coincidentally, SIC was increasing in events of intense storms south of the Bering Sea by approximately 12-15%.

Further, corresponding to intensified cyclone activity during the high number of intense storms, the sea ice in the costal and marginal zones showed vast ice thickness reduction co-locating areas of shrinking ice extent (Fig. 2.7C, D). Due to cyclone activity on the Atlantic side of the Arctic, sea ice was 10-12 cm thinner while along the NE Greenland the sea ice became 15-20 cm thinner than in the low intensity case as compared to high intensity case (Fig. 2.7C). Along the coasts of the Chukchi and Beaufort Seas, the thickness of sea ice was reduced by approximately 10-15 cm. The most dramatic thickness changes occurred in the East-Siberian Sea with below 20 cm difference compared to the low intense storm composite (Fig. 2.7D).

Negative sea ice extent and volume anomalies enhanced heat uptake in the ocean leading to positive mixed-layer ocean temperature anomalies. On the Atlantic side of the Arctic, a pronounced positive SST anomaly (0.5-1°C) extended from the NE Barents Sea into the SW Kara Sea (Fig. 2.7E). Similarly, a positive but less extensive SST anomaly was observed in the Beaufort Sea corresponding to decreasing of SIC and thickness as a result of cyclone activity (Fig. 2.7F).

In order to further explain the aforementioned sea ice mass balance changes occurring during the high number of intense storms, we presented a composite analysis of sea ice drift speed and direction (Fig. 2.8). In the composite with high number of intense storms, sea ice in the central Arctic and along NE Greenland was dominated by the southerly drift. The ice is therefore transported from the NE Kara Sea merging into the main Transpolar Drift Stream through the Fram Strait into the North Atlantic (Fig. 2.8A). The ice in Transpolar Drift Stream moved significantly faster in the intense storm composite than in the composite with no intense storms 0.1-0.14 m/s vs. 0.06-0.1 m/s, respectively. There is noticeable lack of drift change in the SW Kara Sea in intense storm composite compared to no intense storms composite. Negative SIC anomalies east of Novaya Zemlya and near the Yamal peninsula, where polynyas are present, are not related to prevailing ice drift. As illustrated by the composite difference, sea ice drift in the SW Kara Sea tended to move slower during intense than non-intense storms, which is in association with the discussed location of a strong cyclonic circulation anomaly. An amplified drift of sea ice on the Pacific side of the Arctic was discovered along the coasts of the Chukchi Sea and West Beaufort Sea (Fig. 2.8D). In the intense storm composite, the Beaufort Gyre was weakened and displaced towards the Canadian Arctic Archipelago. Corresponding with anticyclonic circulation, it was moving westward from the Beaufort Sea towards Eurasia. Once the ice reached the Chukchi Sea, the pattern of ice movement becomes cyclonic. Transport across the northern Chukchi Sea bifurcated the ice flow with one branch of ice drift moving into the East-Siberian Sea and another directing towards the Laptev Sea. In case of the Pacific side of the Arctic, ice drift composite differences were mostly positive, ranging from 0.02-0.04 m/s in the East-Siberian and Beaufort Seas to 0.04-0.06 m/s in the central Chukchi Sea (Fig. 2.8).

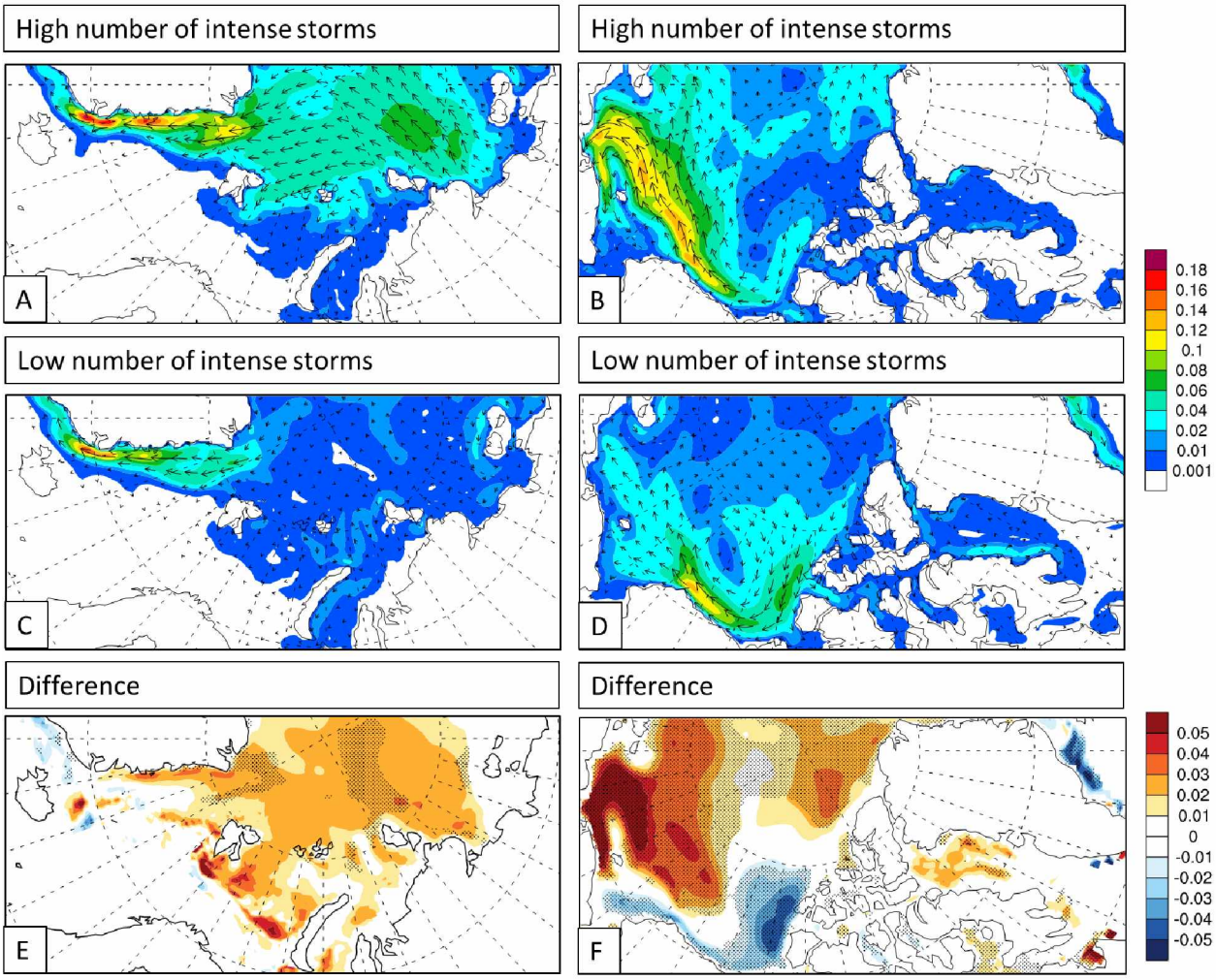


Figure 2.8: Composite differences of sea ice motion (Unit: [m $s^{-1}$]) over the Atlantic side Arctic Ocean (A) and the Pacific side Arctic Ocean (B) from a composite analysis of high and low intense storms during JAS 1948-2008. Ice drift speed is colored shaded. Differences between high and low intense storms with significance greater than 95% confidence are dotted.

As discussed above, thermodynamic (in this case melting) and dynamic forcings during intense storms resulted in sea ice reduction that in turn, affected the amount of heat flux released from the surface into the atmosphere. To address the question of the quantity and spatial distribution of surface heat released into the Arctic atmosphere in summer during storms, we analyzed the composites of the net surface heat flux (Fig. 2.9). The composite analysis was continually extended to the net sea ice heat fluxes, calculated as the difference between the net atmospheric surface heat fluxes and the oceanic heat flux of a model grid

cell. The difference represents the net contribution from all radiative, sensible, and latent heat fluxes from the atmosphere and the turbulent heat flux from ocean, indicating the total thermodynamic contribution to sea ice changes (melt and growth). In this paper, we use the sign convention that negative (positive) net heat fluxes point downward (upward), which we can interpret as snow/ice melt (sea ice growth).

As indicated by the composite analysis, sea ice net heat budgets were negative on the Atlantic side (except for the Central Arctic Ocean) for high as well as low numbers of intense storms ranging from -3 to -10 $W/m^2$ (Fig. 2.9A) and from -5 to -30 $W/m^2$ (Fig. 2.9C), respectively. Negative net heat flux indicated the surface takes up heat from the atmosphere thereby promoting sea ice melt. In time periods with high intensity storms, diminished ice concentration in the Barents and Kara Sea areas exposed areas of open water that increased the upward turbulent heat flux due to storm induced ocean mixing. The difference between composites with high and low numbers of intense storms was positive over the Barents and Kara Seas (Fig. 2.9E). This positive difference was likely caused by the reduced downward solar radiation as a result of increased cloudiness during cyclones.

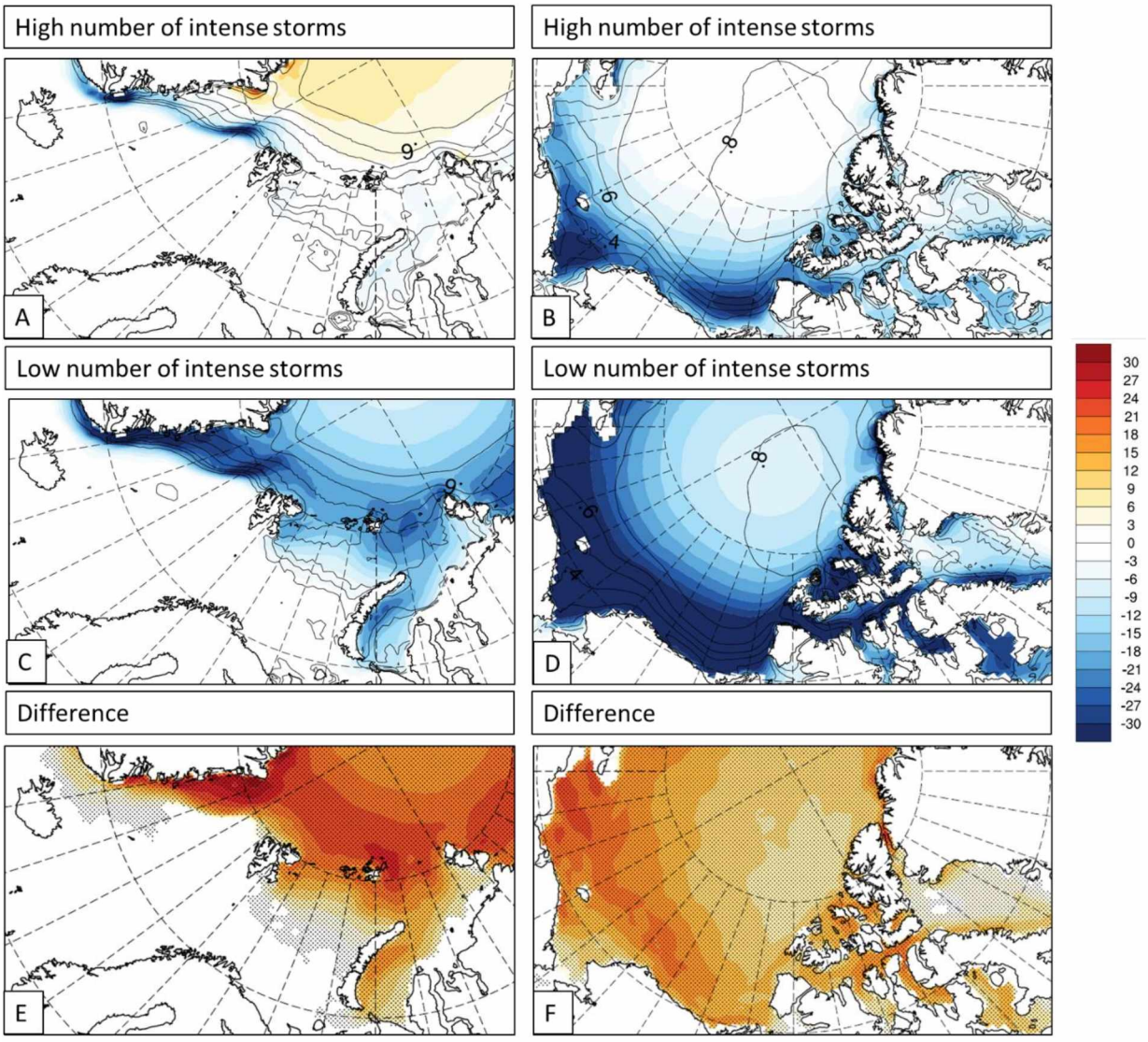


Figure 2.9: Composite differences of surface net heat flux over (Unit: [W $m^{-2}$]) Atlantic side Arctic Ocean (A) and the Pacific side Arctic Ocean (B) from a composite analysis of high and low intense storms during JAS 1948-2008. Positive fluxes point downward. Differences between high and low intense storms with significance at greater than 95% confidence are dotted.

A negative net heat flux was observed on the Pacific side of the Arctic (Fig. 2.9B). Areas of minimum net surface heat flux extended along the coast of the East-Siberian Sea into the southern Chukchi Sea and eastern Beaufort Sea. The net surface heat flux was more apparent in magnitude and spatial extent than on the Atlantic side. In low number of intense storm cases, net surface heat fluxes were approximately -30 to (-50) W/$m^2$ in the Chukchi Sea, East-Siberian and Beaufort Seas (Fig. 2.9D). The corresponding

areas in the high number of intense storm cases showed comparatively higher net surface heat fluxes: -5 to (-15) $W/m^2$ in the Chukchi Sea and -30 to (-40) $W/m^2$ in the East-Siberian and Beaufort Seas (Fig. 2.9B). Similar to the Atlantic side of the Arctic, the differences in net surface heat flux marked positive corresponded to a greater energy release from the surface into the atmosphere in high intense storm case than low intense storms as a result of cyclonic forcing generating sea ice openings. Overall, the difference of the low and high intense storm cases displayed pronounced positive anomalies of net surface heat flux co-locating the areas of largest ice reduction in the marginal ice zones of the Barents and Kara Seas on the Atlantic side (Fig. 2.9E) and along the coasts of Alaska and Chukotka peninsula on the Pacific side of the Arctic (Fig. 2.9F).

The composite analysis showed that there is a climatic (60 years) response of sea ice/ocean to intense summer cyclones. Arctic cyclones were found to result in increased SST and reduced SIC, reduced ice thickness and a reduction of net heat flux. While the composite analysis showed the general large-scale sea ice/ocean response to a combined number of cyclones in the Arctic, it did not show the individual physical mechanisms driving sea ice response to Arctic cyclones.

# Chapter 3 Processes Associated with Cyclone Impacts on Sea Ice: A Case Study Using Sea Ice-Ocean Model Simulations

## 3.1 Introduction

This chapter documents the findings of the sea ice response to two intense Arctic cyclones by utilizing the output of the global coupled climate model Community Earth System Model, version 1.0.4 (CESM 1.0.4) [*Collins at al.,* 2006]. The main objective of this research is to analyze the impact of dynamic vs. thermodynamic forcing by cyclones on sea ice. The hypothesis is that sea ice, ocean, and atmosphere interactions can be amplified during intense storms and this amplification may contribute to further climate change. In order to test this hypothesis, a case study approach was applied to two Arctic cyclones. The key objectives for this study are:

(i) to assess coupled ocean-sea ice model performance to simulate Arctic sea ice and ocean conditions and its applicability for climate research studies;

(ii) to investigate storm-induced dynamic and thermodynamic forcing on sea ice decay/growth processes;

(iii) to investigate storm-induced dynamic and thermodynamic forcing on sea ice energy balance.

Henceforth, the thermodynamic processes in this study include sea ice freezing and melting cycles that are caused by changes in the surface radiation balance and sensible and latent heat fluxes. Dynamic processes refer to sea ice deformation and drift that result from wind forcing, ocean, and internal ice stresses. Sea ice thermodynamic and dynamic growth/reduction processes are not independent in that sea ice dynamics changes may induce thermodynamic changes, and vice versa [e.g. *Thorndike et al.,* 1975]. The present study adopts a similar modeling approach involving the partitioning of cyclone forcing, which was introduced and applied by *Liptak and Strong* [2013], onto sea ice to partition dynamic and thermodynamic forcing components.

### 3.1.1 Dynamic Forcing of Arctic Cyclones on Sea Ice

Dynamic impacts of Arctic cyclones on sea ice constitute an important forcing factor affecting sea ice deformation and motion at various temporal and spatial scales [*Brummer et al.,* 2003; *Herman and Glowacki*, 2012]. Previous studies of interactive processes between ocean, atmosphere, and sea ice in the Arctic indicate that sea ice dynamics is dependent upon a variety of atmospheric variables: forces related to atmospheric circulation [e.g., the Arctic oscillation in *Kwok,* 2006; *Rampal et al.,* 2009; *Comiso,* 2012]

including geostrophic wind *[Thorndike and Colony*, 1982; *Serreze et al.,* 1989], and surface pressure gradient force [*Asplin et al.,* 2009; *Kwok et al.,* 2009]. It also depends on cyclone tracks, number (which can be expressed in counts), intensity [*Screen et al.,* 2011].

Previous studies pointed out that atmospheric circulation is a key factor, determining the Arctic sea ice drift and thickness pattern [e.g., *Deser et al.*, 2000; *Rigor et al.,* 2002; *Hu et al.,* 2002; *Rigor and Wallace,* 2004*; Rothrock and Zhang,* 2005; *Serreze and Francis,* 2006; *Ukita et al.,* 2007]. *Rigor et al.* [2002] as well as *Zhang et al.,* [2003] showed that the phase of the Arctic Oscillation (AO) is another factor that determines annual Arctic sea ice areal and volume distributions. *Zhang et al.* [2003] found reductions of Arctic sea ice area and volume by ~3% and ~9%, respectively, when the AO changes from the negative to the positive phase.

Large-scale synoptic events may determine the sea ice conditions on time scales of several weeks as a result of increased wind-driven advection of sea ice [*Barry and Maslanik*, 1989, *Brummer et al.,* 2003, *Zhang et al.,* 2010]. The Arctic cyclones may result in reversal of the predominant rotational pattern of sea ice from anticyclonic to cyclonic [*McLaren et al.,* 1987; *Serreze et al.,* 1989] as has been observed in the Beaufort Sea where under cyclonic conditions the rotation of the Beaufort Gyre changes from clockwise to counterclockwise [*LeDrew et al.,* 1991, *Asplin et al.,* 2009]. *Barry and Maslanik* [1989] showed that wind speed and divergence of the sea ice pack behind a low pressure system cause sea ice concentration to decrease. Strong winds tend to accelerate sea ice drift by breaking it up and decreasing its internal interaction [*Brümmer et al.,* 2003]. Using satellite imagery, *Holt and Martin* [2001] argued that the cyclone that developed over the Beaufort and Chukchi Seas in August 1992 reduced the size of sea ice floes and increased the open water area. *Brümmer et al.* [2008] showed that sea ice drift diverged along the track of the center of the March 2002 cyclone while it converged over the areas of cyclonic periphery. In summer, extensive open water fetch under strong winds due to migratory cyclones may generate large waves that, if intruded into the ice pack, may induce sea ice break up [*Asplin et al.,* 2012]. Based on the case study about the Arctic storm that occurred in September 2008, *Asplin et al.* [2012] found that the intrusion of strong waves caused sea ice fracturing as far as 250 km from the ice edge. Increased wind speed associated with Arctic cyclones may reveal openings in sea ice known as leads or polynyas [*Barry and Maslanik,* 1989]. Increased winds affecting sea ice motion intensify sea ice inertial fluctuations [*Brümmer et al.,* 2003*; Lammert et al.,* 2009]. In particular, *Brümmer et al.* [2003] demonstrated that inertial and tidal oscillations of sea ice in the Fram Strait were amplified during cyclonic events. Their finding was reinforced later through analysis of cyclonic cases that occurred in the northeast Greenland in March 2007 [*Lammert et al.,* 2009].

Sea ice preconditioning is another factor that affects the sea ice dynamic state on different timescales [*Rigor et al.,* 2002; *Drobot and Maslanik,* 2003; *Nghiem et al.,* 2006; *Lindsay et al.,* 2009].

Long-term preconditioning refers to increased sea ice susceptibility to oceanic and atmospheric forcing as a result of thinning and shrinking of sea ice coverage in the Arctic. Short-term preconditioning refers to sea ice susceptibility as a result of abrupt sea ice changes that can occur, for example, in the event of wind intensification during a cyclone. Mechanical break up and movement of sea ice will increase sea ice vulnerability to oceanographic and atmospheric abrupt changes associated with cyclones [*Parkinson and Comiso*, 2013].

### 3.1.2 Thermodynamic Impact of Arctic Storms on Sea Ice

The balance of oceanic and atmospheric energy, sea ice internal heat conduction, and storage of heat govern sea ice thermodynamic growth and melt. Ice growth or melt at the ice underside results from the difference between the heat conducted away from the water-ice boundary into the ice and the heat flux supplied from the ocean. Ice growth or melt at the ice top side results from the difference between the atmospheric incoming and outgoing radiation and turbulent heat fluxes. Sea ice thermodynamic state is dependent upon a number of cyclonic forcings including advection of warm/cold air masses [*Stroeve et al.,* 2008], ocean heat advection [*Polyakov et al.*, 2003, 2010; *Woodgate et al.,* 2006, 2010], changes in cloudiness [*Francis et al.,* 2005; *Schweiger et al.,* 2009, *Kay and Gettelman,* 2009], and alterations of the ice albedo feedback [*Perovich et al.,* 2007, 2008].

Sea ice thermodynamic characteristics are subject to changes in surface turbulent heat fluxes under cyclonic conditions. The impact of openings in the sea ice on heat and moisture content of the Arctic atmospheric boundary layer varies subject to the season [*Brummer et al.,* 2003]. In winter, sea ice leads cause turbulent heat release into the atmosphere. In summer, leads promote increased absorption of down-welling shortwave radiation in the ocean that results in a surplus of heat in the uppermost ocean layer. This radiative transfer of energy may have an impact on the sea ice melt/freeze cycle [*Perovich et al.,* 2008; *Kriegsmann and Brummer,* 2014]. Open water amplifies sea ice melt [*Brummer et al.,* 2003; *Perovich et al., 2008*; *Kriegsmann and Brummer,* 2014]. The direction of turbulent heat fluxes is subject to rapid changes, resulting from sea ice motion and formation of open water leads [*Dierer et al.,* 2005]. Exerted wind and wave forcing on sea ice results in a reduced ice floe size and an increased total ice floe perimeter [*Zhang et al.,* 2015]. An increase in the ice floe perimeter allows for efficient distribution of oceanic and atmospheric fluxes into sea ice and, therefore, causes intensified lateral melting [*Steele,* 1992; *Asplin et al.,* 2012]. Analysis of in-situ observations collected in the Arctic as a part of the SHEBA experiment showed that turbulent heat fluxes have larger daily variability as compared to radiation fluxes [*Persson et al.,* 2002].

The SHEBA experiment also showed that maxima of sensible and latent heat fluxes were recorded in events of Arctic cyclones.

The rapid summer sea ice decline observed over the recent decades resulted in open water that stores additional atmospheric heat and delays the freeze-up onset [*Screen and Simmonds,* 2010, *Blanchard-Wrigglesworth et al.,* 2011, *Overland et al.,* 2011]. This, ultimately, results in thinning of winter sea ice [*Blanchard-Wrigglesworth et al.,* 2011]. The reduction of sea ice extent and sea ice thickness explains why the strongest observed warming occurs in the marginal ice zones, with the strongest signature in fall and winter [*Screen and Simmonds,* 2010; *Overland et al.,* 2011].

The impact of Arctic cyclones on the stratigraphy of upper ocean layers has been a focus of many previous research studies [*Shimada et al.,* 2006; *Woodgate et al.,* 2006; *Steele et al.,* 2008; *Perovich et al.,* 2008; *Stroeve et al.,* 2011]. Sea ice reduction observed during and after Arctic cyclones was found to lead to an increase in the summer ocean mixed layer depth [*Stroeve et al.,* 2011], oceanic heat fluxes increase [*Shimada et al.,* 2006; *Woodgate et al.,* 2006; *Steele et al.,* 2008], and solar heating increase [*Perovich et al.,* 2008]. Associated with strong winds increased sea ice movement accelerates ocean mixing and heat exchange within the oceanic boundary layer, therefore, causing sea ice reduction due to enhanced basal melt [*Zhang et al.,* 2013].

Cloudiness, associated with cyclone activity, has been shown to intensify fluctuations of the sea ice energy balance components including short and longwave radiation fluxes, and latent and sensible turbulent fluxes, causing further changes within the sea ice thermodynamic structure [*Persson et al.,* 2002; *Kay and Gettelman*, 2009]. Based on SHEBA field experiment data, the total energy flux into the surface varies from -25 W/m$^2$ to +12 W/m$^2$ in winter and +37 W/m$^2$ to +129 W/m$^2$ in July. This large variability in total energy flux was attributed to day-to-day variability in radiation and turbulent heat fluxes. The total energy flux is positive in winter, during cloudy periods, when the difference between incoming and outgoing longwave radiation is near zero [*Persson et al.,* 1999].

### 3.1.3 Sea Ice Momentum and Mass Balance

Sea ice mass balance is determined by its growth and melt processes, transport and deformation, ultimately resulting in an increase or reduction of sea ice thickness and extent.

The mass balance of sea ice is governed by ice motion (momentum balance), accretion, sublimation, freezing and evaporation and melting (as resulting from surface energy balance), and the transport and redistribution of ice thickness (mass conservation) (Eq. 3.1).

$$m\frac{dU}{dT} = -mfk \times \vec{u} + \tau_a + \tau_w - mg_r\nabla Y + \nabla \cdot \sigma \quad (3.1)$$

where $f$ is the Coriolis parameter, $m$ is the ice mass per unit area, $g_r$ is the acceleration due to gravity, $u$ is the geostrophic wind. The terms in Eq. (3.1) signify the following: $m\frac{dU}{dT}$ is the sea ice momentum, $-mfk \times \vec{u}$ is the Coriolis stress, $\tau_a$ is the air (wind) stress, $\tau_w$ is the ocean stress, $mg_r\nabla Y$ is the sea surface slope, and $\nabla \cdot \sigma$ is internal ice stress [e.g. *Hibler*, 1979].

Air and ocean stresses include forces associated with wind drag on the upper surface and water drag on the ice underside. Triggered by the tilt of the sea surface, the sea surface component is generally less notable in magnitude. The final term of the equation is the force, arising from gradients in the internal ice stress field, i.e., the force resulting from the resistance of sea ice to deformation.

### 3.1.4 Sea Ice Surface Heat Budget

The energy balance at the sea ice – atmosphere interface under steady-state temperature conditions dictates that the heat fluxes out of, and into, the surface of sea ice must be balanced:

$$(1-\alpha)F_r - I_o + F_l\downarrow + F_l\uparrow + F_s + F_e - F_c + F_m = 0 \quad (3.2)$$

where the individual heat flux terms are the incoming solar shortwave flux, $F_r$, with ice albedo, a, (the ratio between incident and reflected shortwave energy for a given ice surface); the shortwave radiation flux into the ice/water, $I_0$; the incoming longwave radiation flux, $F_l\downarrow$; outgoing longwave radiation flux, $F_l\uparrow$; turbulent atmospheric sensible and latent heat fluxes $F_s$ and $F_e$; the heat flux due to melting of ice at the surface (typically only relevant during the summer melting phase), $F_m$; and the conductive heat flux from the interior of the snow/ice to the ocean water, $F_c$. More detailed information of the surface energy balance can be found in *Maykut* [1986] and *Steele and Flato* [2000]. The total energy flux at a given time may be positive, negative, or zero. If a total energy flux is positive, snow or ice is gaining energy. This scenario can result from an increase in the temperature of the snow or ice (energy storage). When the total energy flux is negative, the surface slab of sea ice loses energy and sea ice temperature decreases.

In subsequent sections, the analysis of the sea ice energy balance is based on the comparison of the temporal variability of individual energy fluxes and the net energy fluxes during two cyclonic cases that occurred in the Arctic Ocean and were reproduced in different modeling experiments. To quantify sea ice energy flux variability, area-integrated sea ice energy fluxes were calculated for the Kara and Barents Seas

for the March 2011 cyclone and for the East-Siberian, Chukchi and Beaufort Seas for the August 2012 cyclone.

The principle of conservation of energy (Eq. 3.3) is the basis for the simplistic expression for the energy balance at an ideal, planar surface.

$$F_{\text{total surface energy balance flux}} = (SW_{\downarrow} - SW_{\uparrow}) + (LW_{\downarrow} - LW_{\uparrow}) - SHF - LHF + CHF \quad (3.3)$$

where *SW* and *LW* denote the shortwave and longwave radiation fluxes, *SHF* is the sensible turbulent heat flux, *LHF* is latent turbulent heat flux, *CHF* is the conductivity heat flux, and *OHF* is the oceanic heat flux.

The following fluxes are denoted positive when pointed downward: net surface heat flux, latent heat, sensible heat, conductive heat fluxes. Oceanic heat flux is positive when the ocean gains heat.

## 3.2 Data and Methods

### 3.2.1 Model Description

Modeling experiments are carried out using the sea ice and ocean components of the National Center for Atmospheric Research's Community Earth System Model (CESM) version 1.0.4 [*Gent et al.*, 2011]. CESM is a fully coupled Earth System Model that simulates all major components of the physical climate system including land surface, atmosphere, sea ice, and ocean. Considering the study objectives, only the sea ice and oceanographic model components of CESM were integrated in a two-way coupled setting: Sea Ice Model – Community Ice Code version 4 (CICE4; *Hunke and Lipscomb* [2008]) and Parallel Ocean Program (POP) version 2 model [*Smith et al.* 1992].

The POP and CICE model components were configured and integrated on the identical resolution dipole displaced-pole grid. The CICE-POP model utilizes the nominal 1° resolution and was employed on a displaced pole grid (gx1v6) with one pole co-located at the South Pole and the other pole centered over Greenland. The displaced grid is a rotated coordinate system with a horizontal dimension of 320 zonal points by 384 meridional points and geographically-varying longitudinal and latitudinal spacing. Grid spacing is roughly 1.125° in the zonal direction and 0.5° in the meridional direction. Due to the displacement of the "North Pole", the POP and CICE models utilize a non-uniform horizontal resolution that is variable depending upon the proximity to the displaced pole. Consequently, horizontal resolution for the Arctic Ocean domain is comparatively high in the Atlantic sectors of the Arctic and low in the Pacific sectors.

The Community Ice CodE, or CICE, version 4.0 is a Los Alamos Sea Ice Model [*Hunke and Lipscomb*, 2008]. CICE is a dynamic-thermodynamic model that includes a subgrid-scale ice thickness

distribution [*Bitz et al.,* 2001; *Lipscomb*, 2001]. The ice dynamics utilize the elastic-viscous-plastic (EVP) rheology approach introduced by *Hunke and Dukowicz* [1997]. Subgrid-scale ridging and rafting is parameterized according to *Rothrock* [1975] and *Thorndike et al.* [1975]. In our study, the CICE model was set up to simulate parameters at five discrete ice thickness categories. The CICE model uses the energy conserving thermodynamics of *Bitz and Lipscomb* [1999], with four ice layers and one snow layer in each thickness category, and accounts for the influences of brine pockets within the ice cover. Horizontal advection is calculated via the incremental remapping scheme of *Lipscomb and Hunke* [2004].

The Parallel Ocean Program, or POP, is a depth-based, level-coordinate ocean general circulation model [*Smith et al.,* 1992]. A full description of the POP model is available in *Collins et al.* [2006] and *Danabasoglu et al.* [2006]. In this study, POP was integrated at 60 non-uniformly spaced vertical levels with the uppermost level at 5 m depth. Vertical levels have a 10 m spacing for the upper most 20 levels. Below 200 m levels increase with depth down to the lowest level in ~5400m.

### 3.2.2 Forcing and Initialization

Prescribed atmospheric forcing from the ERA-interim reanalysis surface fields developed at the European Centre for Medium-Range Weather Forecasting (ECMWF) was used to initialize and force POP-CICE model [*Berrisford et al.,* 2011]. ERA-Interim is a global reanalysis dataset covering the period from 1979 and continuing [*Dee et al.,* 2011]. ERA-Interim is discretized on an approximately 80 km horizontal grid increment (T255 spectral) at 60 levels with vertical steps of variable distance from the surface up to 0.1 hPa [*Dee et al.,* 2011]. Prescribed atmospheric forcing for CICE and POP models comprised the following fields: 6-hourly sea level pressure (SLP), u- (u10), v-component (v10) of wind, air temperature (t10), specific humidity (q10); daily average downward shortwave (SW↓) and longwave (LW↓) radiation fluxes; and monthly precipitation rate (pr. rate). For the purposes of this study, the ERA-interim fields for the years 1979 to 2012 (33 years) were utilized.

### 3.2.3 Experimental Design

The investigation of the sea ice response to storms was carried out by performing five sets of simulations that employ different treatments of atmospheric forcing: model spin-up, time-varying (hindcast), control (CTR), dynamic (DYN), and thermodynamic (THERMODYN). Model spin-up and time-varying simulations were used for the CICE-POP model evaluation. Upon attainment of simulated reliable sea ice and ocean conditions by running CICE-POP with the same forcing (1979) for 200 years, the

CTR, DYN, and THERMODYN experiments were performed. In each of the CTR, DYN, THERMODYN experiments, CICE-POP utilized a different set of prescribed atmospheric forcing. CTR experiments were integrated with the real-time, unperturbed atmospheric forcing as was observed during each of the storm cases. A modified atmospheric forcing was employed for the time when the storm case was present in the Arctic Ocean in the DYN and THERMODYN simulations. The overview of the performed modeling experiments, including forcing data, time step, and integration period are given in the Table 3.1.

Table 3.1: Model configuration of the Hindcast, Time-Varying, Control, Thermodynamic and Dynamic experiments

| Experiment | Forcing data | Model run time | Resolution |
|---|---|---|---|
| Spin-up | ERA-Interim | 1979 run for 200 years | monthly |
| Time-varying | ERA-Interim | 1979-2011 | monthly |
| CTR | ERA-INTERIM, real-time during storm: u10, v10, SLP, q10, t10, SW↓, LW↓, | 2011-2012 | 6-hourly |
| Thermodyn | ERA-INTERIM, 1) real-time during storm: t10, q10, SW↓, LW↓ 2) fixed to climate: u10, v10, SLP | 2011-2012 | 6-hourly |
| DYN | ERA-INTERIM, 1) real-time during storm: u10, v10, SLP, q10, 2) fixed to climate: SW↓, LW↓, t10 | 2011-2012 | 6-hourly |

The sea ice mass balance and heat budget responses were studied by analyzing two Arctic cyclones that occurred in different seasons and over different Arctic Sectors. To capture geographical differences in storm – sea ice interaction, we selected one cyclone that developed on the Atlantic side of the Arctic and one on the Pacific side. To capture the seasonality difference of the storm impact on sea ice, we analyzed one summer and one winter cyclone. The overview of investigated cyclones is given in Table 3.2.

Table 3.2: Overview of investigated cyclone cases

| Cyclone Case | Season | Location |
|---|---|---|
| **March 2011** | Winter (ice growth) | Atlantic Side of the Arctic |
| **August 2012** | Summer (ice melt) | Pacific Side of the Arctic |

#### 3.2.3.1 Model Spin-up Experiment

The spin up simulation is run by using one year (1979) forcing data for over 200 years, until equilibrium sea ice and ocean conditions were reached.

#### 3.2.3.2 Time-varying Experiment

To re-create sea ice and ocean conditions for 1979 to 2012, sea ice and ocean data from model spun-up data were used as initial conditions to perform the time-varying simulation once a sea ice and oceanic equilibrium was attained. In this run, continuous time-varying atmospheric data were utilized to force the model for 33 years, spanning from January 1979 to December 2012.

#### 3.2.3.3 Control Experiment

The control experiment (CTR) is a run forced with reanalysis using the following variables u10, v10, SLP, t10, q10, SW↓, LW↓ observed during the storm case. The control simulation is obtained by integrating CICE-POP with a 6-hourly time-step over the cyclonic life time.

#### 3.2.3.4 Thermodynamic Experiment

The thermodynamic experiment (THERMODYN) is a run forced with monthly climatological variables such as u10, v10, SLP and reanalysis datasets including t10, q10, SW↓, LW↓. THERMODYN otput is obtained by integrating CICE-POP with a 6-hourly time-step over the cyclonic life time. Modified forcing was applied for the duration of the storm only. The purpose of THERMODYN is to separate the thermodynamic impact of the cyclone on sea ice by setting dynamic impacts (wind) to climatology. In the

case of the thermodynamic experiment, surface turbulent heat fluxes were computed by combining modified forcing (u10, v10) and reanalysis (t10, q10).

#### 3.2.3.5 Dynamic Experiment

The dynamic experiment (DYN) is a run forced with monthly climatological variables such as t10, SW↓, LW↓ and reanalysis u10, v10, SLP, q10. The ensemble set was obtained by integrating CICE-POP with a 6-hourly time-step over the cyclonic life time. Modified forcing was applied for the duration of the storm only. Fixing surface air temperature and radiation fluxes to climatology allows independent evaluation of the dynamic of the storm impact on sea ice.

### 3.2.4 Model Validation

An assessment of CICE-POP's ability to reliably reproduce Arctic sea ice and ocean temperatures was performed by comparing modeled against available observational data that included upper-surface ocean temperature (PHC 3.0 climatology Polar Science Center [*Steele et al.,* 2001]) sea ice concentration (passive microwave SSMI-derived 1979-2012), sea ice thickness (laser altimetry ICESat (Ice, Cloud and land Elevation Satellite) data collected over the years 2004 to 2008 [*Kwok et al.,* 2009]), and sea ice drift data (International Arctic Buoy Program (IABP), [*Rigor et al.,* 2002]).

Sea ice concentration (SIC) was validated by comparing modeled and SSMI-derived average September mean sea ice concentrations in the Arctic (1979-2012) and March sea ice concentrations (Fig. 3.1). The overall spatial pattern of sea ice distribution in the Arctic is well-represented by CICE-POP in both months. Sea ice conditions, including the location of the sea ice edge and areal coverage, is reproduced more accurately in September than in March. As shown by sea ice concentration (SIC) differences, SIC is overestimated in the western Barents Sea, which is likely associated with a cold bias of surface ocean waters north of the Kola Peninsula, and the White Sea (Fig. 3.6). Increased SIC south of Fram Strait represents an overestimated sea ice outflow from the Arctic into the Atlantic Ocean. The modeled SIC is greater in the coastal areas of the East-Siberian Sea and less in the coastal areas of the Beaufort Sea compared to SSMI data (Figs. 3.6C, 3.6D).

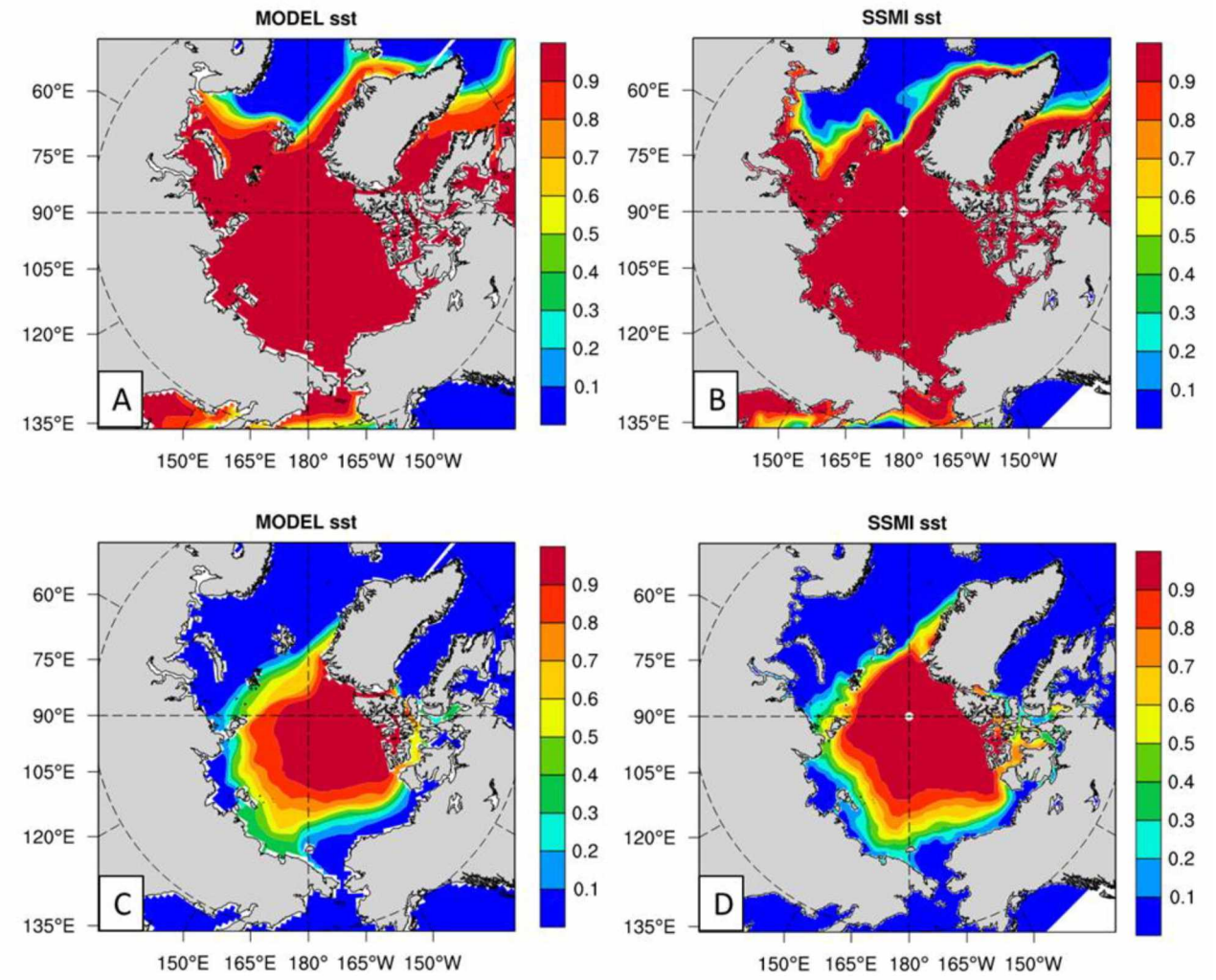


Figure 3.1: Mean sea ice concentration (1979-2011) (Unit: [fraction of 1]) in JFM: CICE-POP (A), SSMI (B); and in JAS: CICE-POP (C), SSMI (D).

As seen from the interannual variability of the sea ice area in SSMI and CICE-POP data in Fig. 3.2, the model generally captures the long-term decreasing trend of sea ice area. The interannual variability of simulated sea ice area experiences a larger amplitude compared to SSMI data with a greater and smaller sea ice area in JFM and JAS, respectively.

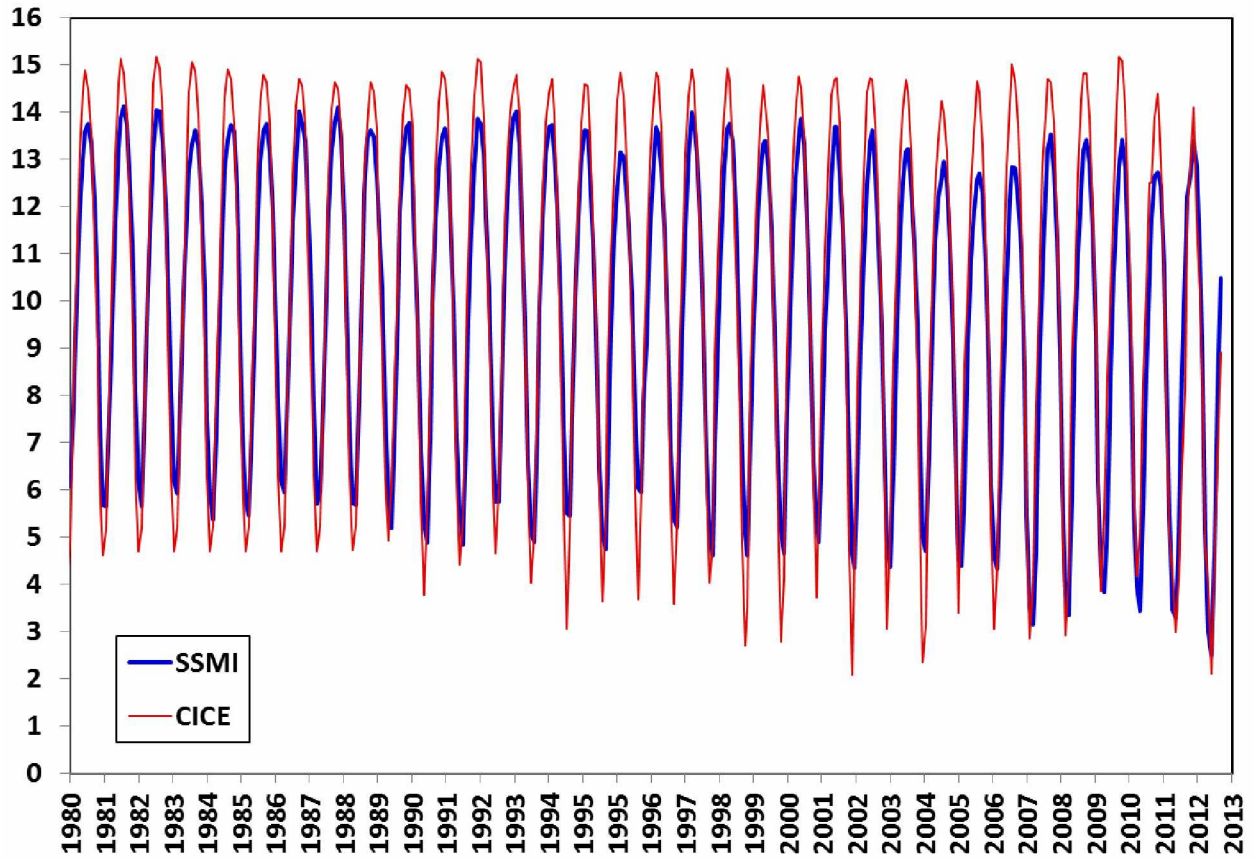


Figure 3.2: Sea ice area comparison 1979-2012 (Unit: [$10^6$ $km^2$]): CICE-POP (red line), SSMI (blue line).

CICE-POP – SSMI sea ice area differences were calculated to assess seasonality in bias between modeled and remote sensing data. Modeled sea ice area average bias is positive in March, ranging from +0.1 $10^6$ $km^2$ in 1979 to +1.78 $10^6$ $km^2$ in 2007 (Fig. 3.3). Sea ice area average bias shows both positive and negative difference in September ranging from -1.58 $10^6$ $km^2$ in 2004 to a maximum of +1.63 $10^6$ $km^2$ in 2010. In this analysis, we consider areal coverage as a main metric for assessing sea ice response to storms so the ability to reproduce sea ice variability subject to external factors (atmosphere and ocean) is critical.

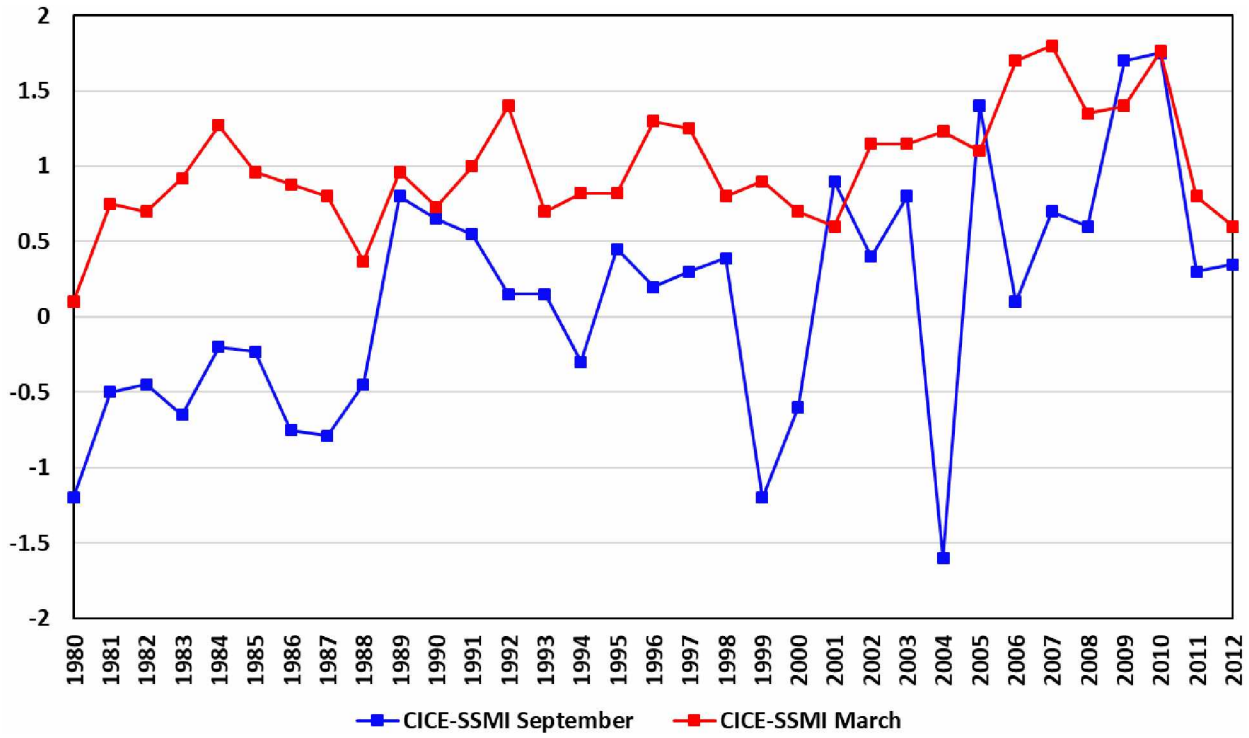


Figure 3.3: CICE-SSMI sea ice area (Unit: [$10^6$ $km^2$]) difference in September (blue line), March (red line).

Observations of sea ice thickness are very limited in covered area and time. One of the recent campaigns (ICESat) collected sea ice thickness data over the Arctic from 2004 to 2008 (February to April). The quality of simulated sea ice thickness was assessed by comparing model output to the data obtained from ICESat freeboard measurements of sea ice thickness (Fig. 3.4). CICE-POP captures acceptably well the general pattern of sea ice thickness including the thicker sea ice north of the Canadian Arctic Archipelago and thinner sea ice along the Eurasian Arctic coast. Simulated sea ice thickness is underestimated north of the Canadian Arctic Archipelago by approximately 1-2 m; it is overestimated in the Central Arctic, eastern Laptev, and west East-Siberian Seas by approximately 1 m (Fig. 3.4).

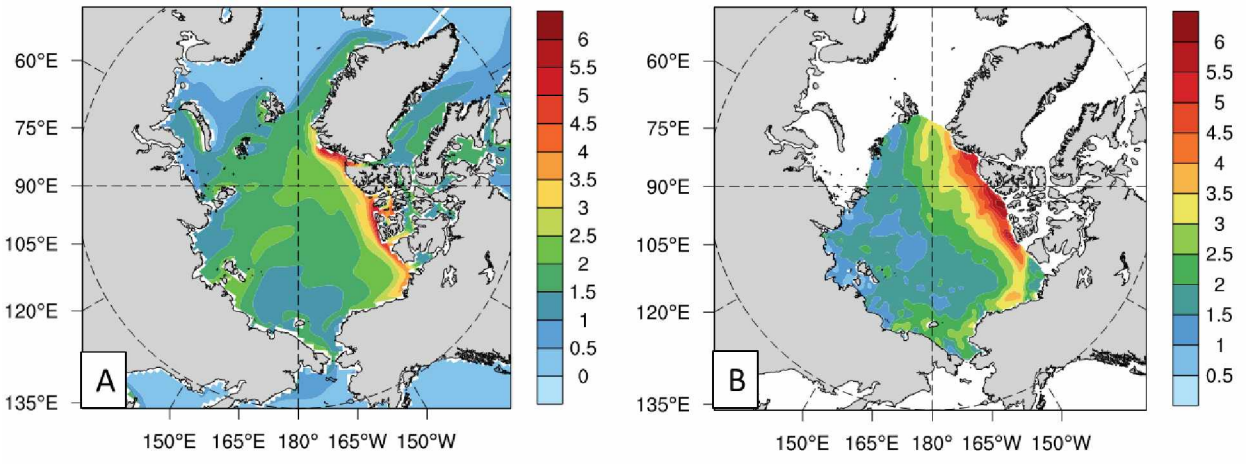


Figure 3.4: Sea ice thickness (Unit: [m]) averaged over February-March-April of 2004-2008: CICE-POP (A); ICESat (B).

The main sea ice drift patterns in the Arctic Ocean, such as the Transpolar Drift Stream and the Beaufort Gyre, have been well reproduced by CICE-POP (Fig. 3.5); however, the Beaufort Gyre is slightly displaced westward of the Chukchi Sea. CICE-POP tends to overestimate the speed of sea ice drift by approximately 3-4 cm/s within the Transpolar Drift Stream and 1-2 cm/s within the Beaufort Gyre.

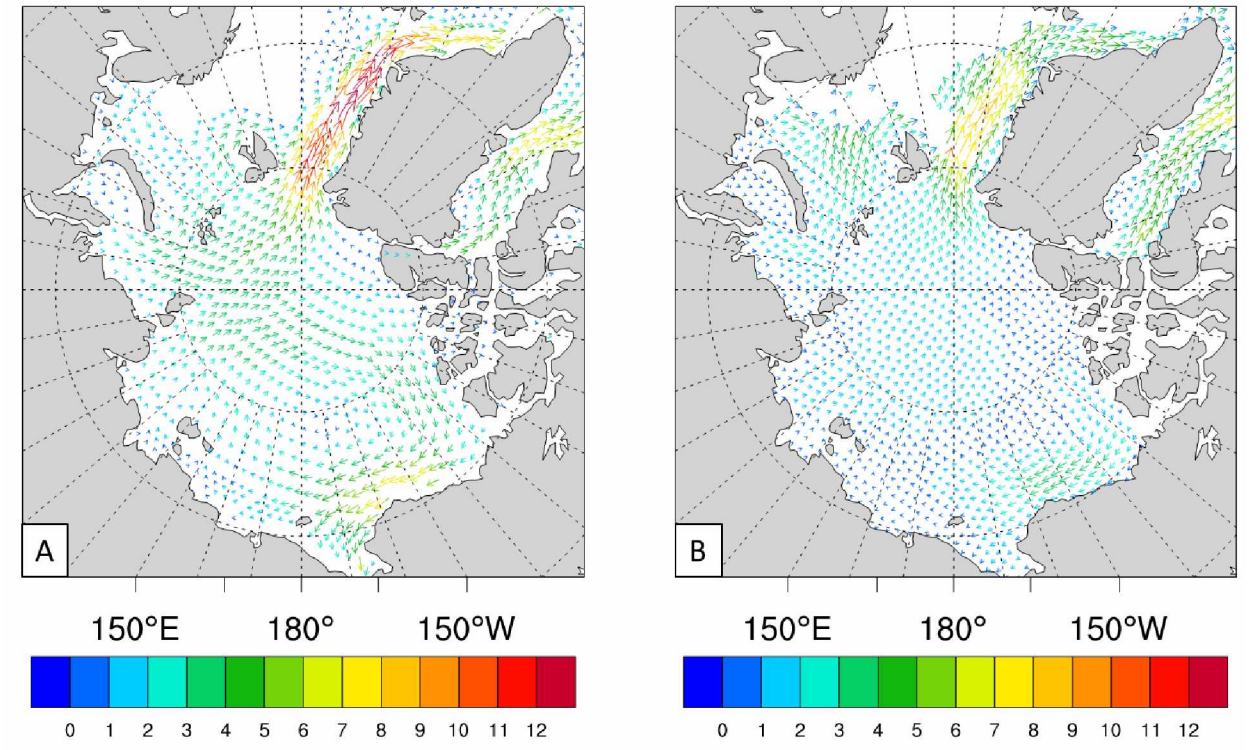


Figure 3.5: Annual mean sea ice drift (1979-2012) (Unit: [cm $s^{-1}$]): model-simulated (A), and observed (IABP) (B).

The CICE-POP performance to simulate ocean surface temperature was assessed by comparing modeled and Polar Science Center Hydrographic Climatology (PHC) data [*Steele et al.,* 2001] (Fig. 3.6). The CICE-POP mean ocean water temperature was computed by averaging the output of the time-series simulation for ocean temperature at levels 5 m, 15 m, 25 m, and 35 m, over 25 years, from 1979 to 1994. The PHC climatology is obtained by extrapolating and averaging compiled in-situ measurements of ocean temperature and salinity collected between 1979 and 1994. Simulated surface water temperatures in the Arctic Ocean have a positive bias of 1-2°C at the Atlantic side of the Arctic. This bias is characteristic for both summer and winter seasons. The bias could be explained by overestimated heat transport into the Arctic. A plausible explanation to the ocean temperature bias is the difference of oceanic depths in the datasets. The upper-level surface in the model is 5m and represents the averaged mixed layer temperature in the upper 10m of oceanic water. In the PHC, the upper-level surface is 0 m and represents the temperature of the atmosphere-ocean interface.

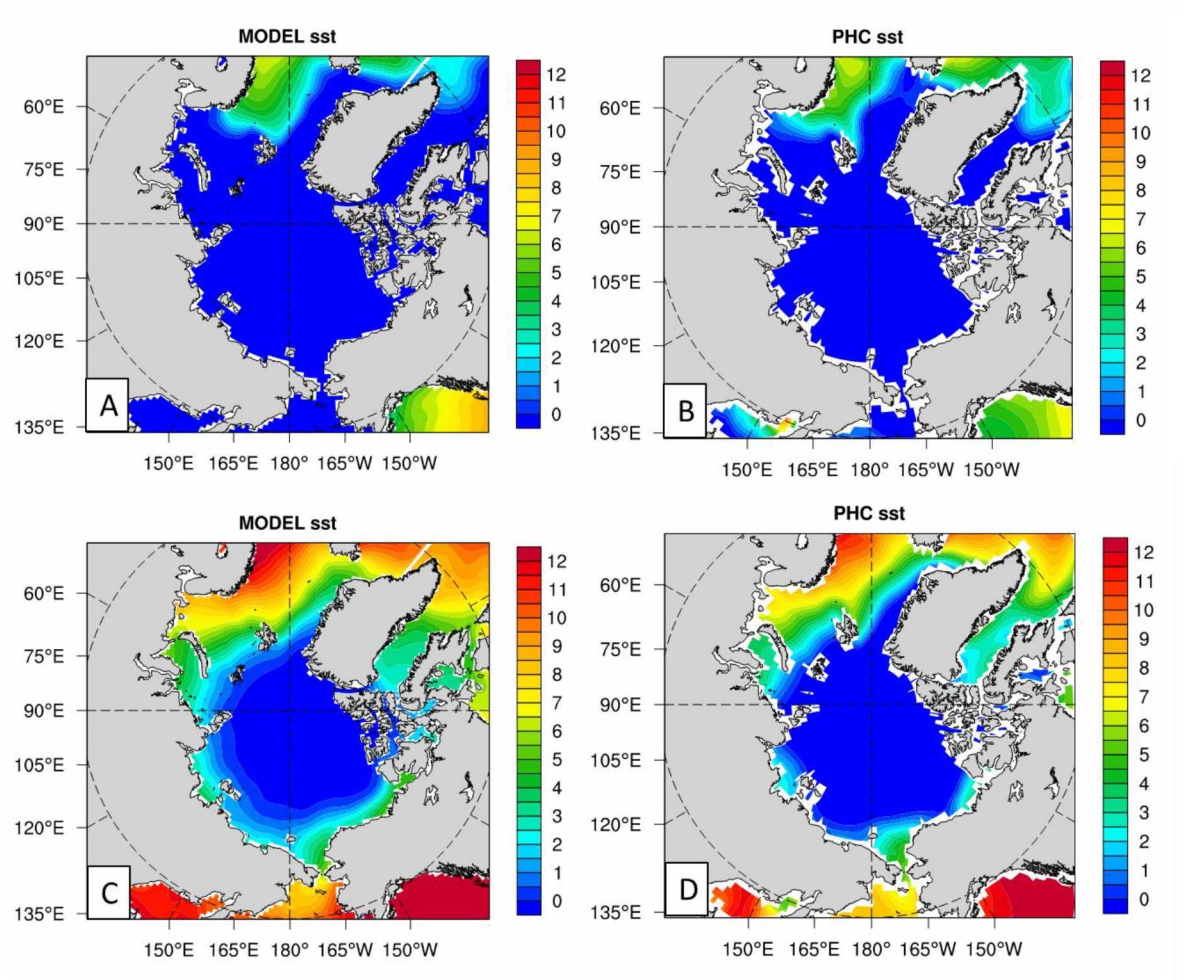


Figure 3.6: Mean sea surface temperature (1979-2011) (Unit: [°C]): CICE-POP in JFM (A), in JAS (C); PHC in JFM (B), in JAS (D).

CICE-POP reliably reproduced inter-annual sea ice area variability for 1979 to 2011, and the Arctic sea ice concentration, motion, and thickness patterns; however, it noticeably overestimated sea ice drift speed. Overall sea ice positive bias in winter and negative bias in summer was less in 2011 and 2012 was less in magnitude as compared to 1979-2008 period, suggesting the model data was more accurate during the two storm case studies that occurred in these years. Sea ice drift bias while being relatively high along the northeast coast of Greenland needs to be taken into account as the outflow of sea ice through the Transpolar Drift Stream will likely be overestimated. Sea ice concentration was reproduced more accurately in summer than in winter as compared to remote sensing data; SIC tended to be overestimated in the Atlantic Ocean, and slightly underestimated in the Pacific side of the Arctic.

The differences between the CICE-POP ocean temperature and the PHC-interpolated ocean temperature to 5 m, 15 m, 25 m and 35 m show that CICE-POP tends to overestimate water temperatures in the upper 40 m (Fig. 3.7). The maximum difference of 2-4°C is observed south of the Svalbard. Ocean temperature bias over the Central Arctic Ocean is positive but small (0.5 – 1°C), i.e. within measurement uncertainty. Negative bias of -1°C to -2°C is observed in the northern White Sea, Bering Strait, and in the Labrador Sea.

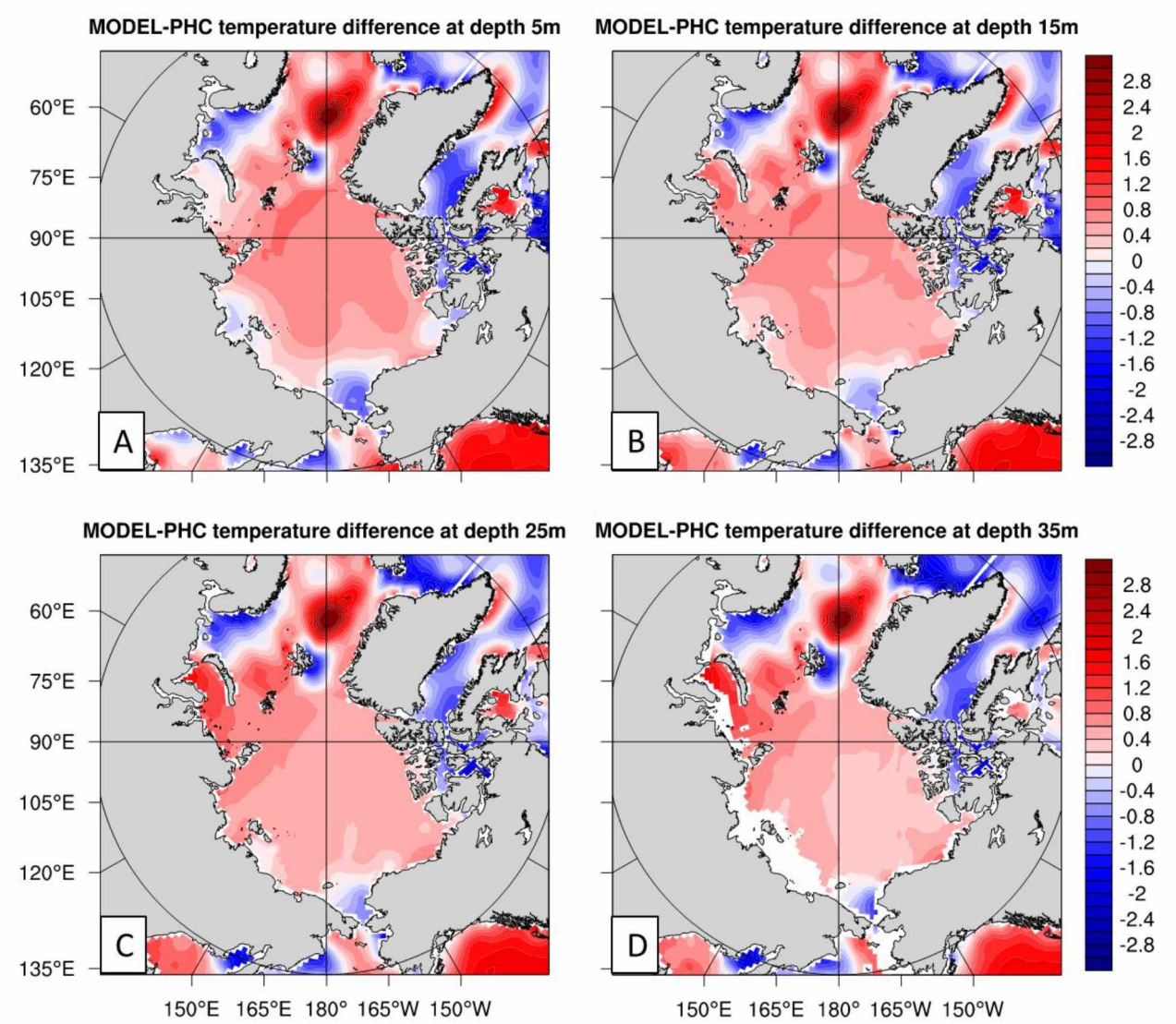


Figure 3.7: Annual mean sea surface temperature difference (1979-2011) (Unit: [°C]) between CICE-POP and PHC: at 5m (A), 15m (B), 25m (C), and 35m (D).

### 3.3 March 2011 Cyclone

This section explores possible forcing, exerted by the March 2011 cyclone on sea ice based on the output of the CTR and sensitivity experiments (DYN, THERMODYN).

The lifecycle of the March 2011 cyclone is detailed in chapter 4 of this thesis document. Before the March 2011 cyclone fully developed, sea ice was at the winter maximum extent (14.6 $10^6$ $km^2$) and sea ice was deteriorating primarily in the marginal zones: the northeastern part of the Barents and the southwestern part of the Kara Seas (Fig. 3.8). When the center of the cyclone reached the Central Arctic, it stalled from March 17 until March 22, the surface pressure gradient tightened up. Consequently, particularly strong winds occurred over the Eurasian Arctic coast that encompassed the Barents Sea and eastward into the East-Siberian Sea. Following the wind increase over the northeastern parts of the Barents Sea, the edge of the sea ice shifted poleward. The poleward displacement of the sea ice edge in the Barents Sea was concurrent with formation of polynyas on the leeward (eastern) side of the islands, including Novaya Zemlya, Svalbard, and Franz-Joseph Land.

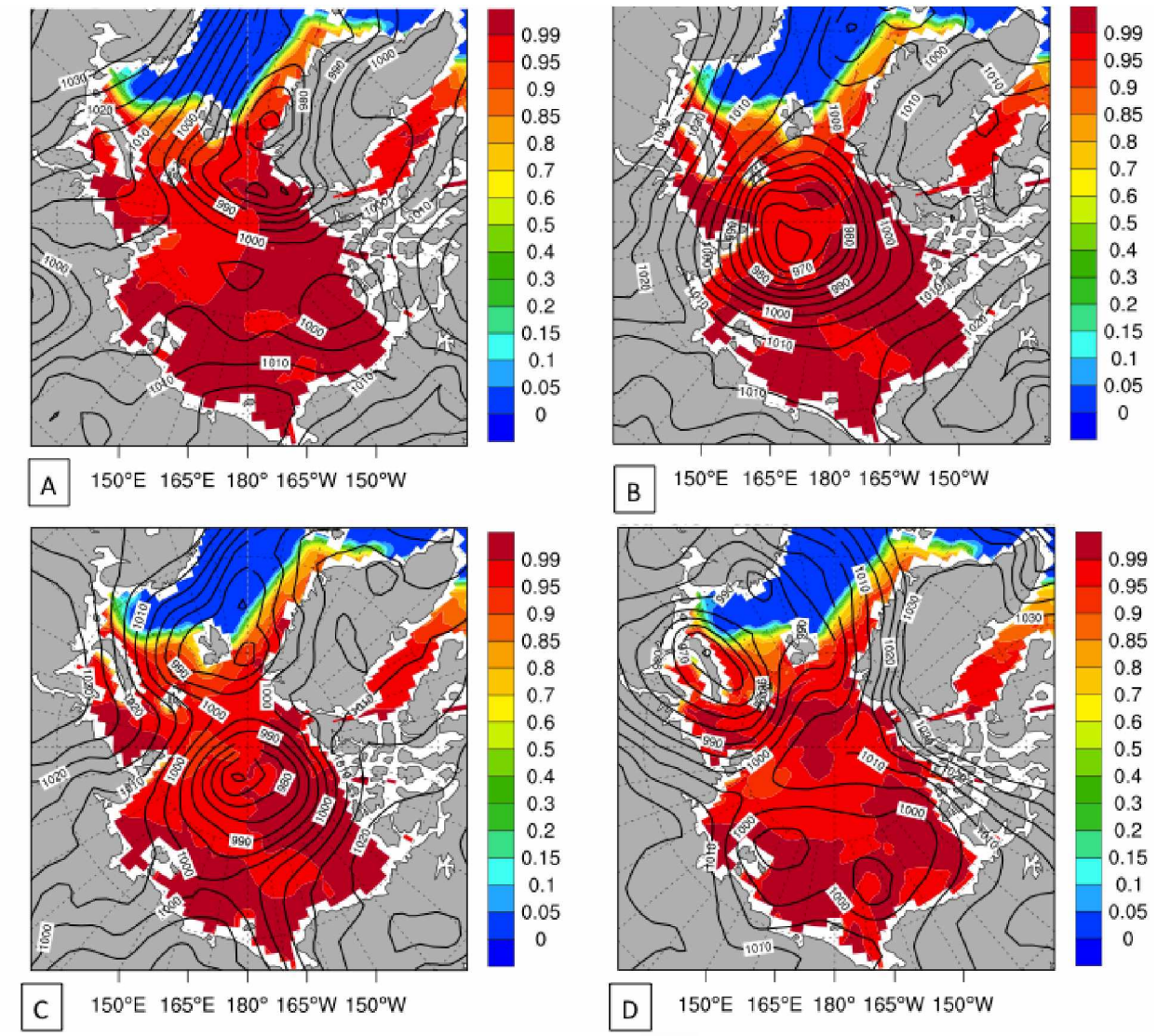


Figure 3.8: CICE-POP sea ice concentration (colors) (Unit: [fraction of 1]) and ERA-Interim reanalysis sea level pressure (contours) (Unit: [hPA]) valid for March 15 1800 UTC (A), March 17 1800 UTC (B), March 19 0000 UTC (C), March 22 1200 UTC (D).

Maximum surface wind speed throughout the lifecycle of the March 2011 cyclone was observed over the Barents and Kara Seas. Less strong winds were observed over the Laptev and East-Siberian Seas. Winds along the Eurasian Arctic coast had a sustained speed of over 17 m/s (near-gale to gale force on Beaufort scale) for a duration of five days (Fig. 3.9). Given orographic effects, winds on the leeward side of the mountains of Novaya Zemlya initiated sea ice recession and created a notable coastal polynya in the Kara Sea. Over the marginal ice zone in the northeastern Barents Sea, wind speed was approximately 15-

20 m/s (Fig. 3.9A). Strong surface winds observed along the Eurasian coast of the Arctic Ocean continued until the March 2011 cyclone weakened on March 21 (Fig. 3.9D).

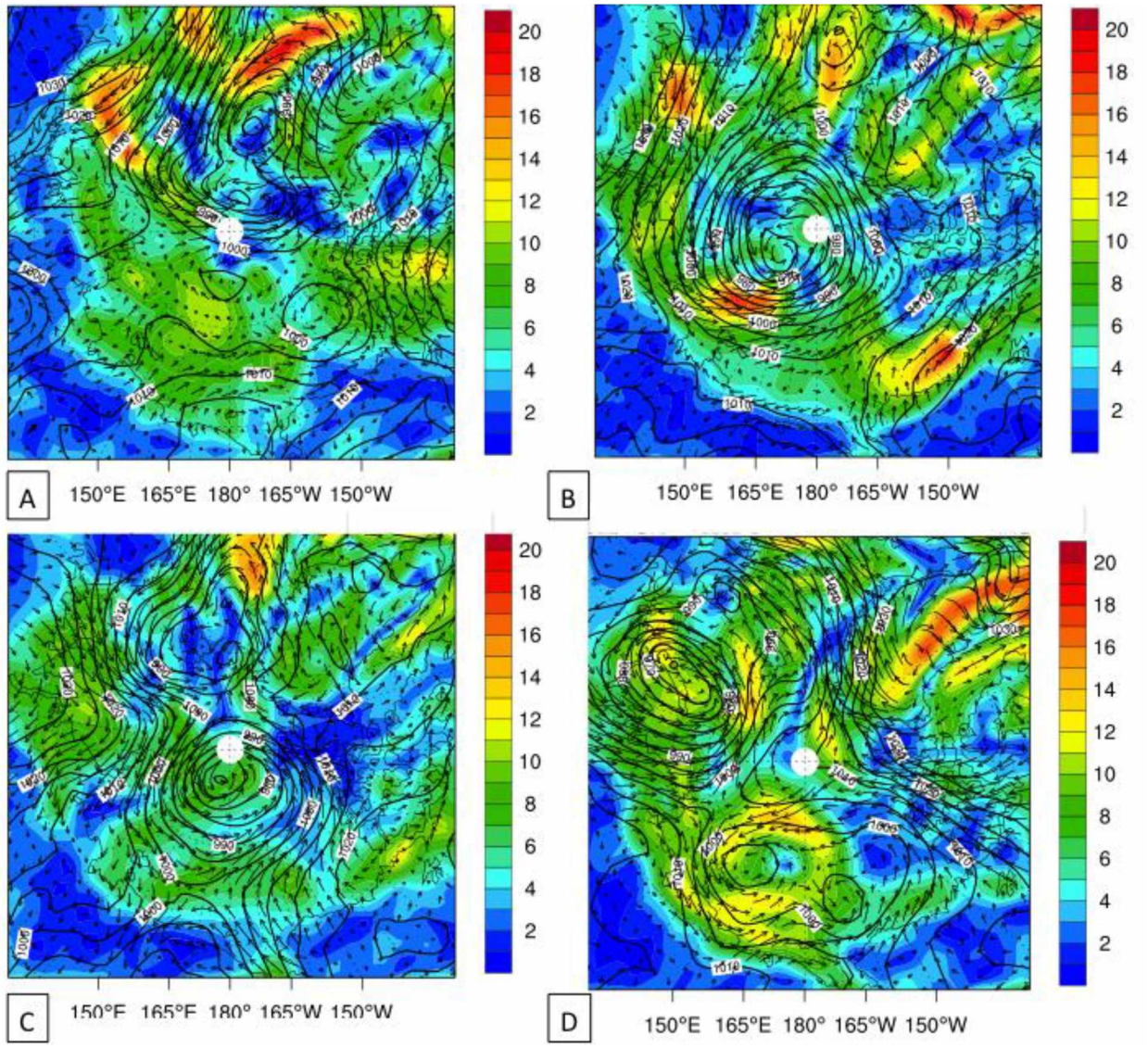


Figure 3.9: ERA-Interim reanalysis surface wind speed (colors) (Unit: [m $s^{-1}$]), direction (arrows), and sea level pressure (contours) (Unit: [hPa]) valid for March 15 1800 UTC (A), March 17 1800 UTC (B), March 19 0000 UTC (C), and March 22 1200 UTC (D).

The pattern of atmospheric circulation, long lifecycle of the March 2011 cyclone, and elevated wind speed determined the sea ice drift speed and sea ice drift direction. The speed of sea ice drift varied in various regions of the Arctic Ocean, depending on the predominant wind speed and direction. It ranged from 20-25 cm/s in the Barents Sea to 10-15 cm/s in the central part of the Arctic Ocean. As the March

2011 cyclone was developing, the maximum drift speed of sea ice (20-25 cm/s) was observed in the marginal ice zones of the Barents and Kara Seas (Fig. 3.10). When the March 2011 cyclone reached its maximum intensity, increased sea ice drift was observed in the Central Arctic and the Laptev Sea. Robust counterclockwise sea ice motion led to the intensification of ice outflow from the Arctic Ocean through Fram Strait.

Corresponding to the winds, sea ice drift was to the northeast. The pattern of sea ice drift assumed a circumpolar shape after the March 2011 cyclone intensified and moved poleward. Corresponding to cyclonic winds, the pattern of sea ice drift during March 2011 was counterclockwise, including the Beaufort Sea where the predominant direction of sea ice motion was reversed (Figs. 3.10B, C, and D). Counterclockwise sea ice movement in the Arctic was sustained through the dissipation phase of the March 2011 cyclone on March 22.

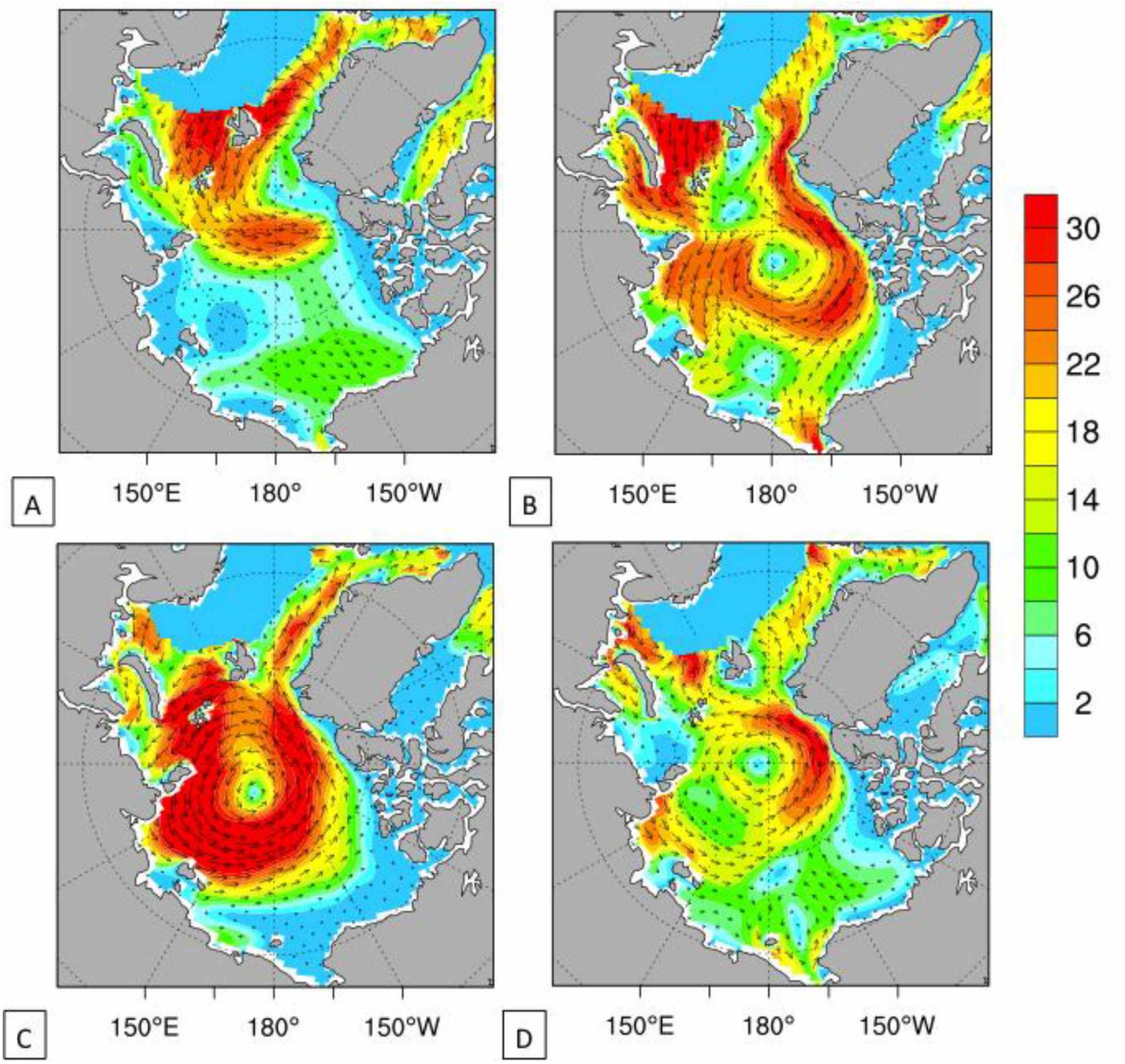


Figure 3.10: CICE-POP sea ice drift (colors) (Unit: [cm $s^{-1}$]) and direction (arrows) valid for March 15 1800 UTC (A), March 17 1800 UTC (B), March 19 0000 UTC (C), and March 22 1200 UTC (D).

### 3.3.1 Dynamic vs Thermodynamic Forcing on Sea Ice

Cyclonic forcing exerted on sea ice during the March 2011 cyclone was analyzed through a comparison of model output of CTR and sensitivity experiments. We selected the region of the Barents and Kara Seas for analysis because that region was characterized by the maximum sea ice reduction during the cyclone passage.

Sea ice growth occurred in the Barents and Kara Seas through March 16, 2011, when the maximum sea ice area reached 1.57 $10^6$ $km^2$ (Fig. 3.11). Between March 17 to March 24 sea ice area in the Barents-Kara Seas underwent a rapid decline from 1.57 $10^6$ $km^2$ to 1.4 $10^6$ $km^2$. The sea ice area was decreasing at an approximate rate of 37.500 $km^2$ per day from March 16 to March 20, 2011, when sea ice reduction was driven by the immediate impact of increased cyclone winds (Fig. 3.9) and melting. The rate of sea ice retreat decreased to approximately 5.000 $km^2$ per day on March 20. The decreased retreat rate lasted until March 24, 2011, which coincided with the weakening and gradual dissipation of the March 2011 cyclone. The decrease in sea ice reduction rate after March 20 was a result of the inertial response of slow-reacting sea ice to rapidly reacting atmospheric changes. The decreased rate of sea ice reduction on March 20, and thereafter, is associated with the lagging sea ice response to diminished wind speed. The sea ice area resumed a gradual growth on March 24 continuing into early April of 2011.

The sea ice reduction rate in the DYN experiment during the March 2011 cyclone was less abrupt than in CTR run. The sea ice area in DYN run was at minimum on March 20 (1.48 $10^6$ $km^2$), which was 0.06-0.08 $10^6$ $km^2$ greater than in the CTR run. There is a difference in the time of minimum sea ice area: CTR - March 24 and DYN - March 20 due to inability to sustain robust baroclinic instability in DYN as compared to CTR.

To estimate the impact of wind forcing on sea ice during the March 2011 cyclone, we compared the output of the CTR and THERMODYN runs. Simulated sea ice area in the CTR and THERMODYN runs show notable differences; sea ice in the CTR case experienced a sharp decrease during the March 2011 cyclone whereas the sea ice in the THERMODYN case continued steady winter growth. The fact that the sea ice area did not experience a drop during a cyclone in THERMODYN demonstrates that the modified wind forcing was too weak to result in sea ice deterioration. Lower wind speeds, causing lower wind stress, resulted in slower ice drift in the Barents-Kara Seas in THERMODYN than CTR.

Based on a comparison of the CTR-THERMODYN and CTR-DYN differences, it can be concluded that the cyclonically-driven wind forcing had a more pronounced impact on sea ice reduction than thermodynamic melting (Fig. 3.11).

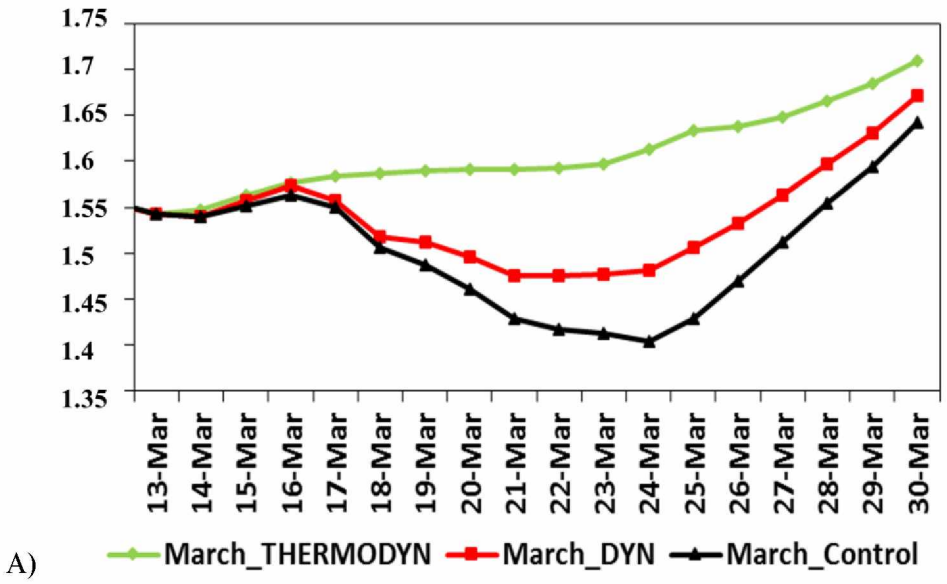


A)

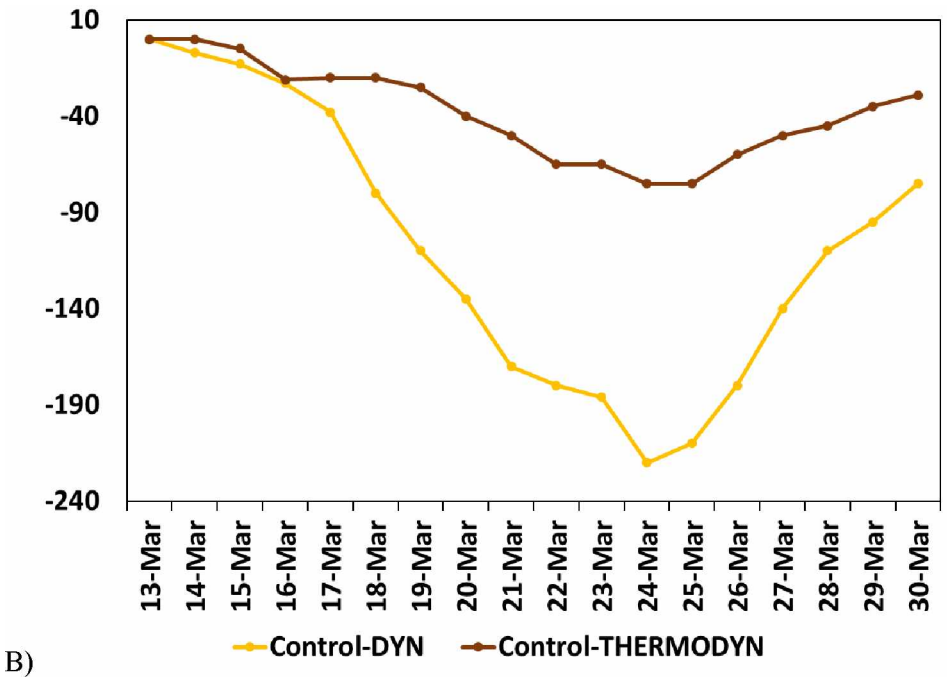


B)

Figure 3.11: CICE-POP simulated sea ice area (Unit: [$10^6$ $km^2$]) over the Barents and Kara Seas in the Control, Thermodynamic, and Dynamic experiments (A). CTR-DYN (brown) and CTR-THERMODYN (yellow) difference in sea ice area (Unit: [$10^3$ $km^2$]) over the Barents and Kara Seas (B).

The geographical pattern of where dynamic and thermodynamic cyclonic forcing had their maximum impact on sea ice was analyzed by investigating the difference in simulated sea ice concentration (SIC) fields between CTR and DYN (Fig. 3.12A) and CTR and THERMODYN experiments (Fig. 3.12B).

SIC difference is more significant in the CTR-THERMODYN case than in CTR-DYN. This finding supports the evidence that during the March 2011 cyclone, the wind forcing was the primary forcing causing the sea ice recession; surface heating and radiation fluxes were secondary. The areas of maximum impact of thermodynamic forcing on sea ice concentration is observed east of Novaya Zemlya, Franz-Joseph Land, and Svalbard (Fig. 3.12B).

The CTR-THERMODYN difference of sea ice concentration, valid for March 19, 2011, is negative in the marginal ice zone in the NE Barents Sea and, to the east of the islands, in the Barents and Kara Seas (Fig. 3.12B). Sea ice concentration west of Novaya Zemlya increased as a result of sea ice compression due to increased east-northeasterly drift of sea ice during the March 2011 cyclone. Strong winds pushed thinner ice eastward and amplified sea ice dynamic growth as a result of sea ice piling west of the Novaya Zemlya Archipelago.

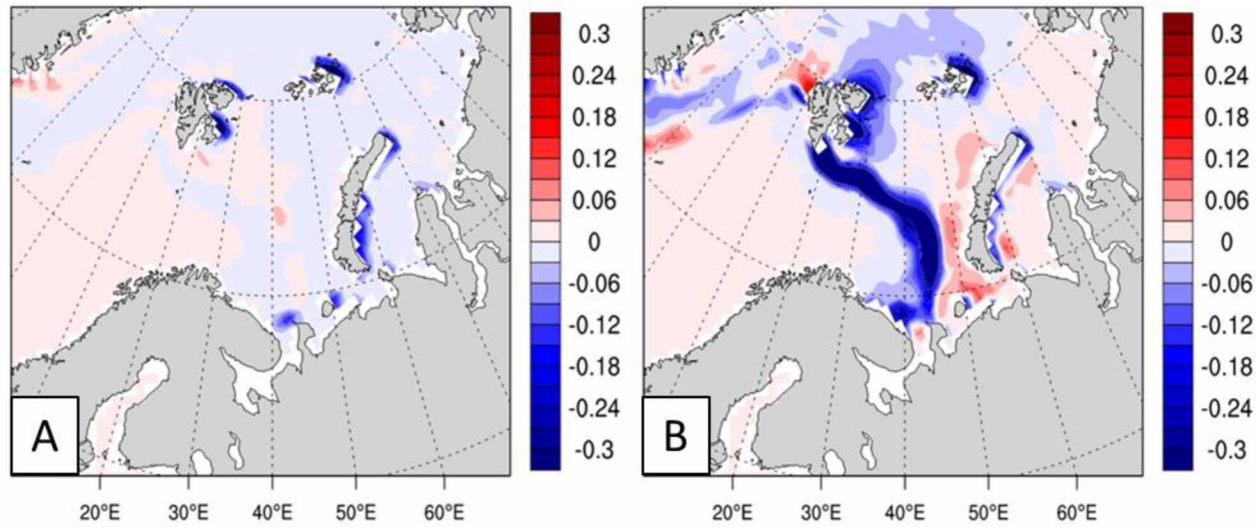


Figure 3.12: CICE-POP sea ice concentration (Unit: [fraction of 1]): CTR-DYN (A), CTR-THERMODYN (B) differences.

### 3.4 August 2012 Cyclone

Another cyclone discussed in this chapter occurred on the Pacific side of the Arctic Ocean in August 2012. The August 2012 cyclone was a deep low pressure system that developed off the East Siberian Sea coast and moved into the Central Arctic Ocean in the summer of 2012. Concurrent with the movement and intensification of the August cyclone, sea ice concentration dramatically deteriorated [*Zhang et al.,* 2012].

Areas of low sea ice concentration, encompassing coastal parts of the East-Siberian, Chukchi, and Beaufort Seas, were most affected by the cyclone (Fig. 3.14). The cyclone developed on August 2, 2012, and deepened to 988 hPa on August 4 (Fig. 3.14A and 3.15C). On August 6, the low developed into a very intense cyclonic system, covering the Central and Western Arctic. In the center of the cyclone, sea level pressure reached 968 hPa. Having stalled over the Central Arctic Ocean, the August 2012 cyclone began to dissipate and eventually split into multiple weaker low pressure systems on August 10.

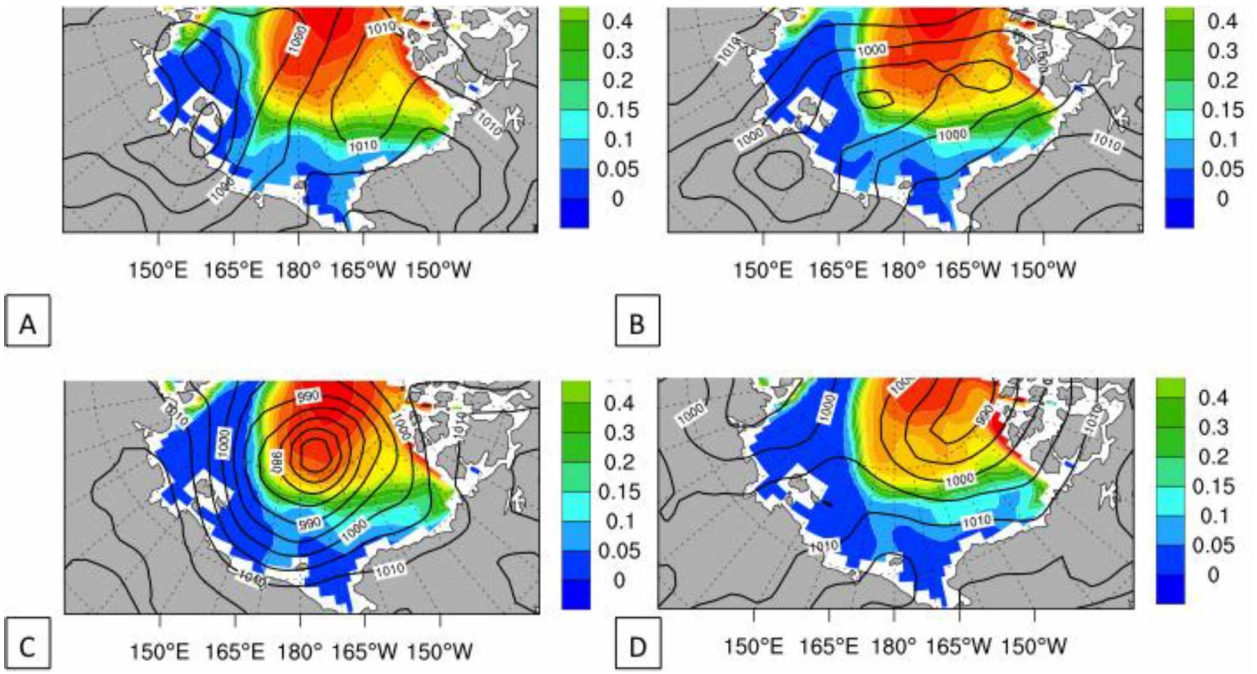


Figure 3.14: Simulated sea ice concentration (colors) (Unit: [fraction of 1]), ERA-Interim reanalysis sea level pressure (contours) (Unit: [hPA]) valid for August 2 0000 UTC (A), August 4 0000 UTC (B), August 6 0000 UTC (C), and August 10 0000 UTC (D).

After the Arctic storm developed on August 8, the area of high pressure gradient resulted in the southerly movement of continental, warm air towards the East-Siberian and Chukchi Seas (Fig. 3.15). Sustained southerly winds on August 2 were increasing during the August 2012 cyclone and reached their maximum speed of 20-25 m/s on August 6.

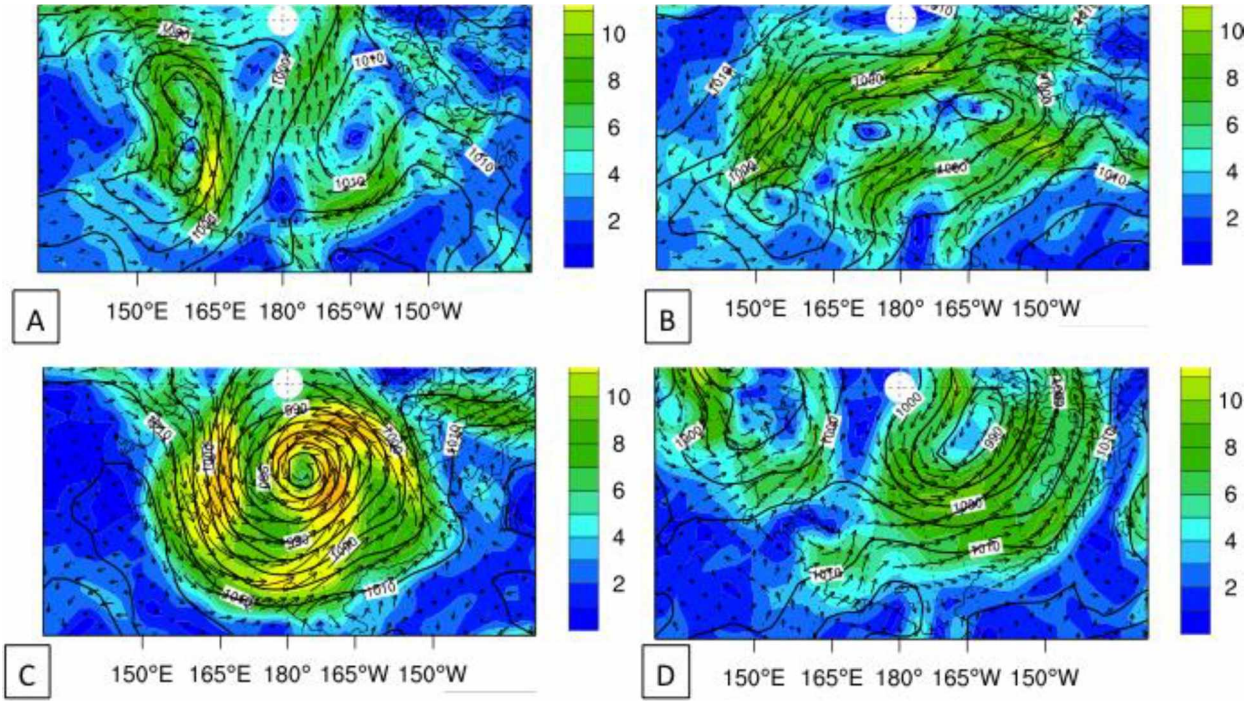


Figure 3.15: ERA-Interim reanalysis surface wind speed (colors) (Unit: [m $s^{-1}$]) and direction (arrows) valid for August 2 0000 UTC (A), August 4 0000 UTC (B), August 6 0000 UTC (C), and August 10 0000 UTC (D).

During the August 2012 cyclone, increased winds determined the pattern and speed of sea ice drift. Moderate sea ice drift at 8 to 12 cm/s prevailed over the Pacific side of the Arctic Ocean from August 3 until August 5 (Fig. 3.16). Sea ice drift speed accelerated up to 15-20 cm/s during the maximum phase of the storm development on August 6 through August 7. Sea ice drift, being primarily wind-driven, was counterclockwise with the maximum drift speed along the coasts of the East-Siberian and Chukchi Sea coasts. As winds diminished during the decay of the cyclone on August 10, the speed of sea ice drift reduced to 5-10 cm/s.

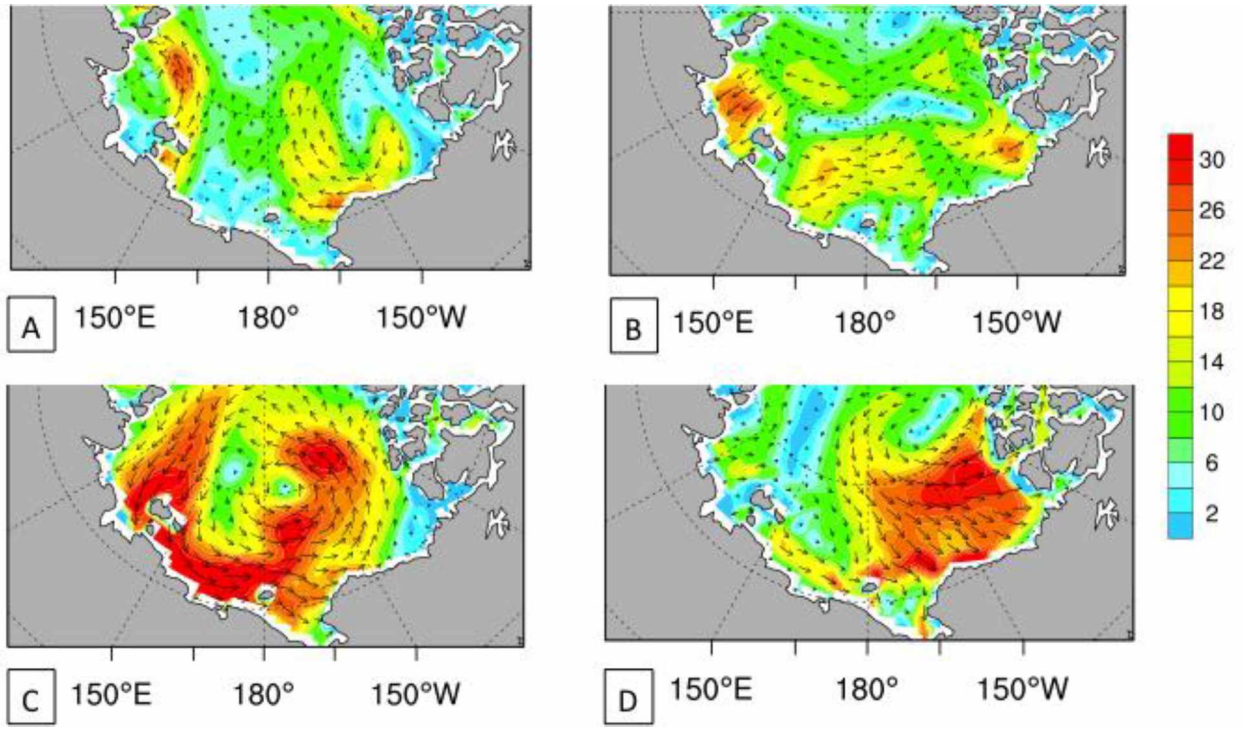


Figure 3.16: Simulated sea ice drift (colors) (Unit: [cm $s^{-1}$]) and direction (arrows) valid for August 2 0000 UTC (A), August 4 0000 UTC (B), August 6 0000 UTC (C), and August 10 0000 UTC (D).

### 3.4.1 Dynamic and Thermodynamic Forcing on Sea Ice

In the Western Arctic, the sea ice area reduced at an accelerated rate during the August 2012 cyclone, resulting in a 20% reduction over the East-Siberian, Chukchi, and Beaufort Seas (Fig. 3.17). On August 1 before the August 2012 cyclone, the sea ice area over the Pacific side of the Arctic was 2.8 $10^6$ $km^2$. On August 12, after the cyclone dissipated, the sea ice area was 1.85 $10^6$ $km^2$. This diminution reveals a rate of sea ice area reduction of approximately 90.000 – 100.000 $km^2$ per day during the August 2012 cyclone.

In CTR, sea ice reduction rate was more robust than in DYN and THERMODYN simulations. The CTR-DYN and CTR-THERMODYN difference in sea ice area was at its maximum on August 12. The sea ice area reduced by 0.65 $10^6$ $km^2$ from August 1 to August 12 in CTR and by 0.45 $10^6$ $km^2$ in DYN and THERMODYN. The equal rates of deterioration of sea ice area in August reveal that thermodynamic and dynamic cyclonic forcing had an equal impact on sea ice area over the East-Siberian, Chukchi, and Beaufort Seas, however, for different reasons

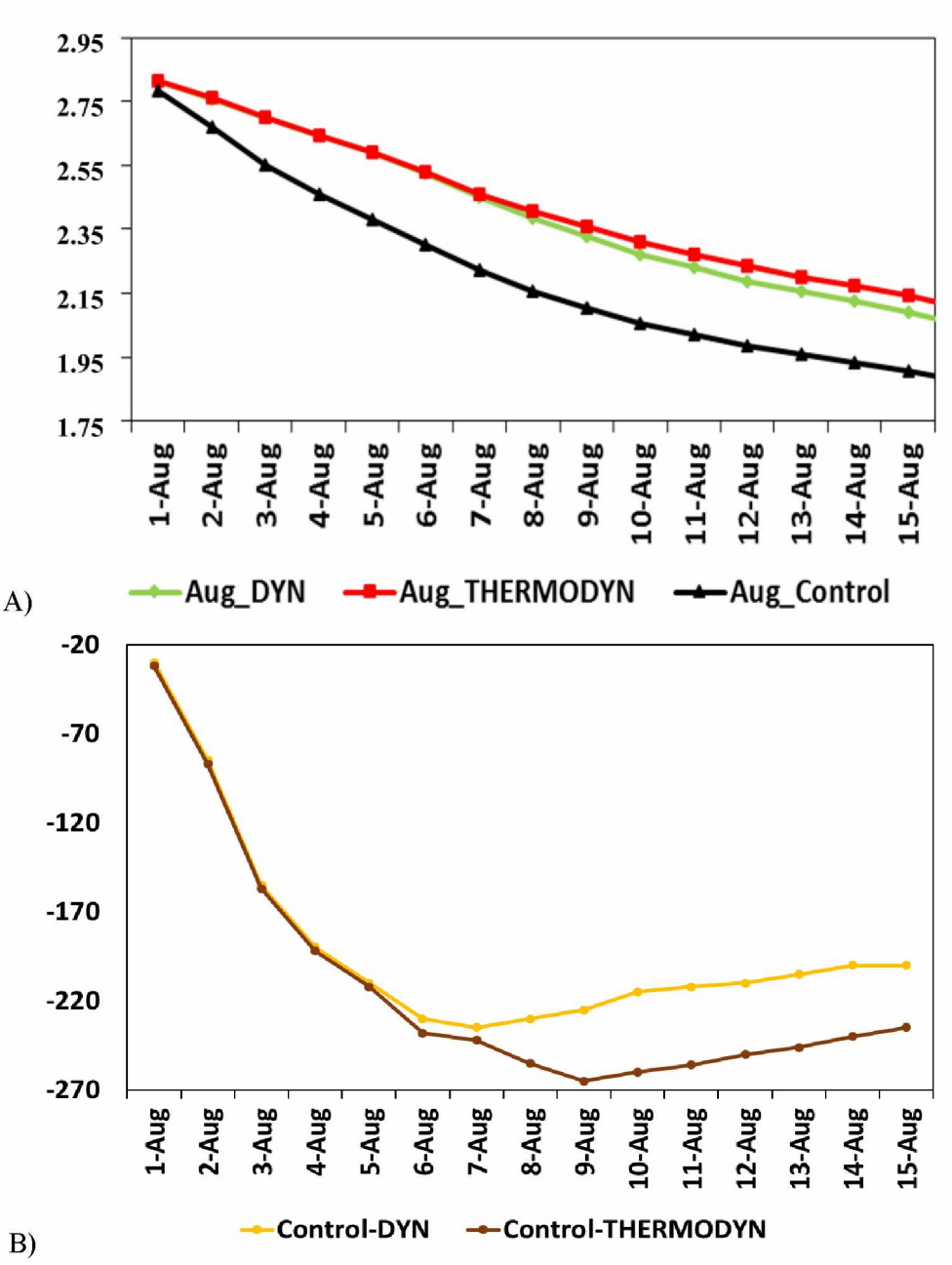


Figure 3.17: CICE-POP-reproduced sea ice area (Unit: [$10^6$ km$^2$]) over the East-Siberian – Chukchi - Beaufort Seas in Control, Thermodynamic, and Dynamic experiments (A). Sea ice area difference (Unit: [$10^3$ km$^2$]) over the East-Siberian – Chukchi - Beaufort Seas between Control and Dynamic; Control and Thermodynamic experiments (B).

The CTR-DYN and CTR-THERMODYN differences of sea ice concentration show that the impact of cyclone dynamic and thermodynamic forcing on sea ice was the most notable in the marginal ice zones

of the northern East-Siberian, Chukchi and Beaufort seas (Fig. 3.18). On August 12, sea ice reduction was at a maximum in the northern Beaufort Sea and was primarily wind-driven (Fig. 3.18B). The impact of surface air temperature and radiation fluxes had a secondary role in sea ice reduction in the East-Siberian, Chukchi, and Beaufort Seas (Fig. 3.18A).

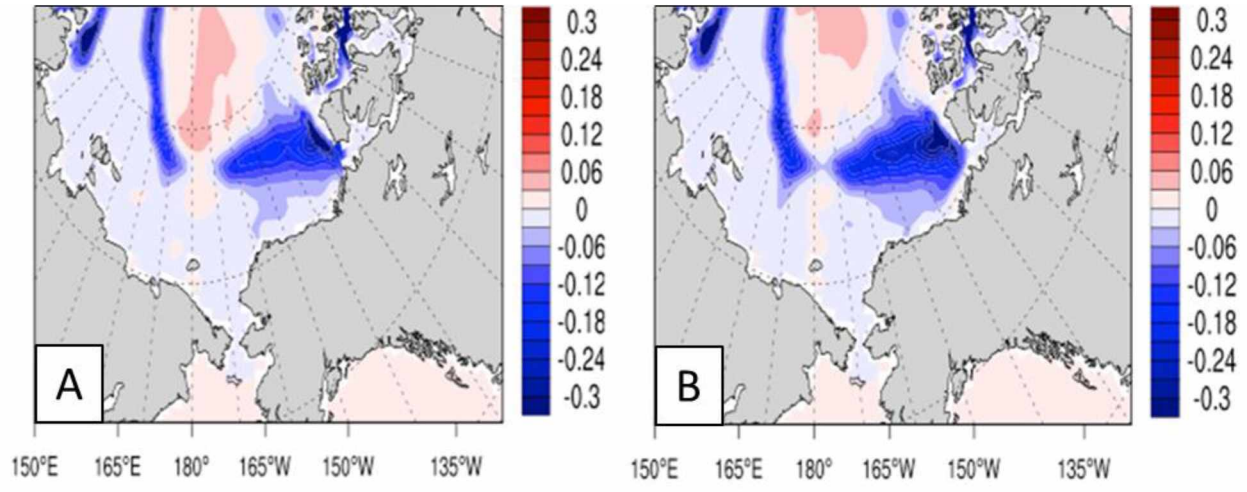


Figure 3.18: Simulated sea ice concentration (Unit: [fraction of 1]) differences between the Control and Dynamic experiments (A), Control and Thermodynamic experiments (B) both valid for August 12, 2012.

### 3.5 Comparison of March 2011 and August 2012 Storms

An important finding in this study is that global climate coupled ocean-sea ice model CICE-POP is able to reproduce the sea ice response to extreme Arctic cyclones (spatial pattern, seasonal variations, dynamic and thermodynamic processes). Verification of CICE-POP output against available observational data showed the sea ice and ocean are well represented in the model data. The model has a positive bias in reproducing ocean temperature in North Atlantic, sea ice area in the Barents Sea, and sea ice thickness in the Canadian Arctic Archipelago, the velocity of sea ice drift along the eastern coast of Greenland is also greater than the observations. Biases of maximum and minimum of model simulated sea ice area vary from year to year and indicate no relation to one another.

The conducted study presents an analysis of two storm cases that occurred over different areas of the Arctic Ocean (Atlantic side and Pacific side of the Arctic) and in different seasons (March and September). Both storms are characteristic for the rapid sea ice area reduction in the area where the storms were occurring. In case of the March 2011 storm, sea ice reduction in the region encompassing the Barents

and Kara Sea was approximately 0.17 $10^6$ $km^2$. In case of the August 2012 storm, sea ice reduction in the area covering the East-Siberian, Chukchi, and Beaufort Seas was approximately 0.95 $10^6$ $km^2$.

Based on the completed analysis of cyclonic forcings on sea ice, it is possible to state that the studied storms resulted in amplification of sea ice, ocean, and atmosphere interactions and sea ice decline. On the basis of the results obtained from the two case studies, we showed that various storm-induced forcings resulted in sea ice reduction and that through time these changes may impact the Arctic weather and climate on short and long-term time scales. The extent of those impacts is left for further analysis.

To understand how much of sea ice loss was resulted from dynamic and how much was from thermodynamic factors, we partitioned prescribed atmospheric forcing utilized by CICE-POP model into thermodynamic forces (air temperature at 2 m, specific humidity, downward shortwave and longwave radiation fluxes) and dynamic factors (surface wind speed and direction, and sea level pressure). This approach enabled to assess actual sea ice loss in comparison to sea ice loss that occurred if only dynamic (or thermodynamic) forcing was considered. Using modified forcing, sensitivity simulations were produced and results analyzed by comparing the output of sensitivity runs with control, unperturbed simulation. We found that there is no clear signal as to whether dynamic mechanisms prevail over thermodynamic or vice versa. For example, in March 2011 storm, the dynamic forcing produced a much stronger reduction of sea ice than thermodynamic forcing, however, in the case of August 2012 storm dynamic and thermodynamic forcings resulted in about equal amount of sea ice reduction. In case of the March 2011 storm, sea ice primarily responded to dynamic forcing in the marginal ice zone in the Barents Sea whilst in case of the August 2012 storm, the dynamic forcing caused sea ice reduction primarily in the coastal areas of the Chukchi, East-Siberian, and Beaufort Seas.

# Chapter 4 Possible Processes and Forcing in Arctic Cyclone Development: A Case Study with WRF Model Simulations

## 4.1 Introduction

The North Atlantic is regarded as one of the world's most cyclonically active regions [*Tsukernik et al.*, 2007]. Intense cyclogenesis in this region is persistently driven by robust baroclinic energy, arising out of contrasting temperature and moisture conditions over the Gulf Stream and Greenland air masses. The high cyclone count over the Atlantic sector of the Arctic Ocean basin extends from the Iceland/Greenland Sea northward into the Barents Sea [*Zhang et al.*, 2004]. Cyclone activity on the Atlantic side of the Arctic has undergone a notable change in recent years that includes a poleward shift of cyclonic tracks, increased cyclonic duration, count, and intensity. Arctic cyclones are key elements in transporting moisture and heat into the Arctic [*Sorteberg and Walsh*, 2008b]. Occasionally, intense cyclones, developing in the Barents/Kara Seas, may lead to extreme and dramatic winter positive temperature and moisture anomalies in the Arctic Ocean [*Boisvert et al.*, 2016]. Sea ice extent and thickness on the Atlantic side of the Arctic has simultaneously experienced rapid and significant decline in recent decades [*NSIDC,* 2016].

The main driving force for mid- and high-latitude cyclogenesis is baroclinic instability [*Eady*, 1949]. Baroclinic instability is strongly dependent on a variety of factors including surface heating, convective instability, reduced static stability, moisture availability, and latent heat release [*Schultz and Vaughan,* 2011]. The release of latent heat as a result of condensation of moisture can contribute notable baroclinic energy to atmospheric eddies, causing the regeneration of a dissipating cyclone [*Branscome et al.,* 1989]. Sea ice and oceanographic conditions are as important to cyclogenesis as the aforementioned factors and vary notably depending on the surface forcing (the ratio of sea ice to open water coverage) [*Walsh et al.,* 1996; *Zhang et al.,* 2004].

Studies show that the high storm count over the Barents/Kara Seas is inconsistent with the variability of sea ice extent in the Barents Sea [*Ruggieri et al.,* 2016]. This contrasts with the observed acceleration of the westerly oceanic inflow by cyclone activity and sea ice reduction in the Barents Sea [*Sorteberg and Kvingedal*, 2006]. Hence, more studies are needed to clarify how cyclone activity interacts with sea ice on the Atlantic Side of the Arctic and what the impact of moisture and ocean heat capacity is on Arctic baroclinic instability.

By employing the high-resolution, state-of-the-art, mesoscale Weather Research and Forecasting Model (WRF) [*Skamarock et al.*, 2008], this study investigated the mechanisms that affected baroclinic instability in the Arctic during the intense cyclone in March 2011.

The underlining objectives for this research were to investigate:

(i) the ability of WRF to reliably reproduce the atmospheric conditions and baroclinic instability during the lifecycle of a cyclone;

(ii) the impact of surface forcing (sea ice and SST);

(iii) the impact of latent heat release (LHR) in the development of the March 2011 cyclone.

This chapter is structured as follows: Synoptic analysis of the storm case is given in Section 4.2; Section 4.3 summarizes the configuration and forcing of the WRF model; a model validation assessment is given in Section 4.5; the model experimental design is described in Section 4.4; the impact of sea ice concentration, SST and latent heat release on the cyclonic lifecycle is discussed in Sections 4.6.2 and 4.6.3, respectively; and the conclusions are given in Section 4.7.

## 4.2 Synoptic Analysis for March 16 – 22, 2011

A low pressure system developed over northeast Greenland on March 16, 2011 (Fig. 4.1A). This Parent Cyclone (PC) moved north from March 16 until March 18. On March 18, the PC stalled over the North Pole as a decaying cold-core cyclone with a central sea level pressure of 972 hPa (Fig. 4.1B). The poleward movement of the PC favored advection of warm air masses from the North Atlantic Ocean along the Eurasian Arctic coast into the Central Arctic. Heat and moisture brought by the PC into the Central Arctic Ocean further increased the temperature gradient and baroclinic instability in the Barents-Kara Sea region. The increased temperature gradient in the North Atlantic and Barents-Kara Seas regions prompted the occurrence of a secondary mesocyclone (MC) that developed in the wake of the PC (Fig 4.1B). After developing in the North Atlantic, the MC moved into the Laptev Sea on March 18 and approached the stalled and decaying PC. On March 19, the PC regenerated after merging with the MC and formed the new, very deep, low pressure system (967 hPa), the Regenerated Cyclone (RC). Before merging with the PC, the MC was a developing low pressure system with robust warm and cold sectors. The warm and moist air of the MC entering the reservoir of cold air in the PC re-enforced the temperature gradient (Fig. 4.1C). After regeneration, the central sea level pressure in the RC experienced a notable drop by ~30 hPa to 945 hPa within 24 hours (Fig 4.1C). The RC was later cut off from the warm sector, which led to gradual weakening and dissipation on March 22, 2011 (Fig 4.1E).

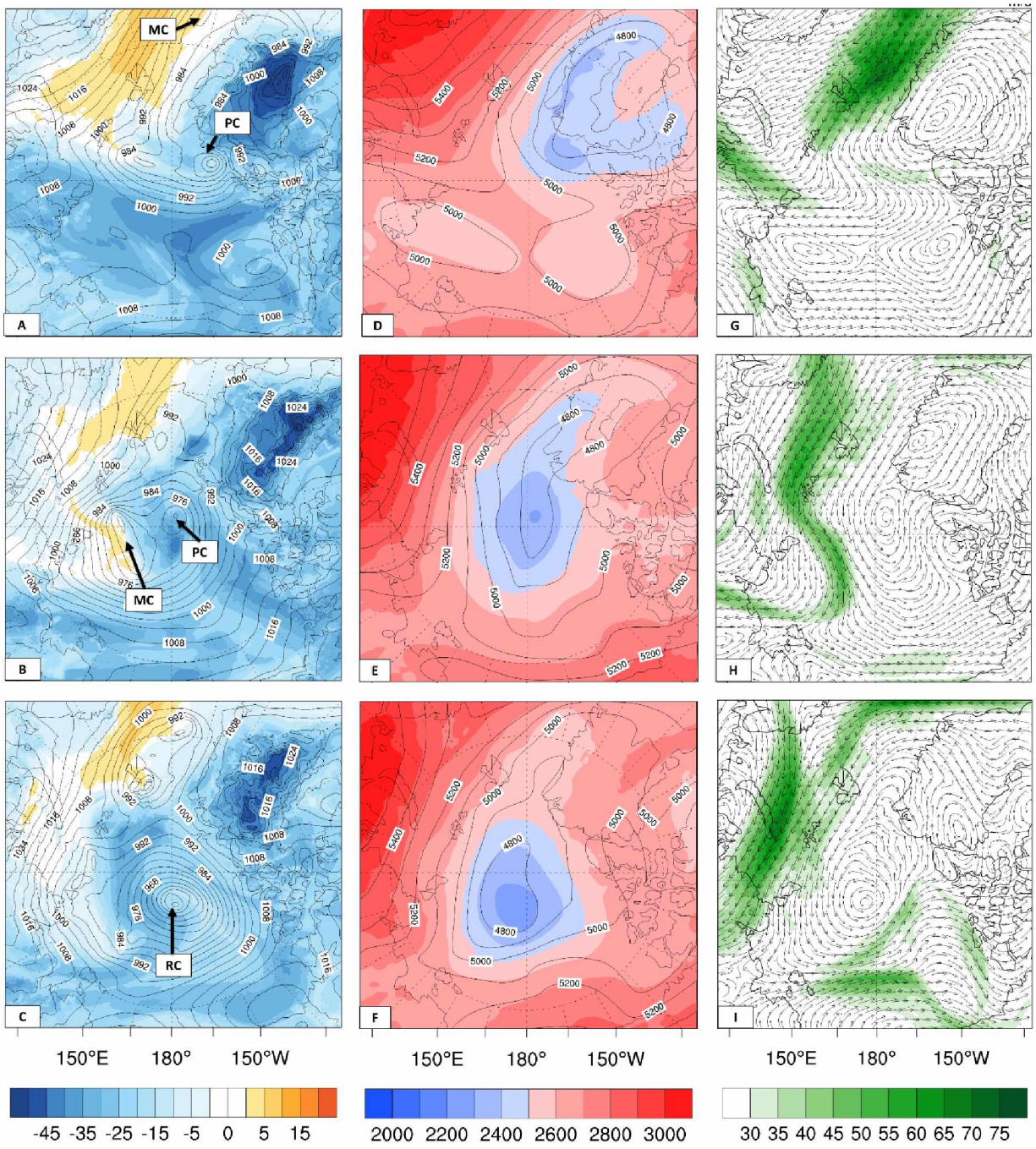


Figure 4.1: Simulated sea level pressure (contours) (Unit: [hPa]) and surface air temperature (shaded) (Unit: [°C]) valid for March 16 1200 UTC (A); March 18 1800 UTC (B); March 19 1800 UTC (C). Simulated geopotential height 700 hPa (shaded) over 500 hPa (contours) (Unit: [gpdm]) valid for March 16 1200 UTC (D); March 18 1800 UTC (E); March 19, 1800 UTC (F). Simulated jet stream at 300 hPa (Unit: [m/s]) valid for March 16 1200 UTC (G); March 18 1800 UTC (H); March 19 1800 UTC (I).

An upper-level jet existed above the surface temperature gradient (Fig. 4.1G). The PC developed over northeast Greenland, co-locating the near left exit region of the upper-level jet where ageostrophic divergence aloft promoted vertical ascent. The upper-level jet at H300 strengthened over Novaya Zemlya and the Taimyr Peninsula while a secondary jet wrapped the Canadian side of the RC (Fig. 4.1I). As indicated by the upper-level atmospheric conditions, the upper-level low and the surface PC were not co-located (Fig. 4.1D, 4.1E). On March 19, the centers of the RC and the upper-level low became stacked upon each other indicating the occluded stage of the low pressure system development (Fig. 4.1F).

### 4.3 Model Configuration

To examine the physical processes responsible for cyclone formation, a series of modeling experiments using version 3.2.1 of the Weather Research and Forecasting (WRF) model were conducted. WRF is a fully compressible and non-hydrostatic Eulerian model that can be used for both idealized and real data applications and applied to the Arctic domain. The European Reanalysis Interim (ERA-Interim), produced by the European Center for Medium-Range Weather Forecasts (ECMWF), was utilized as a source of initial and boundary conditions data. ERA-Interim has a T255 resolution (approximately 0.7 ° x0.7°) and is available at 37 vertical levels for the period from 1979 to present [*Dee et al.,* 2011]. The analysis considers output from March 15 at 0000 UTC onwards, in order to allow for a spin up period of at least 30 hours for all of the simulations. WRF was integrated for ~180 hours. All runs are made with SST and fractional sea ice concentration (SIC) updates every 6 hours. Two domains with 30 km (290×280 grid points) and 10 km (400×430 grid points) grid increments were nested via a two-way approach. The initial data were interpolated to 33 vertical levels with a top pressure of 10 hPa.

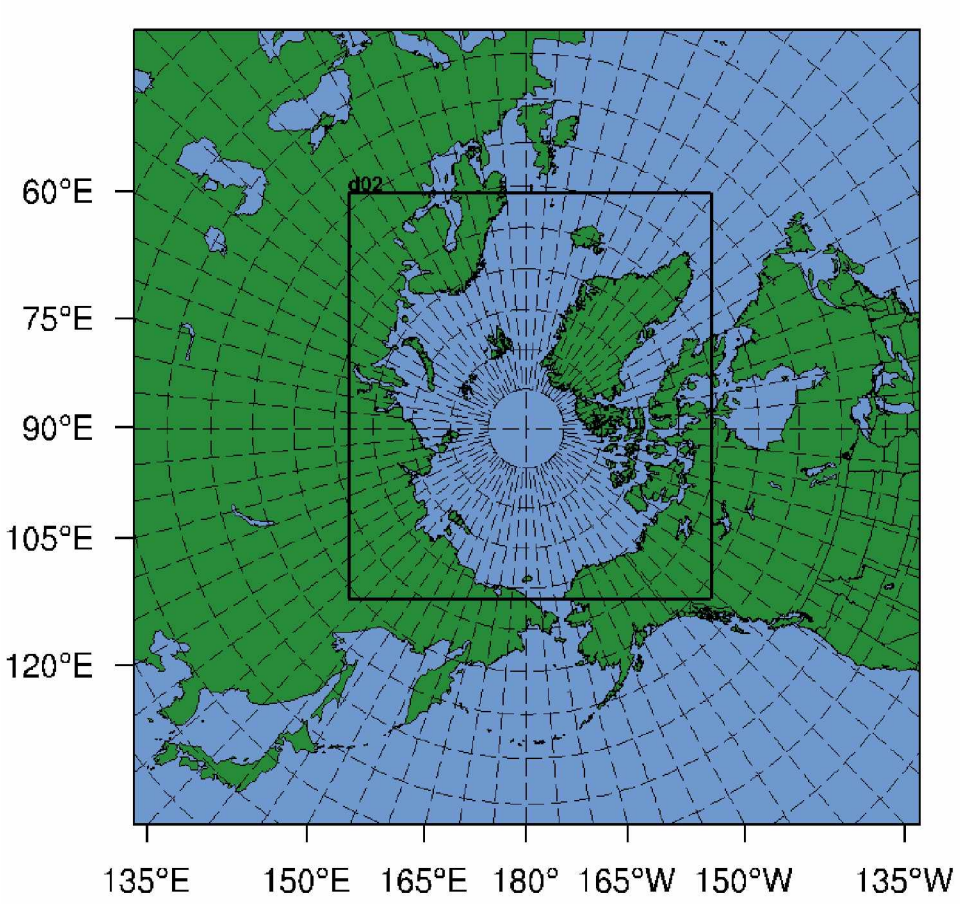


Figure 4.2: Modeling domains for WRF simulation of cyclogenesis in the case study of March 2011 cyclone.

### 4.4 Model Experimental Design

An ensemble set of seven model simulations was obtained by using different initialization times was used to identify robustness of the key findings in the March 2011 Arctic cyclone simulation. Each ensemble simulation was initialized three hours apart. This setup allowed simulation of the storm using perturbed initial conditions. The ensemble simulations utilized identical lateral and surface boundary conditions. The first ensemble member was initialized on March 14, 1700 UTC. The last ensemble member was initialized on March 15, 1500 UTC. All simulations ran to March 22, 1200 UTC.

Ensemble simulations were conducted for each of the modeling experiments: Control (CTR), climatological (CLIM), and no latent heat consumption or release during phase transition processes (DRY). Analysis of the ensemble mean was conducted on all three experiments (Table 4.1). The control experiment

was configured using unperturbed ERA-Interim atmospheric forcing data for March 2011. Similar atmospheric forcing data were utilized for the climatological experiment (CLIM) with the exception that the observed SST and SIC were replaced with climatological mean values averaged daily from 1981 to 2010. SST and SIC data for CLIM was obtained from the NOAA Optimum Interpolation Analysis version 2 [*Reynolds et al., 2002*].

Table 4.1: Suite of WRF simulations that were analyzed in this study

| | CTR | CLIM | DRY |
|---|---|---|---|
| Sea ice concentration | 16 – 22 March 2011 | 16 – 22 March daily climatology 1981-2011 | 16 – 22 March 2011 |
| SST | 16 – 22 March 2011 | 16 – 22 March daily climatology 1982-2011 | 16 – 22 March 2011 |
| Latent Heat Release | Yes | Yes | No |

The latent heat experiment was configured similar to CTR with the exception that the release of latent heat was set to 0 at every time step of the integration.

### 4.5 Model Validation

The model validation presented in this study utilized multiple sources of observational data, including surface stations, sounding sites, and reanalysis products. In order to quantify the errors, a normalized root mean squared error (*NRMSE*) was calculated by normalizing the bias to the standard deviation ($\sigma_0$) of the observations as given by:

$$NRMSE = \sqrt{\frac{\sum_{i=1}^{n}\left(\frac{x_{s_i} - x_{o_i}}{\sigma_o}\right)^2}{N}} \tag{4.1}$$

where $N$ is the total number of data points, $x_s$ is the simulated value, and $x_o$ is the observed value. The model validation assessment was performed by using the observed meteorological data of 101 Arctic coastal stations for surface air temperature, dew point temperature, sea level pressure, wind direction and speed. The simulation with the smallest errors was deemed the best performing one. It is clear from the low NRMSE for the Arctic Ocean domain that the WRF simulation with ERA-Interim is realistic in reproducing the coastal station data (Fig. 4.3). Wind direction has the highest error.

The lowest error, hence, closest alignment between simulated and observed data, is found for sea level pressure and surface air temperature.

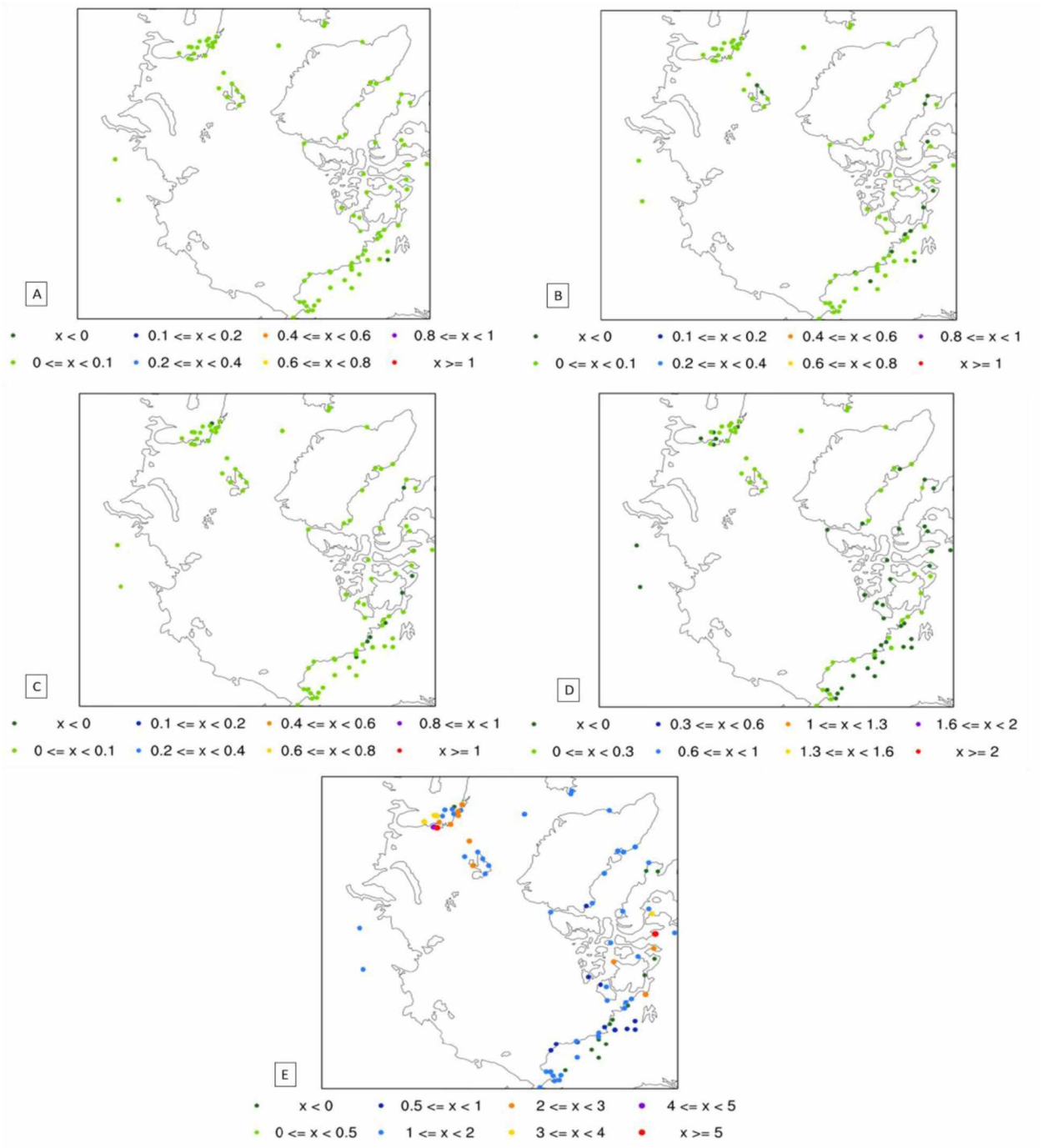


Figure 4.3: Normalized Root Mean Square Errors of WRF-simulated surface air temperature (A), dew point temperature (B), sea level pressure (C), surface wind speed (D), and direction (E) during March 16 to March 22 2011.

The WRF vertical atmospheric profiles from 925 hPa to 100 hPa were validated against three radiosonde sites (ENAS, ENBJ, ENJA) in Svalbard and Scandinavia. Table 4.2 summarizes the statistical measures of model performance: NRMSE, root mean square errors (RMSE), and unbiased RMSE (URMSE) for each of the sounding sites

Table 4.2: Statistical evaluation of WRF-simulated air temperature, dew point temperature, geopotential height, and wind speed against five sounding sites: ENAS – Ny-Alesund (78.91N; 11.93E), ENBJ – Bjornoya (74.5N; 19.5E), ENJA – Jan Mayen (70.93N; 8.66W).

| | Air Temperature | Dew Point Temperature | Geopotential Height | Wind Speed |
|---|---|---|---|---|
| | Correlation | | | |
| ENAS | 0.98 | 0.97 | 1 | 0.86 |
| ENBJ | 0.99 | 0.98 | 1 | 0.94 |
| ENJA | 0.98 | 0.96 | 1 | 0.78 |
| | Air Temperature (°C) | Dew Point Temperature (°C) | Geopotential Height (m) | Wind Speed (m/s) |
| | RMSE | | | |
| ENAS | 4.53 | 5.54 | 64.06 | 6.05 |
| ENBJ | 6.14 | 11.75 | 123.11 | 7.16 |
| ENJA | 4.9 | 8.23 | 84.85 | 12.75 |
| | URMSE | | | |
| ENAS | 2.28 | 1.27 | 34.61 | 0.44 |
| ENBJ | 3.32 | 4.9 | 116.9 | 3.6 |
| ENJA | 4.63 | 7.4 | 64.63 | 9.33 |
| | Mean Bias | | | |
| ENAS | 3.92 | 5.39 | 53.91 | 6.04 |
| ENBJ | 5.17 | 10.68 | 38.61 | 6.19 |
| ENJA | -1.6 | -3.6 | 54.98 | -8.7 |

Two WRF vertical profiles obtained on March 16, 1200 UTC and on March 19, 1200 UTC were compared against the sounding made at the ENAS station (Fig. 4.4). Given the high correlation coefficients and low statistical errors, it can be concluded that WRF realistically reproduced the vertical profiles of the atmosphere at the initial (March 16) and mature stage (March 19) of the March 2011 cyclone.

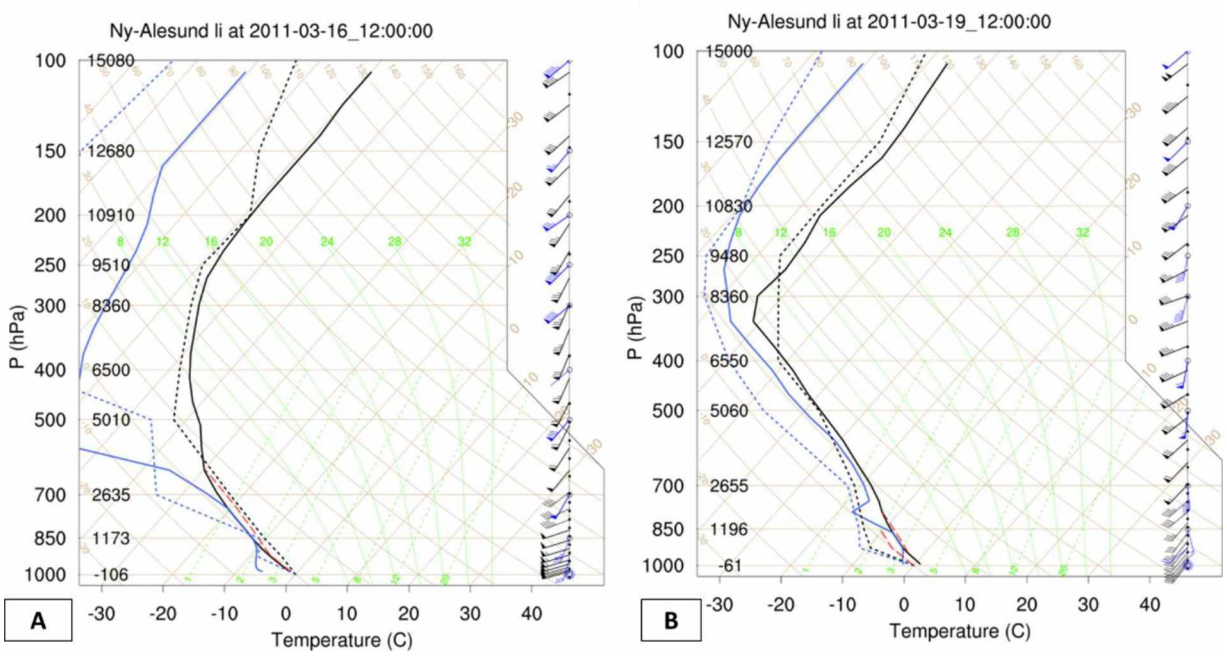


Figure 4.4: Simulated atmospheric vertical profile (black) and observed (blue) at Ny Alesund (78.92N, 11.9E) valid for March 16 1200 UTC (A) and March 19 1200 UTC (B). The dashed red curve is the wet adiabatic curve.

## 4.6 Results and Discussions

### 4.6.1 Baroclinic Instability

As pointed out by *Eady* [1949], a number of diagnostic parameters can be used for analyzing baroclinicity, including the Eady growth rate (*EGR*), which is employed here (Eq. 4.2). The EGR is given as:

$$EGR = 0.31 \frac{f}{N} \left| \frac{\partial v}{\partial z} \right| \tag{4.2}$$

where $f$ denotes the Coriolis parameter, $N$ is the Brunt-Väisälä frequency, $z$ is the vertical distance, and $v$ is the horizontal wind vector. EGR is used to localize baroclinic zones both horizontally and vertically within the troposphere (Fig. 4.5). Throughout the lifetime of the March 2011 cyclone, the observed baroclinic zone extended from ~ 850 hPa to ~ 600 hPa indicating deep baroclinicity. It was found that the maximum values of baroclinic instability were between 700-600 hPa prior to the regeneration of Arctic cyclone (Fig. 4.5A, 4.5B), and between 850-700 hPa after its regeneration (Fig. 4.5C). The lowering of the altitude of the

maximum baroclinic instability is explained in more detail in Section 4.6.3. The area of increased EGR forms a comma shape, characteristic of extratropical low pressure system, and resembles the pattern of the maximum surface temperature gradient. EGR is increasing with time corresponding to the deepening of the low pressure system and increasing temperature gradient. As the MC and, associated with the MC, the warm sector moved poleward, the baroclinic instability in the atmosphere over the Arctic Ocean amplified. On March 19, 1200 UTC, the EGR reached its maximum in the East Siberian Sea while the pattern of increased EGR assumed the characteristic mid-latitude cyclonic "comma" shape.

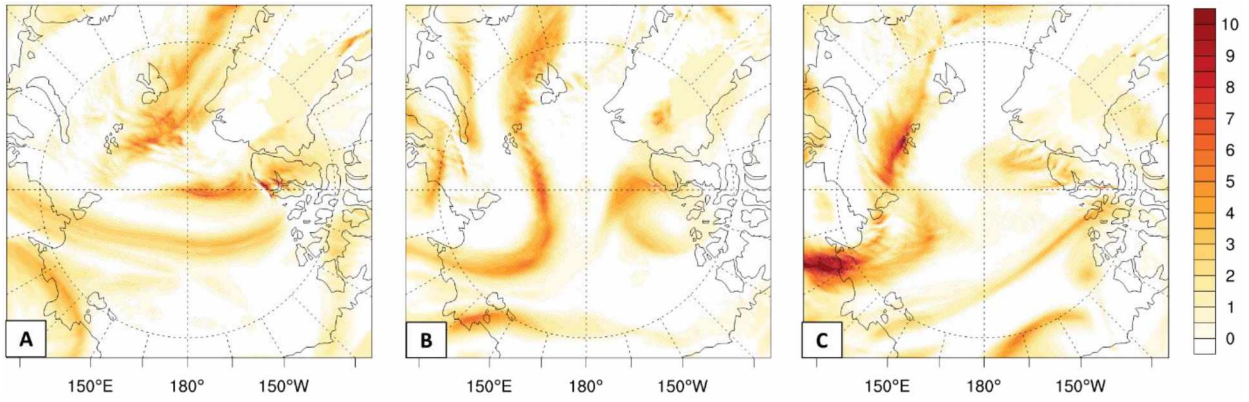


Figure 4.5: Simulated Eady growth rate at 700 hPa (Unit: [day$^{-1}$]) valid for March 17 0600 UTC (A); March 19 1200 UTC (B); March 20 0800 UTC (V).

$$Heat\ advection = u_{lat}\frac{\partial T}{\partial (lat)} + u_{lon}\frac{\partial T}{\partial (lon)} \tag{4.3}$$

In the Arctic, increased EGR is associated with amplified baroclinic instability due to the movement of heat and moisture from the North Atlantic into the Arctic (Fig. 4.6).

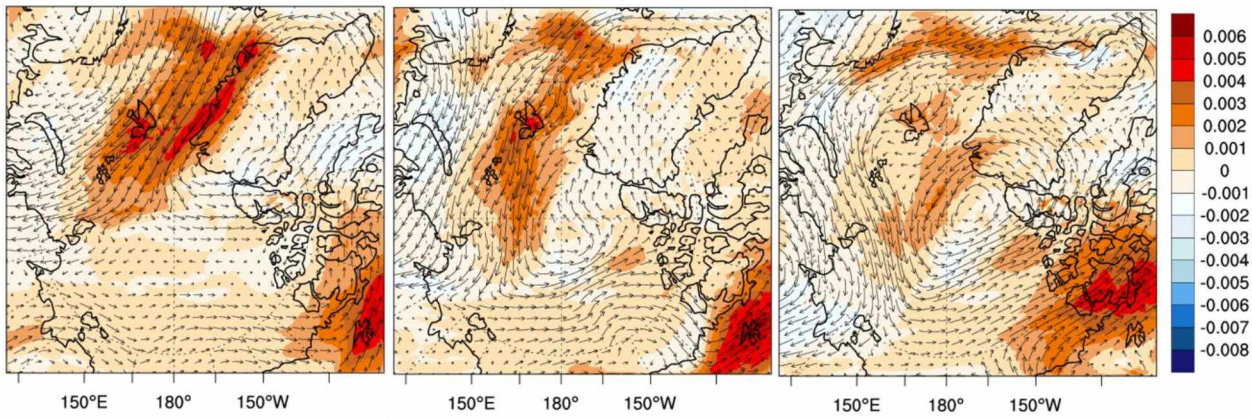


Figure 4.6: Simulated heat advection at 500 hPa (Unit: [K s$^{-1}$]) valid for March 17 0600 UTC (A); March 19 1200 UTC (B); March 20, 0800 UTC (C).

This advection, in turn, resulted in increased baroclinicity in the Arctic and the prolonged lifecycle of the March 2011 cyclone. The following mechanisms were investigated in relation to the increased baroclinic instability during the cyclone: Decreased SIC and elevated SST (4.6.2), and latent heat release (4.6.3).

### 4.6.2 Sensitivity to Decreased Sea Ice Concentration and Elevated SST

According to National Snow and Ice Data Center, the observed sea ice extent in March 2011 was lower than the 1979-2011 climatology by 1.2 $10^6$ $km^2$. Reduced sea ice cover on the Atlantic side of the Arctic, and the associated larger open water exposure with relatively warm SST in March 2011 could be responsible for providing moisture and heat fluxes that triggered and sustained the development of an intense cyclone. To test the validity of this hypothesis, the difference between CTR and CLIM experiments were analyzed. In order to capture the impact of sea ice/SST on baroclinicity in the low- and mid-troposphere during the March 2011 cyclone, the following fields from the output of ensemble mean CTR and CLIM simulations were analyzed: turbulent heat fluxes (sensible and latent heat), sea level pressure (SLP), surface air temperature (SAT), geopotential height H700, and air temperature at 700 hPa.

By using the NOAA Optimum Interpolation Analysis version 2 sea ice concentration data, the difference of observed SST, sea ice concentration averaged over March 16 to March 22, 2011, and SST, sea ice concentration averaged over the same days but using the observed data of 1981-2011 were computed. Sea ice areal coverage in the Barents Sea is significantly lower in 2011 compared to the 29-year climatology (Fig. 4.7B). The difference between the two simulations shows increased SST (Fig. 4.7A) over the areas of pronounced sea ice areal decline, primarily over the Barents and Greenland Seas (Fig. 4.7B). In the marginal ice zone in the Southern Barents Sea, negative SST differences correspond to openings in the sea ice pack in the CLIM cases where SST was higher than in the CTR cases where, due to the wind-induced mixing of water, SST was lower.

The reduced sea ice area in March 2011 led to amplified surface turbulent sensible and latent heat fluxes (Fig. 4.7E and 4.7C). Positive turbulent heat fluxes are defined upward. The difference between the CTR and CLIM experiments shows that sensible and latent heat fluxes were greater in the North Atlantic by 50-100 $W/m^2$ (Fig. 4.7E) and 40-50 $W/m^2$ during the March 2011 cyclone as compared to climatology (Fig. 4.7F). Increased release of turbulent heat fluxes into the atmospheric boundary layer is found over the marginal ice zone along the eastern coast of Greenland and western coast of Novaya Zemlya. Maximum differences of 300-400 $W/m^2$ were found along the sea ice edge. Increasing heat and moisture content of the boundary layer and the reduction of sea ice caused elevated baroclinic instability in the lower atmosphere. The relationship between low-level baroclinicity and surface fluxes is in agreement with *Van*

*Loon* [1967], who found that a release of latent heat may increase atmospheric baroclinicity. In March 2011, elevated SST and turbulent heat fluxes promoted an increase in near-surface air temperatures over the eastern Barents and western Kara Seas of 2K (Fig. 4.7G). The greater sea ice area in CLIM diminished surface turbulent heat fluxes, thereby, decreasing the heat and moisture content of the air over the Barents-Kara Sea region as compared to the CTR case.

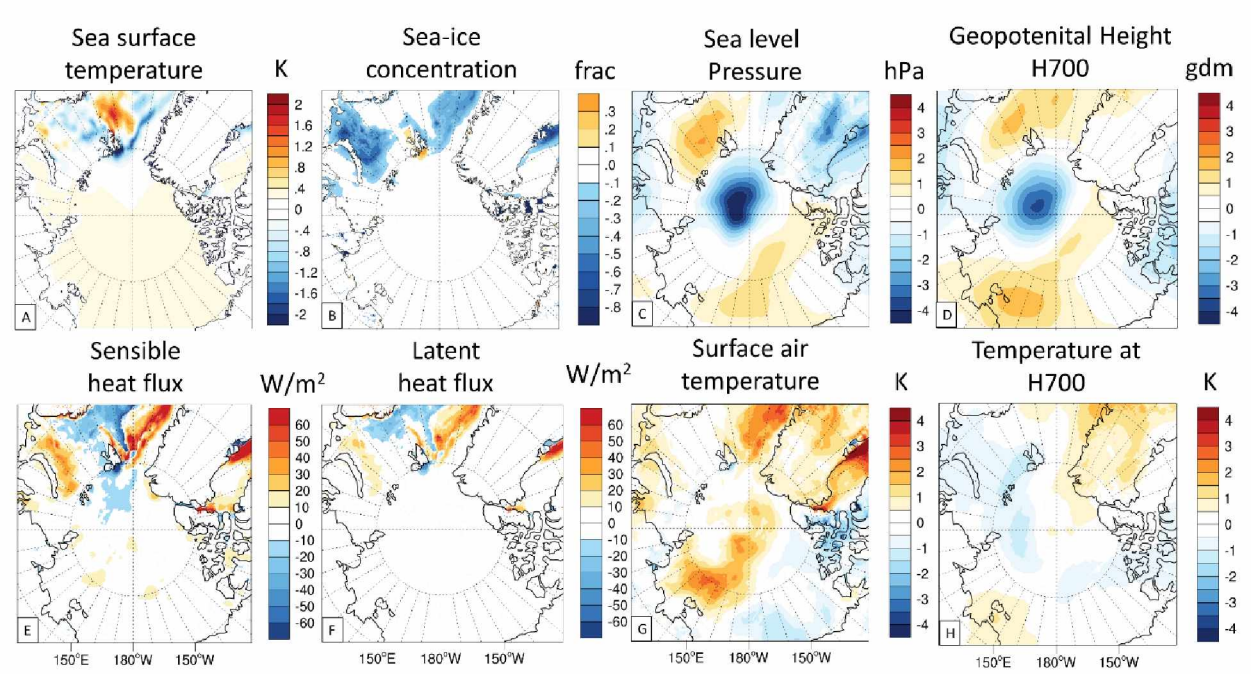


Figure 4.7: CTR – CLIM mean difference for SST (Unit: [K]) (A), SIC (Unit: [fraction of 1]) (B), sea level pressure (Unit: [hPa]) (C), geopotential height 700 hPa (Unit: [gdm]) (D), latent heat flux (Unit: [W $m^{-2}$]) (E), sensible heat flux (Unit: [W $m^{-2}$]) (F), surface air temperature (Unit: [K]) (G), temperature at 700 hPa (Unit: [K]) (H).

Alternation of sea ice / SST conditions during the March 2011 cyclone stimulated a poleward shift of the area of increased baroclinicity (Fig. 4.5). The physical mechanism behind the baroclinicty shift is two-fold: (1) Increased surface warming due to reduced sea ice area and increased SST in March 2011, and (2) MC driven transport of this heat surplus towards the center of the PC. The increased warming that occurred during the March 2011 cyclone shows in the positive air temperature difference along the Eurasian Arctic coast and in the mid-Arctic troposphere at 700 hPa (Fig. 4.7G, 4.7H). The maximum difference of air temperature over the Laptev Sea reached 6K at the surface and 2K at 700 hPa. The positive air temperature difference indicates a more pronounced and long-lasting warm air advection in CTR than in CLIM.

The March 2011 SST and SIC conditions played an important role in intensifying the dynamic development of the March 2011 cyclone. As manifested by a deeper surface low in the CTR compared to CLIM experiment, warm air advection from the North Atlantic into the Central Arctic caused air column stretching along the Eurasian coast. Based on the SLP and geopotential height fields, it can be concluded that the reduced SIC and elevated SST resulted in steepening the sea level pressure / geopotential height gradient. Negative sea level pressure and 700hPa geopotential height differences of -6 hPa (Fig. 4.7C) and -3.5 gdm (Fig. 4.7D) occurred in the center Arctic Ocean while positive SLP and geopotential height differences of 2 hPa (Fig. 4.7C) and 3 gdm (Fig. 4.7D) occurred over the Eurasian Arctic Coast on the periphery of the March 2011 cyclone. The sea level pressure gradient between the center and periphery was over 10 hPa greater in CTR than in CLIM (Fig. 4.7C). Given the pattern and magnitude of the SLP and geopotential height mean difference fields, it therefore can be inferred that perturbed SST and SIC conditions resulted in cyclonic deepening and amplified cyclonic vorticity (Fig. 4.7C, 4.7D).

In order to investigate the impact of SIC and SST conditions at various phases of the March 2011 cyclone development, the time series of central sea level pressure in the PC, MC, and RC phase were used (Fig. 4.8). In the PC, central SLP was close in magnitude in both CTR and CLIM cases while in the MC, central SLP was 5-10 hPa lower in CTR than in CLIM. In the MC, the lower central SLP indicates deeper and, hence, a more intense, low pressure system. As such, it can be stated for the MC in CTR that it developed under elevated baroclinic instability conditions that were driven by unperturbed SIC and SST conditions in CTR.

Based on time series, it was found that the anomalous SIC conditions of March 2011 had an impact on cyclonic regeneration. Under modified SIC and SST conditions in CLIM, regeneration of the PC was noticeably weaker than in CTR. The rate of deepening of the cyclone after the PC merged with the MC in CTR was greater by 10 hPa/12 hours: 35 hPa/12 hours in CTR in contrast 25 hPa/12 hours in CLIM. In addition, the time series demonstrated that reduced SIC and elevated SST led to a prolonged lifecycle of the March 2011 cyclone. In the CTR case, the RC decayed on March 21 1200 UTC, while in CLIM, the RC decayed 36 hours earlier, on March 20 0000 UTC. Also, the merging of the PC and MC occurred 12 hours earlier in CLIM than in CTR: March 19 0000 UTC in CLIM as opposed to March 19 1200 UTC (Fig. 4.8). The March 2011 sea ice and SST conditions imposed a profound impact on cyclone dynamic and thermodynamic development resulting in elevated baroclinic instability in the lower atmosphere, increased near-surface and mid-troposphere warming over the Central and Eurasian Arctic, greater intensity, and a more prolonged lifecycle of the cyclone with sea ice conditions observed in March 2011 as compared to monthly average March sea ice conditions (1981-2011).

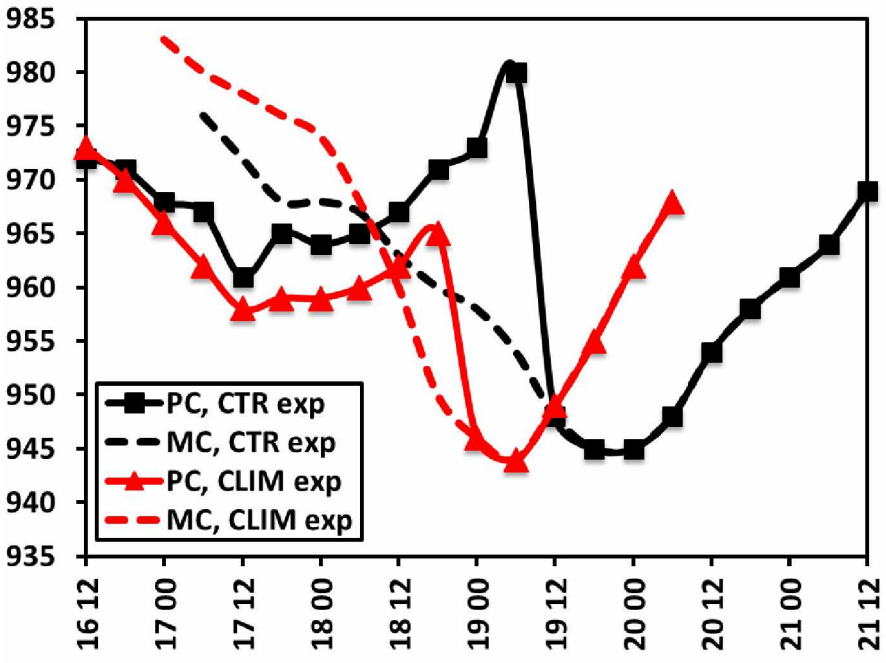


Figure 4.8: Central sea level pressure (Unit: [hPa]) of the PC and MC in the CTR and CLIM experiments.

### 4.6.3 Sensitivity to Latent Heat Release

The process of LHR refers to the release of energy as a result of vertical ascent of air, cooling down and developing condensation. The hypothesis was that the released latent heat during the condensation of warm and moist Atlantic air caused the explosive deepening and regeneration of the March 2011 cyclone. In order to test the validity of this hypothesis, simulated LHR in CTR and a series of atmospheric parameters simulated in CTR and DRY experiments were analyzed.

To capture the spatial distribution of the maximum released latent heat in the Arctic Ocean during the March 2011 cyclone, the simulated LHR in CTR were analyzed. Vertically-integrated LHR fields from the surface up to 100 hPa were calculated and analyzed at three times that corresponded to the various phases of cyclonic development: The initial phase on March 16 1200 UTC (Fig. 4.9A), the mature phase on March 18 2200 UTC (Fig. 4.9B), and the cyclonic decay on March 22 1200 UTC (Fig. 4.9C). The areas of maximum latent heat release in the Arctic (Fig. 4.9) encompass the Norwegian-Barents and East-Siberian Seas and co-located regions of elevated baroclinic instability (Fig. 4.5). The increased LHR over the ice-free Norwegian and Barents Seas is explained by the elevated surface air temperature gradient and ongoing condensation of the warm and moist air that was being advected from the North Atlantic during the March 2011 cyclone. A localized LHR maximum in the East-Siberian Sea occurred on March 18, 2200 UTC during the regeneration of the cyclone (Fig. 4.9b). On that day, the release of latent heat was estimated to

be roughly $2\times10^9$ J $kg^{-1}m^{-2}day^{-1}$; this amount is comparatively higher than on March 16 (Fig. 4.9A) and March 22 (Fig. 4.9C). The increased vertical motion on March 18 2000 UTC was caused by the ascent of advected warmer Atlantic air into the cooler Arctic Ocean, its ascent aloft, subsequent cooling, and condensation. On March 18 2000 UTC, the maximum vertical wind speed was approximately 0.4 m/s at levels 925 hPa up through 500 hPa (Fig. 4.9B). This vertical speed was high compared to the near-zero ascent of air on March 16 1200 UTC (Fig. 4.9A) and descent of -0.2 to -0.1 m/s on March 22 1200 UTC (Fig. 4.9C).

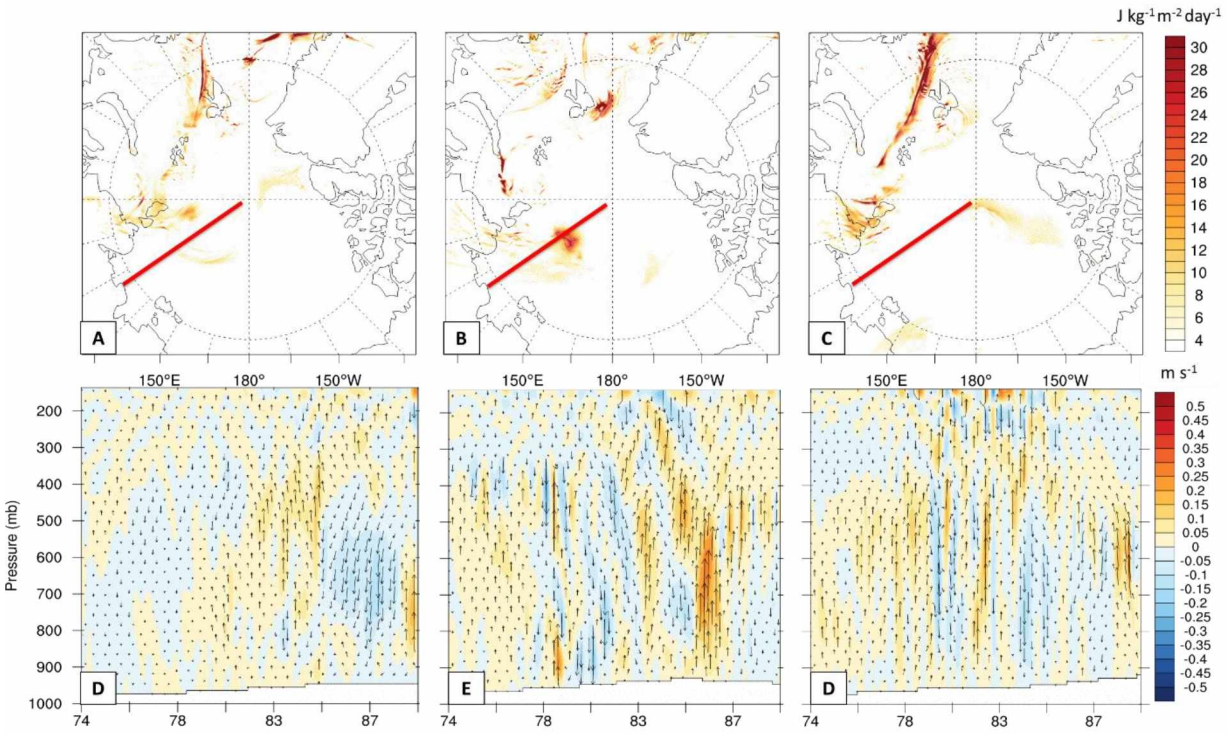


Figure 4.9: Vertically-integrated latent heat release (Unit: [J $kg^{-1}m^{-2}day^{-1}$]) valid for March 16 1200 UTC (a); March 18 1800 UTC (b); March 22 1200 UTC (c) and cross-section of CTR vertical motion (Unit: [m $s^{-1}$]) along (70N, 125E) – (90N, 125E) valid for March 16 1200 UTC (a); March 18 1800 UTC (b); March 22 1200 UTC (c).

On March 18 2000 UTC, the warm sector of the MC reached the cold-core of the PC that at that time, was centered over the East-Siberian Sea. The notable temperature difference between the cold air of the PC and warmer, more humid, air of the warm sector of the MC led to the increased ascent of warm and moist air aloft and its subsequent condensation. When moisture condensed, the released latent heat added additional baroclinic energy into the mid troposphere, increased the temperature gradient between the cold and warm sectors of the storm, and reinforced baroclinicity in the low- and mid- troposphere. A rapid spin

up of the cyclone, or "seclusion" occurred as LHR was introduced to the PC. By releasing latent heat, air in the warm sector became more buoyant resulting in air column stretching, causing increased vorticity.

To assess the vertical distribution of LHR over the East-Siberian Sea, the vertical profile of released latent heat at different atmospheric levels from the surface up to 100 hPa for March 18, 2200 UTC was analyzed (Fig. 4.10). LHR was maximum at two levels: 925 hPa and 750 hPa with ~$2.2\times10^{8}$ J $kg^{-1}m^{-2}day^{-1}$ and ~$0.5\times10^{8}$ J $kg^{-1}m^{-2}day^{-1}$, respectively. Owing to the released latent heat and a subsequent increase of baroclinic energy aloft, the tropospheric height at which the maximum EGR occurred shifted to 850 – 700 hPa as pointed out in Section 4.6.1.

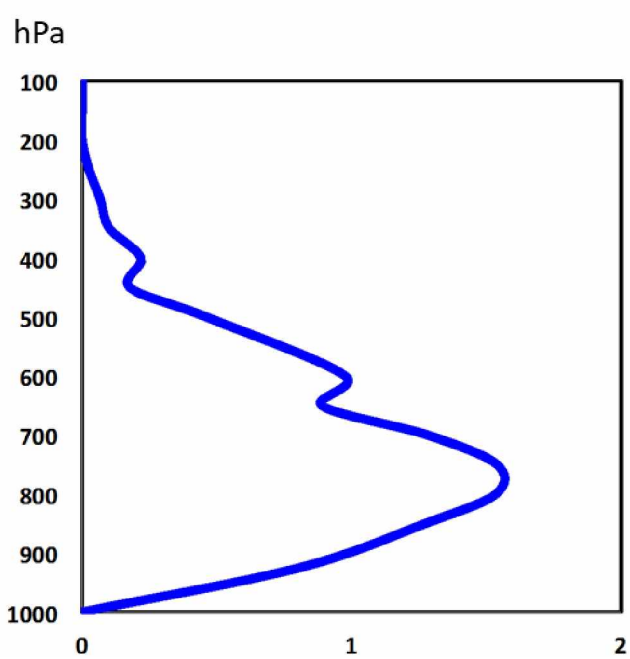


Figure 4.10: Vertical profile of released latent heat (Unit [$10^{8}$ J $kg^{-1}m^{-2}day^{-1}$]) on March 18, 1800 UTC at (81N, 125E).

Analysis of the LHR impact on the cyclonic development, before and after the regeneration of the cyclone was carried out by investigating the mean difference between DRY and CTR for the following variables: SAT; temperature at 700 hPa; SLP; and geopotential height 700 hPa. The CTR-DRY differences of air temperature, SLP, and geopotential height fields were near-zero at times prior to the regeneration of the PC, indicating an insignificant contribution of LHR to baroclinic energy (Fig. 4.11A-D). In contrast, after the regeneration of the PC, the CTR-DRY differences of SLP decreased while those of air temperature increased, proving that the release of latent heat aided the development of RC (Fig. 4.11E-H).

At times after regeneration, the minimum difference of mean SLP between CTR and DRY is negative (-12 hPa) while the maximum difference is positive (5 hPa). Similarly, the minimum difference of geopotential height at 700 hPa between CTR and DRY is negative (-5 gdm) north of Severnaya Zemlya archipelago and positive (3 gdm) over the Canadian Arctic Archipelago (Fig. 4.11B; 4.11D). The pattern of negative SLP and geopotential height mean differences encompassed the areas of the Laptev, East Siberian Sea, and extended into the Central Arctic Ocean. The negative CTR-DRY differences of SLP and geopotential height 700hPa indicated that, owing to LHR, the depth (e.g., intensity) of the March 2011 cyclone lowered (e.g., increased) in both the near-surface and mid troposphere.

In the Central Arctic Ocean, the heat content increased after the regeneration of the cyclone, as is indicated by the CTR-DRY difference of surface and 700 hPa air temperatures. At the surface, the CTR-DRY air temperature differences are positive (2-3 K) over the East Siberian Sea and Central Arctic Ocean (Fig. 4.11F). The area with positive CTR-DRY air temperature differences has the comma shape characteristic of synoptic cyclones (Fig. 4.11G; 4.11H). The maximum CTR-DRY temperature difference is found over the North Atlantic with a near-surface air temperature difference of 8K, and over the Northern East-Siberian Sea with a difference of 6K.

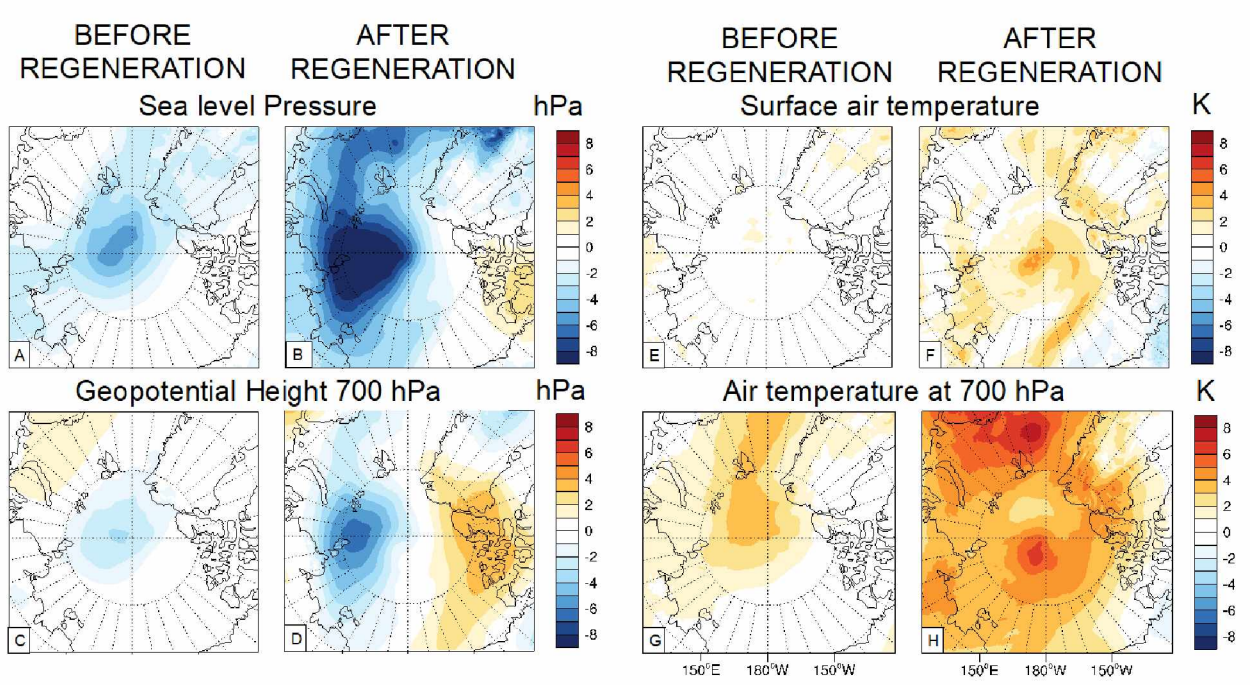


Figure 4.11: CTR – DRY mean differences for sea level pressure Unit: [hPa]) before (A) and after (E) the regeneration; geopotential height at 700 hPa (Unit: [gdm]) before (B) and after (F) the regeneration; surface air temperature (Unit: [K]) before (C) and after (G) the regeneration; air temperature at 700 hPa (Unit: [K]) before (D) and after (H) the regeneration.

In order to better capture the timing of LHR impacts on cyclogenesis, the time series of SLP in the center of the cyclones (PC, MC, and RC) in CTR and DRY experiments were compared (Fig. 4.12). The central SLP of the PC and MC in the DRY case is similar to that in the CTR case indicating that LHR negligibly contributed to the baroclinic energy of the cyclone. After regenerating on March 19, in the RC, the central SLP was 25 hPa lower in CTR than in DRY. Therefore, LHR that was included in CTR had a critical role in the rejuvenation and explosive deepening of the cyclone. Lacking additional baroclinic energy from LHR in DRY, the cyclone was unable to re-develop and continued to slowly decay until it fully dissipated on March 21. Based on the comparison of the CTR and DRY experiments, the release of latent heat had a paramount role in altering the dynamic and thermodynamic structure of the cyclone by contributing additional baroclinic energy and increasing the cyclonic lifecycle.

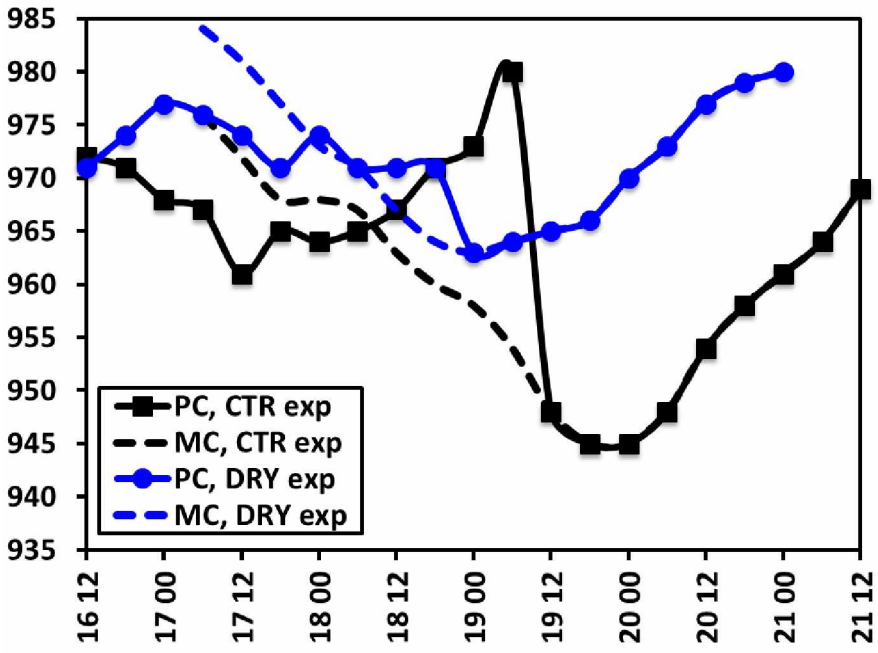


Figure 4.12: Central sea level pressure (Unit: [hPa]) of the PC and MC in the CTR and DRY experiments.

## Chapter 5 Conclusions and Discussions

Arctic storms and sea ice present a complex coupled interaction within the Arctic Climate System. This study focused on investigating the physical processes of ocean – sea ice interaction, in the context of storm dynamics, occurring within the Arctic atmosphere. Combined climatology and case studies, as well as output data from several climate models, were utilized in order to enable the differentiation of processes between ones that occur on a climatological scale versus those that are storm-specific. The coupling mechanisms of the Arctic sea ice – storm interaction can be separated into two main categories: impact of storms on sea ice, and impact of sea ice on storms. The impact of Arctic storms on sea ice is classified as dynamic, i.e., related to wind forcing, or thermodynamic, i.e., related to thermal changes of sea ice. Multiple findings emerged from the research study into sea ice – storm interaction in the Arctic; these are summarized below.

The analysis of the HIRHAM-NAOSIM model output showed the climatological impacts of cyclonic forcing on underlying sea ice and ocean in JAS. It was found that JAS Arctic storm count and intensity experienced large inter-annual variability with distinct regional characteristics. High storms counts were found to occur over the Atlantic side of the Arctic Ocean while fewer storms occurred over the Pacific side. In addition, storm intensity was also found to be greater for the cyclones developing over the Atlantic side versus the Pacific side of the Arctic Ocean.

Composite analysis indicated that the increased number of JAS storms on the Atlantic side of the Arctic Ocean shape a low pressure system that is centered over the Kara Sea. The low pressure system, in turn, leads to increased surface winds, ocean circulation, and sea ice drift in the marginal ice zone, increased upward heat flux from the ocean into the atmosphere and, ultimately, decreased sea ice concentration (10-15%) and thickness (10-20 cm) on average. Composite analysis for the Pacific side of the Arctic suggested that low pressure forms over the Chukchi Sea causing cyclonic surface winds over the Beaufort-Chukchi-East-Siberian Seas, increased ocean circulation and sea ice drift along the coasts, increased upward heat fluxes from the ocean into the atmosphere, and reduced sea ice concentration and thickness. On days with high number of intense storms, positive SST (0.5-1°C) anomaly over the Barents, Kara, and Beaufort Seas was attributed to cyclonically induced sea ice concentration and thickness reduction. During intense storms over the Atlantic and Pacific sides of the Arctic, sea ice drift accelerated by approximately 0.1-0.2 m/s as compared to climatology. Net surface energy fluxes were positive during periods with both high and low numbers of intense storms suggesting that, in JAS, sea ice takes up energy from the atmosphere. On days with high numbers of intense storms, the net heat flux was less than on days with low number of intense storms; this suggests weakened energy transfer between the atmosphere and sea ice due to sea ice reduction

and exposure of open water. During JAS in the Arctic, energy transfer between the surface and the atmosphere is inhibited due to a weak vertical temperature gradient. The temperature gradient between the surface and atmosphere was greater in cases when the underlying surface was sea ice, versus open water. This fact explained why the energy exchange was weakened in periods with high numbers of intense storms.

An in-depth analysis of sea ice - storm interaction was conducted for two storms that occurred in different seasons (August and March) and over different areas (Atlantic side and Pacific side of the Arctic) by employing the sea ice – ocean coupled model CICE-POP. CICE-POP reliably reproduced inter-annual sea ice area variability for 1979 to 2011, and the Arctic sea ice concentration, motion, and thickness patterns; however, it noticeably overestimated sea ice drift speed. Sea ice concentration was reproduced more accurately in summer than in winter as compared to remote sensing data; SIC tended to be overestimated in the Atlantic Ocean, and slightly underestimated in the Pacific side of the Arctic.

The March 2011 storm was a deep low pressure system that developed over the Atlantic side of the Arctic and resulted in a pronounced sea ice retreat over the Barents and Kara Seas. Cyclonic forcing was robust enough to reverse the freeze-up of sea ice and cause it to retreat. The storm-induced reduction of sea ice increased the amplitude of fluctuations of surface radiation and turbulent heat fluxes.

The combined dynamic and thermodynamic forcing exerted on sea ice during March 2011 resulted in sea ice area loss of 150.000 $km^2$, 80.000 $km^2$ of which was loss due to dynamic forcing. In contrast, thermodynamic forcing resulted in a sea ice area gain of 20.000 $km^2$. However, the coupled thermodynamic and dynamic forcing that was represented by the control, unperturbed experiment led to more extensive sea ice area reduction than that in the thermodynamic experiment. Although there were noticeable fluctuations in surface heat energy fluxes, dynamic forcing was deemed to be the main driver for sea ice retreat.

The August 2012 storm was another Arctic low pressure system that caused extensive reduction of sea ice concentration. Turbulent heat fluxes underwent the most notable changes during this cyclone. The storm developed over Eurasia and moved over the East-Siberian Sea poleward to the Central Arctic. Unlike the March 2011 storm where sea ice reduction was predominantly wind-driven, in the case of the August 2012 storm, sea ice area loss was a result of a combination of dynamic and thermodynamic drivers. The total loss of sea ice area over the Beaufort-Chukchi-East-Siberian Seas during the August 2012 cyclone was approximately 900.000 $km^2$. Analysis of the sensitivity experiment results showed that dynamic and thermodynamic drivers resulted in approximately identical impact. These findings suggest that for the August 2012 cyclone, the thermodynamic and dynamic drivers were equally relevant in the deterioration of the sea ice pack. The main factors of accelerated sea ice retreat during the cyclone's passage were revealed to be increased oceanic heat flux and turbulent heat fluxes.

To demonstrate that ongoing changes in sea ice and ocean in the Arctic may have an impact on storm dynamics, a case study was conducted by employing the ERA-Interim forced WRF model and analyzing the output based on the March 2011 storm. WRF yielded realistic and high-resolution simulations of storm dynamics. Surface thermal difference between the Gulf Stream waters and the sea ice along the coast of Greenland, in conjunction with the presence of a cold-core low pressure system, provided favorable conditions for robust baroclinic instability. Sensitivity experiments forced by perturbed boundary forcing (SIC and SST were fixed to climatological conditions, averaged over 1981-2011) showed that warm and moist air advection from the North Atlantic along the Eurasian coast into the Central Arctic was key for storm development. A sustained pattern of warm air advection, increased surface heating due to enhancement of the turbulent heat fluxes through cracks and openings in sea ice, and latent heat release of condensation in the lower-mid atmosphere, further strengthened the surface temperature gradient and allowed continuation of the development of the March 2011 storm. In March 2011, lower than climatologically average (1979-2011) sea ice concentration weakened the surface air cooling leading to a buildup of additional baroclinic energy. The poleward shift of elevated turbulent heat fluxes, associated with diminished sea ice extent and increased SST, contributed an additional source of baroclinic energy that enabled the development of secondary mesocyclones. The merger of the parent cyclone with secondary mesocyclones resulted in sustained and sufficient baroclinic energy and contributed to a continuous and prolonged cyclonic life cycle. Physical analysis of the March 2011 cyclone revealed an increase in poleward moisture and latent heat transport, accompanied by an enhancement of cloud cover, and resulted in positive downward longwave radiation. A persistent warm air advection poleward occurred concurrently with an increased release of surface heat fluxes from open water in the Barents and Kara Sea, making an additional contribution to the surface air warming. The cyclonic deepening and regeneration process on March 19, 2011 was driven by the release of latent heat into the mid-troposphere. The steepening of the temperature gradient between the cyclonic core and periphery reinforced baroclinicity aloft. The mechanism led to rapid increase in cyclonic vorticity and deepening of the low pressure system.

Arctic storm count and intensity has increased as Arctic Climate has been changing to a warmer regime. The poleward movement of the cyclones creates favorable conditions for sea ice reduction in the Arctic Ocean. As sea ice retreats, more energy may be supplied for cyclogenesis and generate more intense cyclones that can further reduce sea ice area. All in all, while more case studies are recommended to determine the role of storm-sea ice interaction in Arctic Climate warming in full climatological scope, the findings of this investigation pointed out the fact that storm – sea ice coupling processes, in certain cases, may increase the pace of Arctic surface air warming.

## References


Akperov, M. G., I. I. Mokhov, A. Rinke, K. Dethloff, and H. Matthes, 2014: Cyclones and their possible changes in the Arctic by the end of the 21st century from regional climate model simulations, Theor. Meteorol. Clim., doi:10.1007/s00704-014-1272-2.

Alekseev G.V., Bulatov L.V., Zakharov V.F., 2000: Fresh Water Freezing/Melting Cycle in the Arctic Ocean. In: Lewis E.L., Jones E.P., Lemke P., Prowse T.D., Wadhams P. (eds) The Freshwater Budget of the Arctic Ocean. NATO Science Series (Series 2. Environment Security), vol 70. Springer, Dordrecht.

Anisimov, O. A., 2007: Potential feedback of thawing permafrost to the global climate system through methane emission., Environ. Res. Lett., 2 045016.

Arctic Council, Protection of the Arctic Marine Environment (PAME) Arctic Marine Shipping Assessment 2009. Project Report. Protection of the Arctic Marine Environment Working Group.

Asplin, M., Lukovich, J., and Barber, D., 2009: Atmospheric forcing of the Beaufort Sea ice gyre: Surface pressure climatology and sea ice motion. J. Geophys. Res., 114, C00A06, doi:10.1029/2008JC005127.

Asplin, M. G., R. Galley, D. Barber and S. Prinsenberg, 2012: Fracture of summer perennial sea ice by ocean swell as a result of Arctic storms. J. Geophys. Res., 117: doi: 10.1029/2011JC007221. ISSN: 0148-0227.

Bader, J., Mesquita, M.d.S., Hodges, K.I., Miles, M., Østerhus, S. and Keenlyside, N., 2011: A review on Northern Hemisphere sea ice, storminess and teleconnection patterns: Observations and projected changes, Atmos. Res., doi:10.1016/j.atmosres.2011.04.007.

Barber, D. G., J. V. Lukovich, J. Keogak, S. Baryluk, L. Fortier, and G.H.R. Henry, 2008: The changing climate of the Arctic. Arctic 61(Suppl.):7–26.

Barry, R. G., and J. A. Maslanik, 1989: Arctic sea ice characteristics and associated atmosphere-ice interactions. Geojournal, 18, 5–44.

Barry, R. G. and A. M. Carleton, 2001: Synoptic and dynamic climatology. Routledge, London and New York. 620 pp. ISBN 0 41503116 8. Q. J. R. Meteorol. Soc., 128: 742. doi:10.1002/qj.200212858018.

Bengtsson L., V.A. Semenov, and O.M. Johannessen, 2004: The early twentieth-century warming in the Arctic – A possible mechanism, J. Clim., 17, pp. 4045-4057.

Bengtsson, L., K. I. Hodges, and E. Roeckner, 2006: Storm tracks and climate change, J. Clim., 19, 3518–3543.

Berrisford, P., Dee, D., Poli, P., Brugge, R., Fielding, K., Fuentes, M., Simmons, A., 2011: The ERA-Interim archive Version 2.0, ERA Report Series 1, ECMWF, Shinfield Park. Reading, UK, 13177.

Bhatt, U.S., Walker, D.A. Raynolds, M.K., Comiso, J.C., Epstein, H.E., Jia, G.-S., Gens, R., Pinzon, J.E., Tucker, C.J., Tweedie, C.E., Webber, P.J., 2010: Circumpolar Arctic tundra vegetation change is linked to sea ice decline, Earth Interact, 14, 1-20.

Bintanja, R. and Selten, F. M., 2014: Future increases in Arctic precipitation linked to local evaporation and sea ice retreat, Nature, 509, 480–482.

Bitz, C.M. and W.H.Lipscomb, 1999: An energy-conserving thermodynamic model of sea ice, J. Geophys. Res., 104, 15, 669-15,677.

Bitz, C. M., M. Holland, M. Eby and A. J. Weaver, 2001: Simulating the ice-thickness distribution in a coupled climate model. J. Geophys. Res., 106, 2441–2463.

Blanchard-Wrigglesworth, E., Armour, K. C., Bitz, C. M., and DeWeaver, E., 2011: Persistence and inherent predictability of Arctic sea ice in a GCM ensemble and observations, J. Clim., 24, 231–250.

Boisvert, L. N., A. A. Petty, and J. C. Stroeve, 2016: The impact of the extreme winter 2015/16 Arctic cyclone on the Barents–Kara Seas. Mon. Wea. Rev., 144, 4279–4287, doi:https://doi.org/10.1175/MWR-D-16-0234.1.

Bonan, G. B., 2008: Forests and climate change: Forcings, feedbacks, and the climate benefits of forests, Science, 320, 1444–1449.

Branscome, L.E., W. Gutowski, and D. Stewart, 1989: Effect of surface fluxes on the nonlinear development of baroclinic waves, J. Atmos. Sci., 46, 460-475.

Brümmer, B., Múller, G., Hoeber, H. 2003: A Fram Strait cyclone: properties and impact on ice drift as measured by aircraft and buoys, J. Geophyis. Res., 108, No. D7, 4217, doi:10.1029/2002JD002638.

Brümmer, B., Schröder, D., Müller, G., Spreen, G., Jahnke-Bornemann, A. and Launiainen, J. 2008: Impact of a Fram Strait cyclone on ice edge, drift, divergence and concentration: Possibilities and limits of an observational analysis, J. Geophys. Res., 113, C12003, doi:10.1029/2007JC004149.

Bunn, A. G., and S. J. Goetz, 2006: Trends in satellite-observed circumpolar photosynthetic activity from 1982 to 2003: The influence of seasonality, cover type, and vegetation density, Earth Interact., 10, 1–9, doi:10.1175/EI190.1.

Chapin, F., M. Sturm, M. Serreze, J. McFadden, J. Key, A. Lloyd, A. McGuire, T. Rupp, A. Lynch, and J. Schimel, 2005: Role of land-surface changes in Arctic summer warming, Science, 310(5748), 657–660.

Clow, G. D., 2008: USGS polar temperature logging system, description and measurement uncertainties, U.S. Geol. Surv. Tech. Methods, 2-E3, 24 pp.

Collins W.D., C.M. Bitz, M.L. Blackmon, 2006: The Community Climate System Model Version 3 (CCSM3). J. Clim., 19: 2122-2143.

Comiso, J.C., 2012: Large decadal decline of the Arctic multiyear ice cover, J. Clim., 25, 1176–1193.

Crook, J. A., Forster, P. M., and Stuber, N., 2011: Spatial Patterns of Modeled Climate Feedback and Contributions to Temperature Response and Polar Amplification, J. Clim., 24, 3575–3592, doi:10.1175/2011JCLI3863.1.

Curry, R., and Mauritzen, C., 2005: Dilution of the northern North Atlantic Ocean in recent decades, Science, 308:1772–1774.

Danabasoglu G., W.G. Large, J.J. Tribbia, et al., 2006: Diurnal coupling in the tropical oceans of CCSM3. J. Clim., 19: 2347:2365.

Dee D.P., Uppala S.M., Simmons A.J., Berrisford P., et al., 2011: The ERA-Interim reanalysis: configuration and performance of the data assimilation system, Q. J. R. Meteorol. Soc., 137: 553–597. DOI:10.1002/qj.828.

Deser, C., 2000: On the teleconnectivity of the "Arctic Oscillation, Geophys. Res. Lett., 27, 779–782.

Deser, C. and Teng, H., 2008: Evolution of Arctic sea ice concentration trends and the role of atmospheric circulation forcing, 1979–2007, Geophys. Res. Lett., 35: doi: 10.1029/2007GL032023. issn: 0094-8276.

Deser, C., R. Tomas, M. Alexander, and D. Lawrence, 2010: The seasonal atmospheric response to projected Arctic sea ice loss in the late 21stcentury, J. Clim., 23, 333–351.

Dethloff, K., A. Rinke, R. Lehmann, J. H. Christensen, M. Botzet, and B. Machenhauer, 1996: Regional climate model of the Arctic atmosphere, J. Geophys. Res., 101, 23,401–23,422.

Dierer, S., Schlunzen, K. H., Birnbaum, G., Brummer, B. and Muller, G. 2005. Atmosphere-sea ice interactions during a cyclone passage investigated by using model simulations and measurements, Mon. Wea. Rev.,133(12), 3678–3692.

Dorn, W., K. Dethloff, and A. Rinke, 2009: Improved simulation feedbacks between atmosphere and sea ice cover over the Arctic Ocean in a coupled regional climate model, Ocean Model., 29, 103-114, doi:10.1016/j.oceanmod.2009.03.010.

Dorn, W., K. Dethloff, and A. Rinke, 2012: Limitations of a coupled regional climate model in the reproduction of the observed Arctic sea ice retreat, The Cryosphere, 6, 985-998, doi:10.5194/tc-6-985-2012.

Drobot, S.D., and J.A. Maslanik, 2003: Interannual variability in summer Beaufort Sea ice conditions: Relationship to spring and summer surface and atmospheric variability, J. Geophys. Res., 108(C7), 3233, http://dx.doi.org/10.1029/2002JC001537.

Eady, E. T., 1949: Long Waves and Cyclone Waves, Tellus, 1: 33–52. doi:10.1111/j.2153-3490.1949.tb01265.x.

Eicken, H., Lovecraft, A.L., and Druckenmiller, M.L., 2009: Sea ice system services: A framework to help identify and meet information needs relevant for Arctic observing network needs, Arctic, 62(2), pp. 119-136.

Feifel, K. and Gregg, R. M., 2010: Relocating the Village of Newtok, Alaska due to Coastal Erosion [Case study on a project of the Newtok Planning Group]. Product of EcoAdapt's State of Adaptation Program. Retrieved from CAKE: www.cakex.org/case-studies/relocating-village-newtok-alaska-due-coastal-erosion.

Francis, J., Hunter, E., and Zou, C.-Z. 2005: Arctic tropospheric winds derived from TOVS satellite retrievals, J. Clim., 18(19):2270 –2285.

Geng, Q., and M. Sugi, 2003: Possible change of extratropical cyclone activity due to enhanced greenhouse gases and sulfate aerosols—Study with a high-resolution AGCM. J. Climate, 16, 2262–2274, doi:10.1175/1520-0442(2003)16,2262:PCOECA.2.0.CO;2.

Gent, P. R., and Coauthors, 2011: The Community Climate System Model version 4., J. Clim., 24, 4973–4991, doi:10.1175/2011JCLI4083.1.

Gitelman, A. I., J. S. Risbey, R. E. Kass, and R. D. Rosen, 1997: Trends in the surface meridional temperature gradient. Geophys. Res. Lett., 24, 1243–1246, doi:10.1029/97GL01154.

Hall, A., 2004: The role of surface albedo feedback in climate, J. Clim., 17, 1550–1568.

Hansen, J., Lacis, A., Rind, D., Russell, G., Stone, P., Fung, I., Ruedy, R., Lerner, J., 1984: Climate sensitivity: analysis of feedback mechanisms. In: Hansen, J., Takahashi, T. (Eds.), Climate Processes and Climate Sensitivity, American Geophysical Union, pp. 130–163.

Herman, A. and Glowacki, O., 2012: Variability of sea ice deformation rates in the Arctic and their relationship with basin-scale wind forcing, The Cryosphere, 6, 1553-1559, doi:10.5194/tc-6-1553-2012.

Hibler, W.D., 1979: A Dynamic Thermodynamic Sea Ice Model, J. Phys. Oceanogr., 9, 815–846, https://doi.org/10.1175/1520-0485(1979)009<0815:ADTSIM>2.0.CO;2.

Holland, M.M., Bitz, C.M., 2003: Polar amplification of climate change in coupled models, Climate Dyn., 21, 221–232.

Holland, M. M., J. Finnis, and M. C. Serreze, 2006: Simulated Arctic Ocean freshwater budgets in the 20th and 21st centuries, J. Clim., 19, 6221–6242.

Holland-Bartels, L., and B. Pierce (Eds.), 2011: An evaluation of the science needs to inform decisions on Outer Continental Shelf energy development in the Chukchi and Beaufort Seas, Alaska, U.S. Geol. Surv. Circ., 1370, 278 pp.

Holt, B., and S. Martin, 2001: The effect of a storm on the 1992 summer sea ice cover of the Beaufort, Chukchi, and East Siberian seas, J. Geophys. Res., 106, 1017–1032.

Hopkins, K., Grove, C., and Dunham, M., 2011: Alaskans weather epic Bering Sea storm. Anchorage Daily News. Accessed November 10, 2011.

Hu, A., C. Rooth, R. Bleck, C. Deser, 2002: NAO influence on sea ice extent in the Eurasian coastal region, Geophys. Res. Lett., 29(22), 2053, doi:10.1029/2001GL014293.

Hunke, E.C. and J.K. Dukowitz, 1997: An elastic-viscous-plastic model for sea ice dynamics, J. Phys. Oceanogr., 27, 1849-1867.

Hunke, E. C., and W. H. Lipscomb, 2008: CICE: The Los Alamos Sea Ice Model user's manual, version 4. Los Alamos National Laboratory Tech. Rep LA-CC-06-012, 76 pp.

Inoue, J., and M. E. Hori, 2011: Arctic cyclogenesis at the marginal ice zone: A contributory mechanism for the temperature amplification? Geophys. Res. Lett., 38, L12502, doi:10.1029/2011GL047696.

Inoue, J., M. E. Hori, and K. Takaya, 2012: The role of Barents Sea ice in the winter time cyclone track and emergence of a warm-Arctic cold-Siberian anomaly, J. Clim., 25, 2561–2568.

Intrieri, J. M., Fairall, C. W., Shupe, M. D., Persson, P. O. G., Andreas, E. L., Guest, P. S., and Moritz, R. E., 2002: An annual cycle of Arctic surface cloud forcing at SHEBA, J. Geophys. Res., 107, 8039, doi:10.1029/2000JC000439.

IPCC (Intergovernmental Panel on Climate Change). 2007: The physical science basis. Contribution of Working Group 1 to the Fourth Assessment Report of the Intergovernmental Panel on Climate Change. New York: Cambridge University Press. 2006GL027341.

Jeoung, S.-J., C.-H. Ho, H.-J. Gim, and M. E. Brown, 2011: Phenology shifts at start vs. end of growing season in temperate vegetation over the Northern Hemisphere for the period 1982–2008, Global Change Biol., 17, 2385–2399, doi:10.1111/j.1365-2486.2011.02397.x.

Johannessen, O. M., L. Bengtsson, M. W. Miles, S. I. Kuzmina, V. A. Semenov, G. V. Alekseev, A. P. Nagurnyi, V. F. Zakharov, L. P. Bobylev, and L. H. Pettersson., 2004: Arctic climate change: Observed and modeled temperature and sea-ice variability, Tellus A, 56(4), 328-341.

Jorgenson M. T. and Brown J., 2005: Classification of the Alaskan Beaufort Sea Coast and estimation of carbon and sediment inputs from coastal erosion, Geo-Marine Letters, vol. 25, pp. 69-80.

Jorgenson, M. T., Y.L.Shur, and E.R. Pullman, 2006: Abrupt increase in permafrost degradation in Arctic Alaska, Geophys. Res. Lett., 25, L02503, doi: 10.1029/2005GL024960.

Kalnay, E., et al., 1996: The NCEP/NCAR 40-Year Reanalysis Project. Bulletin of the American Meteorological Society, 77, 437-471. http://dx.doi.org/10.1175/1520-0477(1996)077<0437:TNYRP>2.0.CO;2

Karcher, M. J., R. Gerdes, F. Kauker, and C. Köberle, 2003: Arctic warming: Evolution and spreading of the 1990s warm event in the Nordic seas and the Arctic Ocean, J. Geophys. Res., 108(C2), 3034, doi:10.1029/2001JC001265.

Kauker, F., R. Gerdes, M. Karcher, C. Köberle, and J. L. Lieser, 2003: Variability of Arctic and North Atlantic sea ice: A combined analysis of model results and observations from 1978 to 2001, J. Geophys. Res., 108(C6), 3182, doi:10.1029/2002JC001573.

Kay, J. E. and L'Ecuyer, T., 2013: Observational constraints on Arctic Ocean clouds and radiative fluxes during the early 21st century, J. Geophys. Res.-Atmos., 118, 7219–7236.

Kay, J. E., and A. Gettelman, 2009: Cloud influence on and response to seasonal Arctic sea ice loss, J. Geophys. Res., 114, D18204, doi:10.1029/2009JD011773.

Koyama, T., J. Stroeve, J. Cassano, and A. Crawford, 2017: Sea Ice Loss and Arctic Cyclone Activity from 1979 to 2014. J. Climate, 30, 4735–4754, https://doi.org/10.1175/JCLI-D-16-0542.1.

Kriegsmann, A. and Brümmer, B., 2014: Cyclone impact on sea ice in the central Arctic Ocean: a statistical study, The Cryosphere, 8, 303-317, doi:10.5194/tc-8-303-2014.

Kwok, R., 2006: Contrasts in sea ice deformation and production in the Arctic seasonal and perennial ice zones, J. Geophys. Res., 111, C11S22, doi:10.1029/2005JC003246.

Kwok, R., and D. A. Rothrock, 2009: Decline in Arctic sea ice thickness from submarine and ICESat records: 1958–2008, Geophys. Res. Lett., 36, L15501, doi:10.1029/2009GL039035.

Kwok, R., G. F. Cunningham, M. Wensnahan, I. Rigor, H. J. Zwally, and D. Yi, 2009: Thinning and volume loss of the Arctic Ocean sea ice cover: 2003–2008, J. Geophys. Res., 114, C07005, doi:10.1029/2009JC005312.

Lammert, A., Brummer, B., and Kaleschke, L, 2009: Observation of cyclone-induced inertial sea ice oscillation in Fram strait, Geophys. Res. Lett., 36, L10503, doi:10.1029/2009GL037197.

LeDrew, E. L., D. Johnson, and J. A. Maslanik, 1991: An examination of atmospheric mechanisms that may be responsible for the annual reversal of the Beaufort Sea ice field, Int. J. Clim., 11, 841–859.

Levis, S., J. A. Foley, and D. Pollard, 2000: Large-scale vegetation feedbacks on a doubled CO2 climate, J. Clim., 13, 1313–1325.

Lindsay, R.W., J. Zhang, A.J. Schweiger, M.A. Steele, and H. Stern., 2009: Arctic sea ice retreat in 2007 follows thinning trend, J. Clim., 22:165–176, http://dx.doi.org/10.1175/2008JCLI2521.1.

Lipscomb, W. H., 2001: Remapping the thickness distribution in sea ice models, J. Geophys. Res., 106, 13,989–14,000.

Lipscomb, W.H. and E.C. Hunke, 2004: Modeling Sea Ice Transport Using Incremental Remapping, Mon. Wea. Rev., 132, 1341–1354, https://doi.org/10.1175/1520-0493(2004)132<1341:MSITUI>2.0.CO;2.

Liptak J. and Strong C, 2013. Propagating atmospheric patterns associated with sea ice motion through the Fram Strait, J. Clim., 26, 2292-2297.

Liu, J., J. A. Curry, and D. G. Martinson, 2004: Interpretation of recent Antarctic sea ice variability, Geophys. Res. Lett., 31, L02205, doi:10.1029/2003GL018732.

Lucarini, V. and Ragone, F., 2011: Energetics of climate models: Net energy balance and meridional enthalpy transport, Rev. Geophys., 49, RG1001, doi:10.1029/2009RG000323.

Manabe, S., Wetherald, R.T., 1975: The effect of doubling the CO2 concentration on the climate of a general circulation model, J. Atmos. Sci. 32, 3–15.

Manabe, S., and R.J. Stouffer, 1980: Sensitivity of a global climate model to an increase of CO2 concentration in the atmosphere, J. Geophys. Res., 85, 5529-5554.

Maykut, G.A., 1986: The surface heat and mass balance. In Untersteiner, N., ed. The geophysics of sea ice. New York, Plenum Press, 395-463. (NATO ASI Series. Ser. B. Physics, 146.

McCabe, G.J., Clark, M.P., and Serreze, M. 2001: Trends in Northern Hemisphere surface cyclone frequency and intensity, J. Clim., 14:2763–2768.McGuire, A.D., F.S. Chapin, J.E. Walsh, and C. Wirth, 2006: Integrated regional changes in Arctic climate feedbacks: Implications for the Global Climate System, Annual Review of Environment and Resources, 31, 61-91, doi:10.1175/JCLI3746.1.

McGuire, A. D., F. S. Chapin, III, J. E. Walsh, and C. Wirth., 2006. Integrated regional changes in arctic climate feedbacks: implications for the global climate system. Annual Review Environment and Resources 31:61–91.

McLaren, A. S., M. C. Serreze, and R. G. Barry, 1987: Seasonal variations of sea ice motion in the Canada basin and their implications, Geophys. Res. Lett., 14, 1123 – 1126, doi:10.1029/GL014i0.

Meehl, G., Washington, W., Collins, W., Arbaster, J., Hu, A., Buja, L., Strand, W., and Teng, H., 2005: How much more global warming and sea level rise? Science 307: 1769–1771.

Mesquita, M. D., Hodges, K. I., Atkinson, D. E., and Bader, J., 2011: Sea ice anomalies in the Sea of Okhotsk and the relationship with storm tracks in the northern hemisphere during winter, Tellus A, 63, 312-329. doi:10.1002/asl.308.

Nghiem, S.V., Y. Chao, G. Neumann, P. Li, D.K. Perovich, T. Street, and P. Clemente, 2006: Depletion of perennial sea ice in the eastern Arctic Ocean, Geophys. Res. Lett., 33, L17501, http://dx.doi.org/10.1029/2006GL027198.

NSIDC, 2016: All About Sea Ice, National Snow and Ice Data Center. Accessed 1 February 2016. /cryosphere/seaice/index.html.

Ogi M, Yamazaki K., 2010: Trends in the summer Northern Annular Mode and Arctic sea ice. Scientific Online Letters on the Atmosphere (SOLA) 6: 41–44, DOI: 10.2151/sola.2010-011.

Ogi, M., and J. M. Wallace, 2012: The role of summer surface wind anomalies in the summer Arctic sea ice extent in 2010 and 2011, Geophys. Res. Lett., 39, L09704, doi:10.1029/2012GL051330.

Ogorodov, S. A., Belova, N. G., Kamalov, A. M., Noskov, A. I., Volobueva, N. N., Grigoriev, M. N., Wetterich, S. and Overduin, P. P., 2010: Storm surges as a forcing factor of coastal erosion in the western and eastern Russian Arctic, Storm Surges Congress, Hamburg, Germany, 1317.

Orlanski, I., 1998: Poleward Deflection of Storm Tracks, J. Atmos. Sci.: Vol. 55, No. 3, pp. 2577-2602.

Overland, J. E., Wood, K. R., and Wang, M., 2011: Warm Arctic-cold continents: climate impacts of the newly open Arctic Sea, Polar Res., 30, 15787, doi:10.3402/polar.v30i0.15787.

Overland, J.E., Francis, J. A., Hanna, E., and Wang, M., 2012: The recent shift in early summer Arctic atmospheric circulation, Geophys. Res. Lett., 39, L19804.

Parkinson, C. L., and J. C. Comiso, 2013: On the 2012 record low Arctic sea ice cover: Combined impact of preconditioning and an August storm, Geophys. Res. Lett., 40, 1356–1361, doi:10.1002/grl.50349.

Pearson, R. G., S. J. Phillips, M. M. Loranty, P. S. A. Beck, T. Damoulas, S. J. Knight, and S. J. Goetz, 2013: Shifts in Arctic vegetation and associated feedbacks under climate change, Nat. Clim. Change, 3, 673–677.

Perovich, D. K., S. V. Nghiem, T. Markus, and A. Schweiger, 2007: Seasonal evolution and interannual variability of the local solar energy absorbed by the Arctic sea ice-ocean system, J. Geophys. Res., 112, C03005, doi:10.1029/2006JC003558.

Perovich, D. K., Richter-Menge, J. A., Jones, K. F., and Light, B., 2008: Sunlight, water, and ice: Extreme Arctic sea ice melt during the summer of 2007, Geophys. Res. Lett., 35, L11501, doi:10.1029/2008GL034007.

Persson, P. O. G., T. Uttal, J. Intrieri, C. W. Fairall, E. L. Andreas, and P. S. Guest, 1999: Observations of large thermal transitions during the Arctic night from a suite of sensors at SHEBA, in Preprints, Fifth Conference on Polar Meteorology and Oceanography, 10 – 15 January 1999, Dallas, Tex., pp. 306 – 309, American Meteorological Society, Boston.

Persson, P. Ola G., C. W. Fairall, E. L. Andreas, P. S. Guest, and D. K. Perovich, 2002: Measurements near the Atmospheric Surface Flux Group tower at SHEBA: Near-surface conditions and surface energy budget, J. Geophys. Res., 107(C10), 8045, doi:10.1029/2000JC000705.

Pithan, F. and Mauritsen, T., 2014: Arctic amplification dominated by temperature feedbacks in contemporary climate models, Nature Geoscience, 7, 181–184, doi:10.1038/ngeo2071.

Polyakov I.V., R.V. Bekryaev, G.V. Alekseev, U.S. Bhatt, R.L. Colony, M.A. Johnson, A.P. Makshtas, D. Walsh, 2003: Variability and trends of air temperature and pressure in the maritime Arctic, 1875–2000, J. Clim., 16, pp. 2067-2077.

Polyakov, I. V., Timokhov, L. A., Alexeev, V. A., Bacon, S., Dmitrenko, I. A., Fortier, L., and Toole, J., 2010: Arctic ocean warming contributes to reduced polar ice cap, J. Phys. Oceanogr., 40, 2743–2756.

Potter, C., S. Li, and R. Crabtree, 2013: Changes in Alaskan tundra ecosystems estimated from MODIS greenness trends, 2000 to 2010, J. Geophys., Remote Sens., 2, 1–7.

Rampal, P., Weiss, J., Marsan, D., and Bourgoin, M., 2009: Arctic sea ice velocity field: General circulation and turbulent-like fluctuations, J. Geophys. Res., 114, C10014, doi:10.1029/2008JC005227.

Reynolds, R.W., N.A. Rayner, T.M. Smith, D.C. Stokes, and W. Wang, 2002: An improved in situ and satellite SST analysis for climate, J. Clim., 15, 1609-1625.

Rigor, I. G., J. M. Wallace, and R. L. Colony, 2002: Response of sea ice to the Arctic Oscillation, J. Clim., 15, 2648–2663.

Rigor, I. G., and J. M. Wallace, 2004: Variations in the age of Arctic sea ice and summer sea ice extent, Geophys. Res. Lett., 31, L09401, doi:10.1029/2004GL019492.

Rinke, A., K. Dethloff, W. Dorn, D. Handorf, and J.C. Moore, 2013: Simulated Arctic atmospheric feedbacks associated with late summer sea ice anomalies, J. Geophys. Res. Atmos. 118, doi: 10.1002/jgrd.50584.

Robock, A., 1983: Ice and snow feedbacks and the latitudinal and seasonal distribution of climate sensitivity, J. Atmos. Sci., 40, 986–997.

Rothrock, D.A., 1975: The energetics of the plastic deformation of pack ice by ridging, J. Geophys. Res., 80, 4514-4519.

Rothrock, D. A., and J. Zhang, 2005: Arctic Ocean sea ice volume: What explains its recent depletion? J. Geophys. Res., 110, C01002, doi:10.1029/2004JC002282.

Ruggieri, P & Buizza, R & Visconti, G., 2016: On the link between Barents-Kara sea-ice variability and European blocking: Barents-Kara sea-ice and the NAO, J. Geophys. Res., 121, 10.1002/2015JD024021.

Schiermeier, Q., 2006: A sea change, Nature, 439, 256–260.

Schultz, D. M. and G. Vaughan, 2011: Occluded Fronts and the Occlusion Process: A Fresh Look at Conventional Wisdom, Bull. Amer. Meteor. Soc., 92, 443–466.

Schweiger, A.J., R.W. Lindsay, S. Vavrus, and J.A. Francis, 2009: Relationships between Arctic Sea Ice and Clouds during Autumn, J. Clim., 22, 2793–2793, https://doi.org/10.1175/2008JCLI3023.1

Screen, J. A. and Simmonds, I., 2010: The central role of diminishing sea ice in recent Arctic temperature amplification, Nature, 464, 1334–1337.

Screen, J., Simmonds, I., and Keay, K., 2011: Dramatic interannual changes of perennial Arctic sea ice linked to abnormal summer storm activity, J. Geophys. Res., 116, D15105, doi:10.1029/2011JD015847.

Sepp M., Jaagus J., 2011: Changes in the activity and tracks of Arctic cyclones, Clim. Change, 105(3–4):577–595. doi:10.1007/s10584–010–9893–7.

Serreze, M., Barry, R., and McLaren, A., 1989: Seasonal variations in sea ice motion and effects on sea ice concentration in the Canada Basin, J. Geophys. Res., 94, 10955–10970.

Serreze, M. C., Carse, F., Barry, R. G. and Rogers, J. C. 1997: Icelandic low cyclone activity: climatological features, linkages with the NAO, and relationships with recent changes in the Northern Hemisphere circulation, J. Clim., 10, 453-464.

Serreze, M. C., Walsh, J. E., Chapin, F. S. III, Osterkamp, T., Dyurgerov, M., Romanovsky, V., Oechel, W. C., Morison, J., Zhang, T. and Barry, R. G., 2000: Observational evidence of recent change in the northern high-latitude environment, Clim. Change, 46, pp. 159–207.

Serreze, M. C., and J. A. Francis 2006: The Arctic amplification debate, Clim. Change, 76, 241–264, doi:10.1007/s10584-005-9017-y.

Serreze, M. C., Holland, M. M., and Stroeve, J., 2007: Perspectives on the Arctic's shrinking sea ice cover, Science, 315, 1533–1536, doi:10.1126/science.1139426.

Serreze, Mark C., Andrew P. Barrett, 2008: The Summer Cyclone Maximum over the Central Arctic Ocean, J. Clim, 21, 1048–1065.doi: http://dx.doi.org/10.1175/2007JCLI1810.1.

Serreze, M. C., Barrett, A. P., Stroeve, J. C., Kindig, D. N., and Holland, M. M., 2009: The emergence of surface-based Arctic amplification, The Cryosphere, 3, 11–19, doi:10.5194/tc-3-11-2009.

Serreze, M.C. and Barry, R.G., 2011: Processes and impacts of Arctic amplification: A research synthesis, Global and planetary change, 77 (2011) 85-96.

Shimada, K., T. Kamoshida, M. Itoh, S. Nishino, E. Carmack, F. McLaughlin, S. Zimmermann, and A. Proshutinsky, 2006: Pacific Ocean inflow: Influence on catastrophic reduction of sea ice cover in the Arctic Ocean, Geophys. Res. Lett., 33, L08605, doi:10.1029/2005GL025624.

Simmonds, I., Burke, C., and Keay, K., 2008: Arctic climate change as manifest in cyclone behavior, J. Clim., 21, 5777-5796.

Simmonds, I., and K. Keay, 2009: Extraordinary September Arctic sea ice reductions and their relationships with storm behavior over 1979–2008, Geophys. Res. Lett., 36, L19715, doi:10.1029/2009GL039810.

Skamarock, W. C., and Coauthors, 2008: A description of the Advanced Research WRF version 3. NCAR Tech. Note NCAR/TN-475+STR, 113 pp., doi:https://doi.org/10.5065/D68S4MVH.

Smith, R. D., J. K. Dukowicz and R. C. Malone, 1992: Parallel Ocean General-Circulation Modeling, Physica, D 60(1-4), 38-61.

Smith, S. L., V. E. Romanovsky, A. G. Lewkowicz, C. R. Burn, M. Allard, G. D. Clow, K. Yoshikawa, and J. Throop, 2010: Thermal state of permafrost in North America: A contribution to the International Polar Year, Permafrost Periglacial Processes, 21, 117–135, doi:10.1002/ppp.690.

Soden, B. J., Held, I. M., Colman, R., Shell, K. M., Kiehl, J. T., and Shields, C. A., 2008: Quantifying climate feedbacks using radiative kernels, J. Clim., 21, 3504–3520.

Sorteberg, A., and B. Kvingedal, 2006: Atmospheric forcing on the Barents Sea winter ice extent. J. Clim., 19, 4772–4784.

Sorteberg, A., and J. E. Walsh, 2008a: Seasonal Cyclone Variability at 70N and its Impact on Moisture transport into the Arctic, Tellus A, 60, 570-586.

Sorteberg, A., and J. Walsh, 2008b: Seasonal cyclone variability at 708N and its impact on moisture transport into the Arctic, Tellus, 60A, 570–586, doi:10.1111/j.1600-0870.2008.00314.x.

Steele, M., 1992: Sea ice melting and floe geometry in a simple ice-ocean model, J. Geophys. Res., 97(C11), 17,729–17,738, doi:10.1029/92JC01755.

Steele, M. and G.M. Flato, 2000: Sea ice growth, melt, and modeling: A survey. In: The Freshwater Budget of the Arctic Ocean, NATO Science Series 2, Vol. 70, E.L. Lewis, editor, Kluwer, pp. 549-587.

Steele, M., R. Morley, and W. Ermold, 2001: PHC: A global ocean hydrography with a high quality Arctic Ocean, J. Clim., 14, 2079-2087.

Steele, M., W. Ermold, and J. Zhang, 2008: Arctic Ocean surface warming trends over the past 100 years, Geophys. Res. Lett., 35, L02614, doi:10.1029/2007GL031651.

Stroeve, J.C., Serreze, M.C., Fetterer, F., Arbetter, T., Meier, W., Maslanik, J., and Knowles, K. 2005: Tracking the Arctic's shrinking ice cover: Another extreme September minimum in 2004, Geophys. Res. Lett., 32, L04501, doi:10.1029/2004GL021810.

Stroeve, J., M. Serreze, S. Drobot, S. Gearheard, M. Holland, J. Maslanik, W. Meier, and T. Scambos, 2008: Arctic Sea Ice Extent Plummets in 2007, Eos Trans. AGU, 89(2), 13–14, doi:10.1029/2008EO020001.

Stroeve J.C., Serreze M.C., Holland M.M., Kay J.E., Maslanik J. et al., 2011: The Arctics rapidly shrinking sea ice cover: A research synthesis, Clim. Change, doi:10.1007/s10584–011–0101–1.

Strong, C. and G. Magnusdottir, 2011: Dependence of NAO on coupling with sea ice, Clim. Dynamics, 36:1681—1689, DOI:10.1007/s00382-010-0752-z.

Sturm, M., C. Racine, and K. Tape, 2001: Increasing shrub abundance in the Arctic, Nature, 411, 546–547.

Tape, K., M. Sturm, and C. Racine, 2006: The evidence for shrub expansion in northern Alaska and the pan-Arctic, Global Change Biol., 12(4), 686–702.

Taylor, P. C., Cai, M., Hu, A., Meehl, J., Washington, W., and Zhang, G. J., 2013: A Decomposition of Feedback Contributions to Polar Warming Amplification, J. Clim., 26, 7023–7043. doi:10.1175/JCLI-D-12-00696.1.

Thorndike, A.S., D.S. Rothrock, G.A. Maykut and R.Colony, 1975: The thickness distribution of sea ice, J. Geophys. Res., 80, 4501-4513.

Thorndike, A. and Colony, R., 1982: Sea ice motion in response to geostrophic winds, J. Geophys. Res., 87, 5845–5852.

Tsukernik, M., D.N. Kindig, and M.C. Serreze, 2007: Characteristics of winter cyclone activity in the northern North Atlantic: Insights from observations and regional modeling, J. Geophys. Res., 112, D03101, doi:10.1029/2006JD007184.

Ukita, J., M. Honda, H. Nakamura, Y. Tachibana, D. J. Cavalieri, C. L. Parkinson, H. Koide, and K. Yamamoto, 2007: Northern Hemisphere sea ice variability: Lag structure and its implications, Tellus, Ser. A, 59, 261–272, doi:10.111/j.1600-0870.2006.00223.x.

Van Loon, H., 1967: The half-yearly oscillations in the middle and high southern latitudes and the coreless winter, J. Atmos. Sci., 24, 472-486.

Vavrus S., 2013: Extreme Arctic cyclones in CMIP5 historical simulations. Geophysical Research Letters, 40 (23): 6208 DOI: 10.1002/2013GL058161

Vavrus, S., M. M. Holland, A. Jahn, D. A. Bailey, and B. A. Blazey, 2016: 21st-century Arctic climate change in CCSM4, J. Clim., 25,2696–2710.

Walsh, J.E., W.L. Chapman, and T.L. Shy, 1996: Recent decreases of sea level pressure in the central Arctic. J. Clim., 9, 480-488.

Walter K. M., Zimov S. A., Chanton J. P., Verbyla D. and Chapin F. S., 2006: Methane bubbling from Siberian thaw lakes as positive feedback to climate warming, Nature 443 71–5.

Wang, W., B. T. Anderson, N. Phillips, R. K. Kaufmann, C. Potter, and R. B. Myneni, 2006: Feedbacks of vegetation on summertime climate variability over the North American Grasslands. Part I: Statistical analysis. Earth Interactions, 10, in press.

Washington, W.M., Meehl, G.A., 1996: High-latitude climate change in a global coupled ocean–atmosphere–sea ice model with increased atmospheric $CO_2$, J. Geophys. Res. 101, 12,795–12,801.

Wendler, G., Chen, L., Moore, B., 2013: Recent sea ice increase and temperature decrease in the Bering Sea area, Alaska, Theoretical and Applied Climatology, 114.

Winton, M., 2006: Amplified Arctic climate change: what does surface albedo feedback have to do with it? Geophys. Res. Lett. 33, L03701, doi:10.1029/2005GL025244.

Wiscombe, W.J. and S.G. Warren, 1980: A Model for the Spectral Albedo of Snow. I: Pure Snow. J. Atmos. Sci., 37, 2712–2733, https://doi.org/10.1175/1520-0469(1980)037<2712:AMFTSA>2.0.CO;2.

Wobus, C., R. S. Anderson, I. Overeem, N. Matell, G. Clow, and F. Urban, 2011: Thermal erosion of a permafrost coastline: Improving process based models using time-lapse photography, Arct. Antarct. Alp. Res., in press. This is from 2011 it should be already published. Please put the actual publication reference.

Woodgate, R. A., K. Aagaard, and T. J. Weingartner, 2006: Interannual changes in the Bering Strait fluxes of volume, heat and freshwater between 1991 and 2004, Geophys. Res. Lett., 33, L15609, doi:10.1029/2006GL026931.

Woodgate, R. A., T. Weingartner, and R. Lindsay, 2010: The 2007 Bering Strait oceanic heat flux and anomalous Arctic sea ice retreat, Geophys. Res. Lett., 37, L01602, doi:10.1029/2009GL041621.

Xu, L., et al., 2013: Temperature and vegetation seasonality diminishment over northern lands, Nat. Clim. Change, 3, 581–586.

Zhang, J., Woodgate R., Moritz R., 2010: Sea Ice Response to Atmospheric and Oceanic Forcing in the Bering Sea, J. Phys. Oceanogr., 08/2010; 40(8):1729-1747. DOI: 10.1175/2010JPO4323.1

Zhang J., R. Lindsay, A. Schweiger, M. Steele, 2013: The impact of an intense summer cyclone on 2012 Arctic sea ice retreat, J. Geophys. Res., 40, 4 doi:10.1002/grl.50190.

Zhang, J., A. Schweiger, M. Steele, and H. Stern., 2015: Sea ice floe size distribution in the marginal ice zone: Theory and numerical experiments, J. Geophys. Res., Oceans, 120, doi:10.1002/2015JC010770.

Zhang, X., Ikeda M., and Walsh J., 2003: Arctic Sea Ice and Freshwater Changes Driven by the Atmospheric Leading Mode in a Coupled Sea Ice–Ocean Model, J. Clim., 16, 2159–2177. doi: http://dx.doi.org/10.1175/2758.1

Zhang, X., J. E. Walsh, J. Zhang, U. S. Bhatt, and M. Ikeda, 2004: Climatology and Interannual Variability of Arctic Cyclone Activity: 1948–2002, J. Clim., 17, 2300–2317.

Zhang, X., He, J., Zhang, J., Polyakov, I., Gerdes, R., Inoue, J., and Wu, P., 2012: Enhanced poleward moisture transport and amplified northern high-latitude wetting trend, Nat. Clim. Change, 3, 47–51, doi:10.1038/nclimate1631.